Università degli Studi di Ferrara

DOTTORATO DI RICERCA IN
Scienze biomediche e biotecnologiche

CICLO *XXXIV°*

COORDINATORE Prof. Pinton Paolo

Age-dependent regulation of co-transcriptional Elp1 exon 20 splicing in Familial Dysautonomia

Settore Scientifico Disciplinare MED/04

Dottorando
Dott. Riccardi Federico

Tutore
Prof. Pinton Paolo

Co-Tutore
Prof. Pagani Franco

Anni 2018/2021

It’s not all about
being *lost in translation*…

ABSTRACT

Spinal Muscular Atrophy (SMA) and Familial Dysautonomia (FD) represent two paradigmatic diseases with a genetic origin associated to exon skipping defects. In both cases, the degree of exon skipping is directly related to the tissue- and phenotypic-severity and rescue of the underlying aberrant splicing events is therapeutic. In common with normal alternative splicing, exon skipping defects might be regulated co-transcriptionally by RNA Polymerase II (Pol II) elongation rate and/or chromatin histone marks. In addition, age-dependent genetic programs that include also co-transcriptional regulation can not only modify splicing globally, but potentially affect disease-causing splicing mutations. In this thesis, I have evaluated temporal changes in aberrant splicing patterns for two exon skipping events in SMA (Smn2 exon 7) and FD (Elp1 exon 20) asymptomatic mice and studied in detail the relationships between chromatin marks and splicing changes in the FD animal and in cellular models. Comparison of patterns at PostNatal Days (PND or P) 10, 90 and 365 showed tissue- and gene-specific splicing changes of the exon skipping events. In muscle, liver, lung and kidney, the Smn2 exon 7 inclusion showed an age-dependent increase, mainly during post-natal development. In central nervous system (CNS), exon 7 inclusion decreased within 3 months of age to then returned to its baseline level at P365 while no changes were observed in heart. In the FD mouse, the inclusion levels of Elp1 exon 20 are reduced in the CNS, liver, muscle and lung between P10 and P90, remaining low at one year of life: no changes were observed for the other organs. To explore the potential co-transcriptional regulation of the exon skipping events *in vivo*, I focused on the FD model and I performed on liver and brain tissues chromatin immunoprecipitation-qPCR experiments (ChIP-qPCR) of Pol II and chromatin marks (H3K4me3, H3K9me3, H3K27me3 and H3K36me3). The analysis was performed on three genomic Elp1 regions corresponding to constitutive exons (exons 10 and 29) and the alternative exon 20. The results showed in both tissues and for all genomic regions an age-dependent decrease in Pol II density profile and a robust increase (approximately 3-fold in liver and 20-fold in brain) of the repressive H3K27me3 mark. Interestingly, the H3K27me3 increased also globally in these tissues. To clarify the role of Pol II and histone modifications on Elp1 splicing regulation, I performed minigene experiments evaluating Pol II mutants with different elongation rate and chemicals that modify the chromatin structure (EED-226 and Valproic Acid) or affect

the Pol II elongation (Camptothecin and DRB). The result I have obtained indicate that a more relaxed chromatin results in exon 20 inclusion while a more compact chromatin or a slow Pol II induce exon 20 skipping. These treatments specifically affect the defective exon 20 with no changes on splicing of minigene or endogenous constitutive exons. Interestingly, EED-226, a drug the specifically targets the repressive H3K27me3 mark induced exon 20 inclusion. These data suggest a co-transcriptional model of Elp1 exon 20 regulation in which an age-dependent increase in the repressive mark H3K27me3 will negatively affect the rate of Pol II elongation along the entire Elp1 gene. This will have a specific effect on the processing of defective exon 20 by inducing its skipping but will spare the other constitutive exons.

RIASSUNTO

L'Atrofia Muscolare Spinale (SMA) e la Disautonomia Familiare (FD) sono due malattie paradigmatiche di origine genetica associate a un difetto di inclusione dell'esone. In entrambi i casi, la severità del salto dell'esone (exon skipping) è direttamente in relazione con la severità della malattia a livello tessutale e fenotipico ed il trattamento del difetto di splicing è terapeutico. In comune con lo splicing fisiologico, i difetti di exon skipping potrebbero essere regolati co-trascrizionalmente dal tasso di elongazione della RNA Polimerasi II (Pol II) e/o dalle modificazioni istoniche della cromatina. In aggiunta, programmi genetici dipendenti dall'età che includono anche una regolazione co-trascrizionale non solo possono modificare lo splicing a livello globale, ma potenzialmente interessare lo splicing aberrante dovuto a mutazioni che causano malattia. In questa tesi, ho valutato i cambi nel tempo di due eventi di splicing difettivi in topi asintomatici SMA (Smn2 esone 7) e FD (Elp1 esone 20) e studiato nel dettaglio la relazione tra modificazioni della cromatina e cambi di splicing nel topo FD e in modelli cellulari. La comparazione dei pattern di splicing a 10, 90 e 365 giorni post-nascita (PND or P) ha mostrato cambi di splicing specifici nello skipping dell'esone per ciascun gene. In muscolo, fegato, polmone e rene, l'inclusione dell'esone 7 del gene Smn2 ha mostrato un incremento dipendente dall'età, soprattutto durante lo sviluppo post-natale. Nel sistema nervoso centrale (CNS), l'inclusione dell'esone 7 è diminuita entro i 3 mesi di età per poi ritornare al livello basale a P365 mentre nessun cambio è stato osservato nel cuore. Nel topo FD, l'inclusione dell'esone 20 del gene Elp1 è ridotta nel CNS, fegato, muscolo e polmone tra P10 e P90, rimanendo bassa all'anno di vita: nessun cambio è stato visto in altri organi. Per esplorare la potenziale regolazione co-trascrizionale degli eventi di exon skipping *in vivo,* mi sono focalizzato sul modello FD e ho effettuato su fegato e cervello l'immunoprecipitazione della cromatina seguita da PCR quantitativa (ChIP-qPCR) verso la Pol II e alcune modificazioni della cromatina (H3K4me3, H3K9me3, H3K27me3 and H3K36me3). Questa analisi è stata fatta su tre regioni genomiche del gene Elp1 corrispondenti a esoni costitutivi (esone 10 e 29) e l'esone alternativo 20. I risultati mostrano che in entrambi i tessuti e su tutte le regioni genomiche avviene un calo nel profilo di densità della Pol II dipendente dall'età ed un robusto incremento (circa 3 volte nel fegato e 20 volte nel cervello) della modificazione repressiva H3K27me3. Interessante notare il fatto che il livello di H3K27me3 aumenta

globalmente in entrambi i tessuti. Per chiarire il ruolo della Pol II e delle modificazioni istoniche nella regolazione dello splicing di Elp1, ho effettuato esperimenti sul minigene valutando l'effetto di mutanti di Pol II con diversi tassi di elongazione della Pol II e composti che modificano la struttura della cromatina (EED-226 e Acido Valproico) o che interessano l'elongazione della Pol II (Camptotecina e DRB). I risultati da me ottenuti indicano che uno stato più rilassato della cromatina risulta nell'inclusione dell'esone 20 mentre una struttura della cromatina più compatta o una Pol II lenta inducono skipping dell'esone 20. Questi trattamenti interessano in maniera specifica questo esone e non indicano cambi nello splicing di esoni costitutivi né sul minigene né su geni endogeni. Interessante il fatto che EED-226, un composto che specificatamente ha come target la modificazione repressiva H3K27me3, induce inclusione dell'esone 20. Questi dati suggeriscono un modello co-trascrizionale di regolazione dell'esone 20 del gene Elp1 in cui un incremento della modificazione repressiva H3K27me3 dovuto al tempo ha un impatto negativo sul tasso di elongazione della Pol II lungo l'intero gene. Questo ha un effetto specifico sul processamento dell'esone 20 inducendo il suo skipping ma non interessa lo splicing di altri esoni costitutivi.

CONTENTS

Abbreviations

The standard abbreviations used in this thesis follow IUPAC rules. The abbreviations are explained also in the text when they are used for the first time.

A	Adenine
AS	Alternative splicing
ATP	Adenosine tri-phosphate
BAC	Bacterial artificial chromosome
BBP	Branch point binding protein
bp	Base pair
BP	Branch point
C	Cytosine
CBC	Cap binding complex
cDNA	complementary DNA
CHD	Chromodomain
CPSF	Cleavage and polyadenylation specificity factor
CPT	Camptothecin
CRC	Chromatin remodelling complexes
CS	Constitutive splicing
CTD	C-terminal domain
DAB1	Disabled homologue 1
DSB	Double strand brake
DRB	5,6-Dichloro-1-β-D-ribofuranosylbenzimidazole
Elp1	Elongator acetyltransferase complex 1 gene
ESE	Exonic splicing enhancer
ESPR2	Epithelial splicing regulatory protein 2
ESS	Exonic splicing silencer
FD	Familial dysautonomia
FGFR2	Fibroblast growth factor receptor 2
FUS	Fused in sarcoma
G	Guanine
H1	Histone 1
H2A	Histone 2A
H2A.Z	Histone 2A.Z
H2B	Histone 2B
H3	Histone 3

H4	Histone H4
hnRNP	heterogeneous ribonuclear protein
hnRNP A1	heterogeneous ribonuclear protein A1
Ikbkap	Inhibitor of κ light polypeptide gene enhancer in B-cells, kinase complex-associated protein gene
ILS	Intron lariat intermediate
INO80	INO80 Complex ATPase Subunit
ISE	Intronic splicing enhancer
ISS	Intronic splicing silencer
ISWI	Imitation SWItch
K	Lysine
kDa	Kilodalton
LB	Luria-Bertani medium
M	Adenine or cytosine
m^7G	7-methylguanosine
me3	Tri-methylation
MRG15	MORF4-related gene on chromosome 15
mRNA	messenger RNA
N	Nucleotide (A,G,C, or T)
ncRNA	non-coding RNA
NMD	Non-sense mediated RNA decay
ng	nanograms
NOVA2	Neuro-oncological ventral antigen 2
nt	nucleotide
NTD	N-terminal domain
P (or PND)	Post-natal day
P	Proline
PABP	Poly(A)-binding protein
PAP	PolyA polymerase
PCR	Polymerase chain reaction
PPT (or $Y_{n)}$	Polypyrimidine tract
PTB	Polypyrimidine tract binding protein
pre-mRNA	precursor messenger RNA
pre-snRNA	precursor small nuclear RNA
Pol I	RNA Polymerase I
Pol II	RNA Polymerase II
Pol III	RNA Polymerase III
PSE	Proximal sequence element

PTM	Post-translational modification
R	Purine (A or G)
RBD	RNA binding domain
RBFOX3	RNA Binding Fox-1 Homolog 3
RBM24	RNA Binding Motif Protein 24
RBM20	RNA Binding Motif Protein 20
RBM38	RNA Binding Motif Protein 38
RBP1	RNA Polymerase II Subunit A
RBP2	RNA Polymerase II Subunit B
RNA	Ribonucleic acid
RNP	Ribonuclearprotein
RRM	RNA recognition motif
RS	Arginine/serine dipeptide-rich motif
qRT-PCR	Quantitative reverse transcriptase PCR
S	Serine
SAM68	SRC associated in mitosis of 68 kDa
SFPQ	Splicing Factor Proline And Glutamine Rich
Sm	Smith protein
SMA	Spinal muscular atrophy
Smn	Survival motor neuron protein gene
SMN	Survival motor neuron protein
Smn1	Survival motor neuron protein 1
Smn2	Survival motor neuron protein 2
SNAPc	small nuclear RNA activating complex polypeptide 1
snRNA	small nuclear RNA
snRNP	small nuclear ribonuclearprotein particles
SR	Serine/arginine rich protein
SRE	Splicing regulatory element
SRSF1	Serine/arginine-rich splicing factor 1
SRSF2	Serine/arginine-rich splicing factor 2
SRSF3	Serine/arginine-rich splicing factor 3
SRSF9	Serine/arginine-rich splicing factor 9
ss	Splice site
SWI/SNF	SWItch/Sucrose Non-Fermentable
T	Threonine
TSS	Transcription start site

U	Uracyl
U2AF	U2 snRNP auxiliary factor
U snRNA	Uridine-rich small nuclear RNA
U snRNP	Uridine-rich small nuclear ribonucleoparticle
VPA	Valproic acid
WT/wt	Wild-type
Y	Pyrimidine (C or T)
Y	Tyrosine

List of figures

Chapter 1

Chapter 3

Chapter 4

List of tables

Chapter 1 – Introduction

1.1 The process of gene expression: where it all begins

In molecular biology, the term "gene expression" refers to the process by which the information encoded in a gene is used to direct the assembly of function macromolecules. These molecular products could be either a protein (in case of coding DNA sequences) or non-coding RNA (in case of non-coding DNA sequences). A wide variety of core biological processes are under the control of gene expression, such as tissue homeostasis, organismal development and cell differentiation to cellular stress responses ad many others (Pope & Medzhitov, 2018). The process is very complex and involves several steps that must be fine regulated. Specifically, these steps in coding DNA sequences are DNA replication, transcription and RNA processing (including 5'capping, splicing and 3'poly-Adenylation) followed by translation and additional post-translational modifications. In the cell nucleus DNA molecules, upon replication, are transcribed into precursor mRNAs (pre-mRNAs) by RNA polymerase II (Pol II) and then are processed through several dynamic co- or post-transcriptional events like 5'-end capping, introns removal and exons splicing and the 3'-end processing and polyadenylation (Proudfoot et al., 2002). After these steps, mature mRNAs are ready to be exported to the cytoplasm where they will undergo translation, being used as templates for protein synthesis (Maniatis & Reed, 2002). All this must be performed correctly by different cellular machines that create a complex network of coupled interactions (Figure 1.1). Furthermore, superimposed on these pathways there is a RNA surveillance system that can act on any steps of gene expression by eliminating potential threats for the physiological state of cells, such as aberrantly processed or mutant transcripts (Maniatis & Reed, 2002).

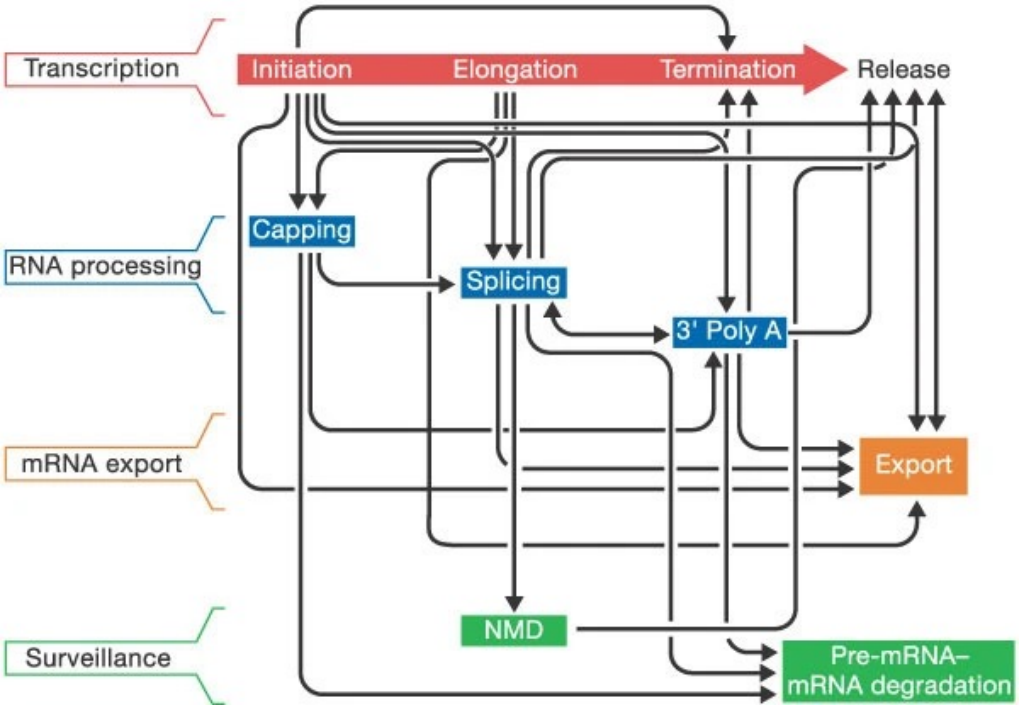

Figure 1.1: ***A complex network of coupled interactions in gene expression.***

The major steps of gene expression are indicated on the left and each stage in transcription is shown along the top in the red arrow. The black arrows indicate physical and/or functional coupling between two steps in gene expression. Adapted from (Maniatis & Reed, 2002).

1.2 Chromatin encloses the information stored in DNA

In eukaryotic cells, genetic information stored in DNA is present in the form of chromatin, a highly organized and dynamic nucleoprotein structure composed of nucleic acids, histones and "non-histone" proteins. Chromatin controls all DNA-templated processes by modulating the accessibility of DNA to nuclear factors, such as the ones implicated in transcription, splicing, DNA repair (Giono & Kornblihtt, 2020). The basic unit of chromatin is the nucleosome, which is made up of 147 bp of DNA left-handed wrapped 1.67 times around an octameric particle consisting of two copies of each core histone (H2A, H2B, H3 and H4) all assembled in a hierarchical manner (G. Li & Zhu, 2015). The primary structure of chromatin is the so-called "beads on a string" which represents a 10 -12 nm thick fiber in which single nucleosomes lie in a linear formation. These strings are then folded into a fiber-like structure of about 30 nm in diameter, further stabilized by a fifth histone, the linker histone H1, that can physically bind a region of 20 bp between the inter-nucleosomic DNA and the nucleosome. Next, 30 nm fibers can self-associate into larger 300 nm structures that are compressed and folded to produce a 250 nm wide fiber. At the end, tight coiling of these fibers produces the chromatid of a chromosome (Figure 1.2) (Even-Faitelson et al., 2016; G. Li & Zhu, 2015). Originally, chromatin has been divided into two major subtypes, according to the intensity of their staining: euchromatin and heterochromatin. Euchromatin exists in a decondensed form and is found in the distal arms of the chromosome. It is usually dispersed all around the nucleus and it is the transcriptionally active form of chromatin, replicated in early S phase. On the other hand, heterochromatin exists in a more condensed form and is usually present toward the end or pericentric region of the chromosome. It is usually replicated toward the end of the S phase and is transcriptionally inactive. Heterochromatin can be further distinguished in "constitutive" or "facultative". Constitutive heterochromatin contains few genes and is formed principally of repetitive sequences located in large regions coincident with centromeres and telomeres. Facultative heterochromatin can be defined as transcriptionally silent regions that can decondense to allow transcription depending on specific needs of the cell. Thus, its formation is regulated and it is often associated with space-temporal morphogenesis and differentiation (Morrison & Thakur, 2021; Tamaru, 2010).

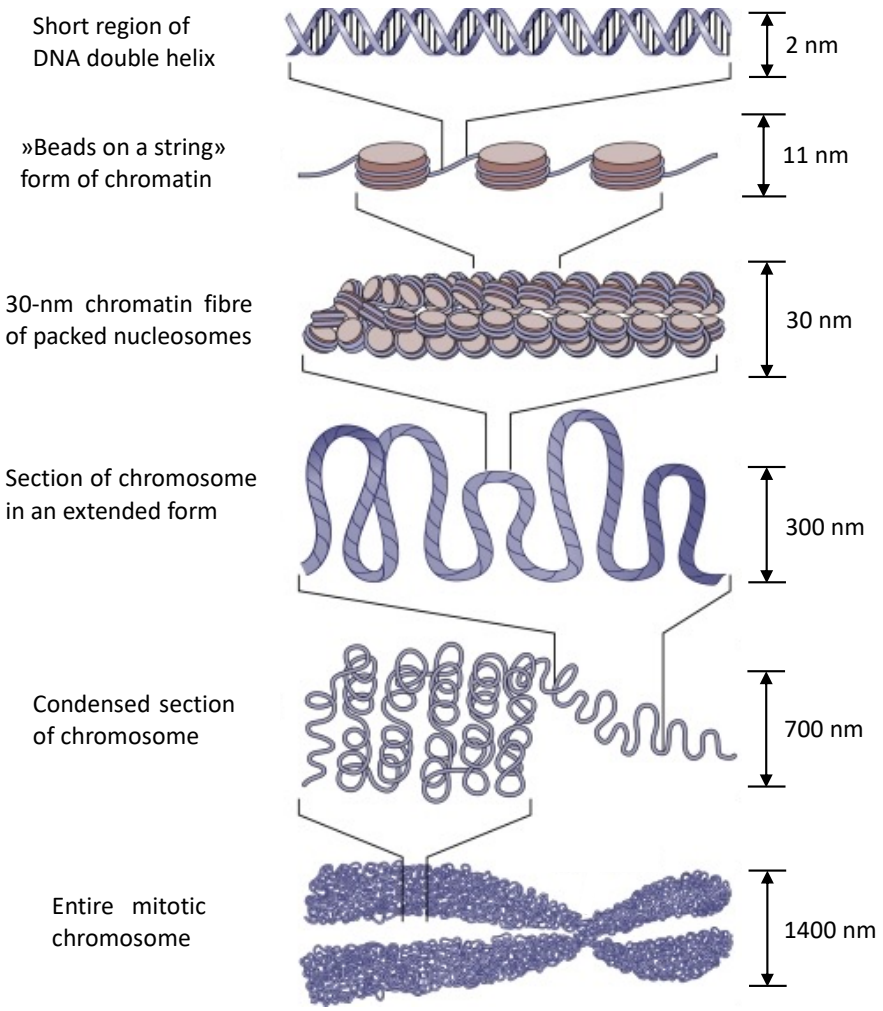

Figure 1.2: ***Chromatin structure at different levels.***

DNA is wrapped around a histone octamer to form nucleosomes, which interact with each other to form the "beads on a string" structure. This basic nucleosome structure winds on itself to form a fiber-like structure of about 30 nm that extends and folds to form loops. These loops are then condensed to form entire mitotic chromosomes. On the right dimensions of each chromatin form are indicated. Adapted from (Jansen & Verstrepen, 2011).

1.2.1 Chromatin is a finely-modified dynamic structure

Since chromatin is a highly-dynamic structure and needs to be easily accessed for basic processes like replication, transcription or DNA damage repair, eukaryotic cells have established precise methods and mechanisms to alter its structure. To make high-compacted regions more accessible to cellular machineries, cells take advantage of groups of factors known as chromatin remodeling complexes (CRCs). These factors, that can be divided in 4 categories according to properties of their ATP-ase subunit, use ATP energy to disrupt the DNA-histone interactions and modulate chromatin structure (Figure 1.3) (Magaña-Acosta & Valadez-Graham, 2020). Specifically, SWI/SNF (Switching defective/Sucrose Non-Fermenting) family members trigger chromatin access to transcription factors by spacing and ejecting nucleosomes, whereas ISWI (Imitation Switch) family facilitates nucleosome sliding during replication and histone maturation. The CHD (Chromodomain-Helicase-DNA binding) family, similarly to ISWI complex, promotes nucleosome maturation and INO80 members are involved in nucleosome editing and are responsible of the incorporation of H2A.Z variant in chromatin during double strand (DSB) break repair (Magaña-Acosta & Valadez-Graham, 2020; Sundaramoorthy & Owen-Hughes, 2020). Besides, histone chaperones, that are key proteins that function at multiple steps of nucleosome formation, guide reversible nucleosome assembling and disassembling processes to maintain chromatin dynamic and ready for use by cell's machineries (Kobayashi & Kurumizaka, 2019). Another method used to alter chromatin structure consists in the substitution of the core canonical histones with similar proteins called histone variants. Basically, they are non-allelic isoforms of conventional histones that arbore structural and functional features capable of drastically modify structure and function of chromatin (Biterge & Schneider, 2014). Furthermore, histones can be post-translational modified to regulate chromatin architecture and function and to provide binding platforms for diverse transcription factors (Venkat Ramani et al., 2021). Over the course of time, all these notions brought to the "histone code" hypothesis, stating that histone post-translational modifications (PTMs) provide an extra layer of information that cooperate in gene regulation, increasing the possibilities of the genetic code. Nowadays, the best-studied PTMs are the one that occur on histones' protruding, intrinsically disordered N-terminal "tail" domain, even though also other regions, such as the structured (globular) surface of the core particles themselves, can be modified (Morgan & Shilatifard, 2020). These modifications mainly consist of the addition of a

small chemical group (for instance in the case of acetylation, methylation and phosphorylation) or of a peptide to a specific amino acid of the histone tail (that is the case of SUMOylation or ubiquitylation), although not all of amino acid residues are prone to PTMs since they have distinct chemical properties (Figure 1.4) (Zhang et al., 2021). As expected, installing these modifications is not a passive process but it is catalyzed by a specific class of enzymes that form a complex interplay among them; the "writers" are the one involved in marks deposition, the "erasers" remove these marks, if they are reversible, and the "readers" are effectors proteins that recognized these marks, triggering a molecular response to fine-tune the control of gene transcription (Hyun et al., 2017). Nowadays, it is well known that the amino acid that is modified, the type of PTM and the other PTMs nearby determine their exact functional outcome.

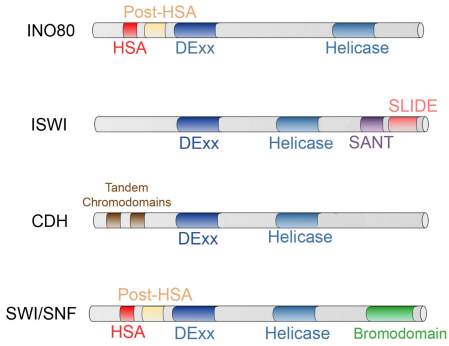

Figure 1.3: ***Main characteristics and domains of CRC families.***

HSA – helicase-SANT domain, DExx – Aspartate Glutammate helicase domain, SANT - Swi3, Ada2, N-Cor, and TFIIIB domain, SLIDE – SANT-like. Adapted from (Magaña-Acosta & Valadez-Graham, 2020).

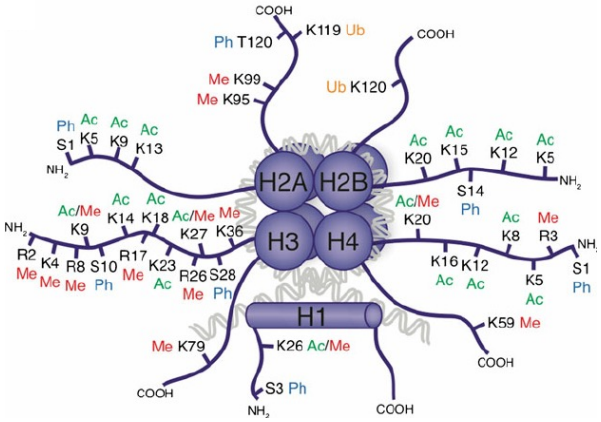

Figure 1.4: ***Histones post-translational modifications.***

Schematic representation of a nucleosome with the 4 canonical histones (H2A, H2B, H3 and H4), the linker histone H1 and DNA wrapped around the octamer. Ac – acetylation, Me – methylation, Ph – phosphorylation, Ub – ubiquitination. Adapted from (Zhao et al., 2013).

1.3 RNA Polymerase synthetizes RNA from a DNA template

RNA Polymerases (Pols) represent the core of the transcription machinery. They are large multi-protein complexes composed by several subunits with the aim of catalyze DNA-directed RNA synthesis. Eukaryotes have three types of nuclear Pols, each one responsible for the synthesis of a distinct subset of RNA classes, but it is thought that all three Pols employ similar mechanisms to start transcription (Figure 1.5) (Yokoyama, 2019);

- **RNA Polymerase I** (Pol I) is located in the nucleolus and it is implicated in the synthesis of the 47S pre-mRNA that is processed into mature 28S, 18S and 5.8S rRNA, but not 5S rRNA. Its promoters lie for most part upstream of the TSS (Khatter et al., 2017);
- Protein-coding genes, as well as most of snRNAs and miRNAs, are transcribed by **RNA Polymerase II** (Pol II), the most studied type of Pol. It consists of 12 subunits, from RBP1 to RBP12, with the two largest subunits (RBP1 and RBP2) structured opposite to each other (X. Liu et al., 2013; Schier & Taatjes, 2020). Their location allows the formation of a "cleft" in which DNA is inserted and new pre-RNA molecules are synthetized. The largest subunit of mammalian RNA Pol II (RBP1) is equipped with a unique appendage, the conserved CTD (carboxy-terminal domain), that comprises 52 tandemly repeated heptapeptides with consensus sequence YSPTSPS (Tyr-Ser-Pro-Thr-Ser-Pro-Ser) (Naftelberg et al., 2015) and it is necessary for the proper functioning of Pol II. The promoters of Pol II are composed of a core (TATA box - binding side for Transcription factor II D (TFIID)) and additional regulatory sequences (*cis*-acting elements), eg. CAAT sequence, enhancers and response elements (RE elements) (Widen et al., 1988);
- **RNA Polymerase III** (Pol III) shares the location with Pol I and transcribes 5S rRNA genes, tRNA genes and various snRNAs. All Pol III transcripts are untranslated and less than 300 bp long. It uses three types of promoters, two of them are downstream from the TSS and a third one upstream from the TSS, composed by TATA box, DSE and PSE (Khatter et al., 2017; Ramsay et al., 2020).

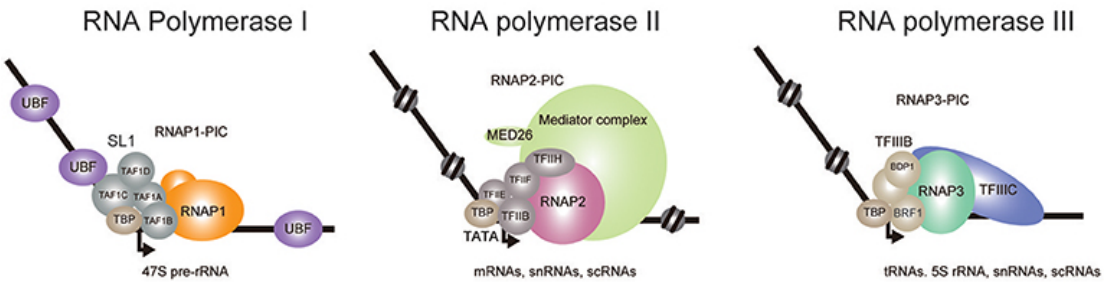

Figure 1.5: ***Transcriptional initiation complexes of eukaryotic RNA Pols.***

In all pre-initiation complexes, the universal role of TBP is to bend template DNA, while TAF1B, TAFIIB and BRF1 proteins recruit corresponding Pols to the promoter, respectively. Adapted from (Yokoyama, 2019).

1.4 pre-mRNA processing events

1.4.1 Capping the 5’ end of mRNA

During the early stage of Pol II transcription, all mRNAs have a cap-structure at their 5'-end added co-transcriptionally to the pre-mRNA. This cap consists of 7 methyl-guanosine (m7G) linked to the 5’end of the nascent pre-mRNA via a 5′-5′ triphosphate linkage. The m7G cap performs multiple functions including nucleus-cytoplasmic transport and the formation of an assembly platform to facilitate translation (Jiao et al., 2017) and its formation involves three sequential enzymatic steps: first, the 5′ triphosphate end of the pre-mRNA is hydrolysed to a diphosphate by RNA 5′ triphosphatase (RTPase); second, the diphosphate RNA is capped with GMP by RNA guanylyltransferase (GTase) and third, the GpppRNA cap is converted to m7GpppRNA by AdoMet:RNA(guanine-N7)-methyltransferase (MTase) (Shuman & Schwer, 1995) (Figure 1.6 A).

1.4.2 polyA-tail addition to the mRNA 3’ end

Beside the 5’-capping, eukaryotic mRNAs are post-transcriptionally modified also at their 3’end by the addition of a poly Adenosines (poly(A)) tail. Poly(A) tails are generated in the nucleus in a two-step reaction that involves the cleavage of the nascent transcript and subsequent polyadenylation of the upstream RNA fragment. Once the mature mRNA is shuttled to the cytoplasm, poly(A) tail helps to stabilize the transcript and increases the efficiency of translation initiation (Calado & Carmo-Fonseca, 2000). The formation of poly(A) tails in the nucleus involves different *trans*-acting factors that include Cleavage and Polyadenylation Specificity Factor (CPSF), Cleavage stimulation Factor (CstF) and poly(A) polymerase (PAP) and poly(A)-binding protein (PABP) (Calado & Carmo-Fonseca, 2000). In the first step of the reaction, CPSF promotes the cleavage at a 5’-CA-3’ dinucleotide that is located 10-35 bases downstream from its binding site. The site of cleavage is known as poly(A) site (PAS) and it is defined by surrounding sequence motifs, such as A[A/U]UAAA hexamers (Clerici et al., 2018). The second step of the reaction occurs after the cleavage and it involves the PAP enzyme that is able to add 200/250 adenine residues to form a poly(A) tail. During this process, PABP-2 binds the nascent poly(A) tail with high affinity and it has three main functions: stabilization, protection against exonucleases digestion and interaction with the nuclear export machinery in order to transport spliced mRNA to

the cytoplasm (Calado & Carmo-Fonseca, 2000) (Figure 1.6 B). Transcription factors and the C-terminal domain (CTD) of Pol II are interacting with the 3′-end processing to help in the control of initiation of the transcription. Essential for transcriptional termination is the proper poly(A) signal. Any alterations in these processes lead to improper polyadenylation and mRNA degradation.

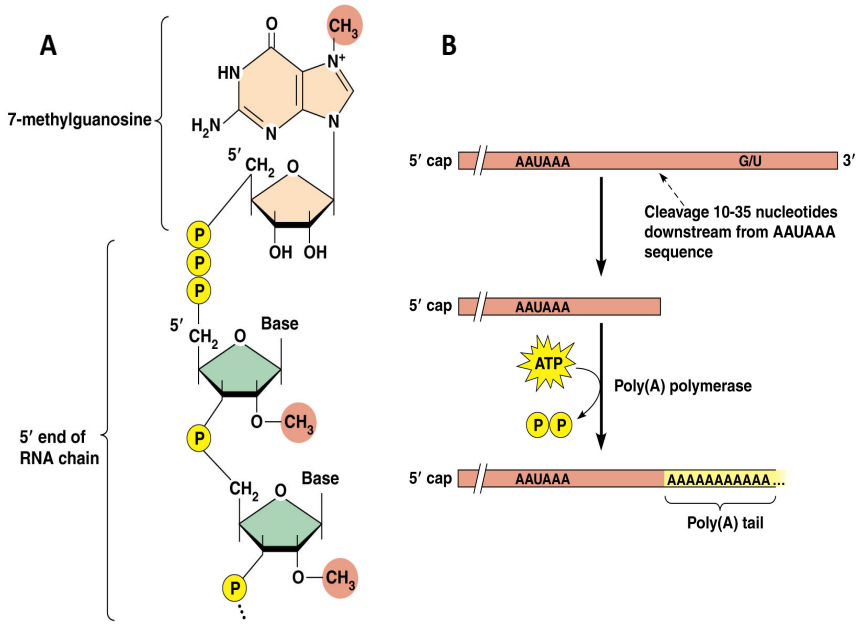

Figure 1.6: ***5'-end capping and 3'-end polyadenylation processes.***

A) Schematic representation of a bond between the 7-methylguanosine and 5' end of primary transcript. **B**) Endonucleolytic cleavage between the AAUAAA sequence and the downstream element generates an upstream fragment terminating with 3P-OH and a downstream fragment starting with 5P-phosphate. The upstream fragment is polyadenylated, the downstream fragment is degraded. Adapted from Pearson Education Inc.

1.5 pre-mRNA splicing reaction is simple and affects eukaryotic genes

Eukaryotic genes are discontinuous because they are transcribed as pre-mRNAs containing non-coding sequences (introns) as well as expressed sequences (exons) (Lee & Rio, 2015). Splicing process is a co- or post-transcriptional event that takes place in the nucleus and allows introns to be snipped out from the pre-mRNA and exons to be stitched back together to produce mature mRNA (Matera & Wang, 2014b; Will & Luhrmann, 2011). From a chemical point of view, the reaction itself is quite simple and to be carried out needs a multiprotein complex called "spliceosome" that requires a large quantity of ATP (Matera & Wang, 2014b). Whereas some exons are constitutively spliced and present in every mRNAs produced from a given pre-mRNA, human genes typically have multiple introns/exons and it has been estimated that at least 90% of them undergo alternative splicing (AS). Because of this event, a large number of mRNA transcripts can be generated from a single gene, increasing proteome diversity (Lee & Rio, 2015). The splicing machinery recognizes exons and introns by using multiple signals, which presumably results in a network of interactions across exons and/or introns. In general, to initiate the splicing reaction very conserved motifs are necessary: the GU dinucleotide at the 5' splice site (5'ss) and the AG dinucleotide at the 3' splice sites (3'ss) located downstream and upstream, respectively, of the exon–intron junctions; the A residue at the branch site (BS) and the polypyrimidine tract (PPT) that are situated upstream of the 3'ss (Herzel et al., 2017; Keren et al., 2010b). Pre-mRNA splicing is a two-step transesterification reaction: the first step is a hydrophilic attack in which the 2'-hydroxyl group of the A residue at BP attacks the phosphodiester bond at the 5'ss, leading to the cleavage of the 5'-exon from the intron and the concerted ligation of the intron 5'-end to the BP 2'-hydroxyl group in a lariat form. Two reaction intermediates are then produced, a detached 5'-exon 1 and an intron-3' exon 2 fragment in a lariat configuration. A rearrangement of spliceosomal components must happen to allow the second transesterification reaction (Figure 1.7) (Herzel et al., 2017). The second step occurs when the 3'-hydroxyl from the detached exon is acting on the phosphate at 3'-end of the intron (Cech 1986, Moore and Sharp 1993). This step results in the ligation of two exons via a phosphodiester bond and the release of the intron in the form of a lariat. This lariat formation is debranched to give a linear intron. Afterwards, intron RNA will be degraded in the nucleus, while snRNPs will be recycled (Ramanouskaya & Grinev, 2017).

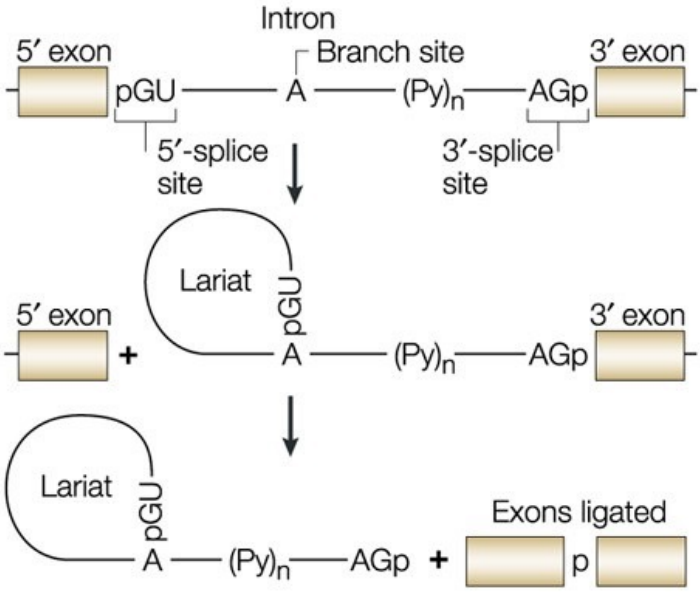

Figure 1.7: ***Splicing occurs in two transesterification reactions.***

Boxes represent exons and solid line represent intron sequences. The consensus sequences found at the mammalian 5', 3' splice sites and branch site are indicated. N = any base, Y = C, T or U and R = A or G. The asterisk marks the adenosine of the branch site and the polypyrimidine tract is indicated by Yn. The nucleophilic attacks on the splice sites by the 2'- OH of the branch site adenosine (step 1) and of the 3′-OH of the cleaved 5′ exon (step 2) are depicted by dashed arrows. Adapted from (Pagani & Baralle, 2004b).

1.5.1 The Spliceosome: the protagonist of the splicing reaction

As aforementioned, the two-step reaction is catalyzed by a complex macromolecular machine known as the spliceosome, which comprises five Uridine-rich small nuclear RNA molecules (UsnRNAs) and approximately 70 proteins in the yeast *Saccharomyces cerevisiae* and over 200 in humans (Wilkinson et al., 2020). Two types of spliceosomes coexist in most eukaryotes: the U2-dependent (or major) spliceosome catalyses the removal of U2-type introns, while the U12-dependent (or minor) spliceosome splices the rare U12-type class of introns, present in only a subset of eukaryotes (Matera & Wang, 2014b; Will & Luhrmann, 2011). The major and the minor spliceosomes employ functionally analogous but structurally distinct snRNAs to facilitate recognition of different splice sites, albeit the principles of the two-step splicing reaction are essentially the same (Kavalecz et al., 2019). In more detail, the U2-dependent spliceosome is assembled from the U1, U2, U4, U5 and U6 small nuclear ribonuclear protein (UsnRNPs) and numerous non-snRNP proteins, whereas the main subunits of the minor spliceosome are the U11, U12, U4atac/U6atac and U5, the latter shared between the two spliceosomes (Pessa et al., 2006). Because of its complexity,

during the splicing process this molecular machine undergoes numerous structural and compositional rearrangements that lead to the formation of its active site in a stepwise manner. For this purpose, divalent cations, such as $Mg^{2+,}$ participate either directly in the catalytic reactions or help to maintain the active RNA conformation (Kastner et al., 2019) and ATPases and/or RNA helicases mainly trigger RNA–RNA and RNA–protein rearrangements. In addition, spliceosome assembly is a cyclic process in which all the snRNPs, once fulfilled their role, are detached from the complex for a successive reuse (Lee & Rio, 2015; Matera & Wang, 2014b; Will & Luhrmann, 2011). The assembly of the spliceosome starts when the U1 snRNP interacts with the pre-mRNA via base-pairing between its 5′ RNA tail and the consensus sequence at the 5′ ss, forming the early (E) complex (Figure 1.8). Since this interaction is fairly weak, other factors such as U1-70K and Cap-Binding Complex (CBC) help its stabilization (Matera & Wang, 2014a). A second important event that occurs during the E complex formation is the stable interaction between the U2 snRNP and the BS, resulting in the A complex formation. This complex is then reinforced by the U2AF65/35 heterodimer, which binds the PPT, and by SF3a and SF3b proteins in order to form the U2-associated heteromeric protein complex. It contacts the intron from 6 to 26 nucleotides upstream of the BS-A (the so-called anchoring site) (Kastner et al., 2019). After that, there is the formation of the pre-B complex that occurs via the recruitment of the U4/U6-U5 preassembled tri-snRNP in an ATP-dependent way, even if this new subunit is not yet stably bound and for this reason this complex is still catalytically inactive (Boesler et al., 2016). Subsequently, with the formation of a short duplex (U2/U6 helix II) between the 5'end of the U2 snRNA and 3' end of the U6 snRNA, there is an initial docking of the tri-snRNP and, thanks to the action of a specific helicase, there is the formation of a stable tri-snRNP interaction. For the generation of the B-act complex is necessary the displacement of U4snRNP and the integration of numerous proteins. The action of a second RNA helicase transforms B-act into a catalytically competent B∗ complex, which catalyses step I of splicing (branching), yields in the C-complex and contains the cleaved 5′ exon and the intron lariat-3′ exon. The latter complex is then remodelled for the generation of the C∗ complex that performs the second catalytic step (exon ligation) followed by the creation of the P (post-splicing) complex (Horowitz, 2012). After that, there is the action of a third helicase that catalysed the reaction that causes the release of the mRNA and the generation of the intron lariat spliceosome (ILS). Finally, the ILS is disassembled by PRP43 helicase and the U2, U5, and U6 snRNPs,

that are released, are recycled for additional rounds of splicing (Kastner et al., 2019; Will & Luhrmann, 2011).

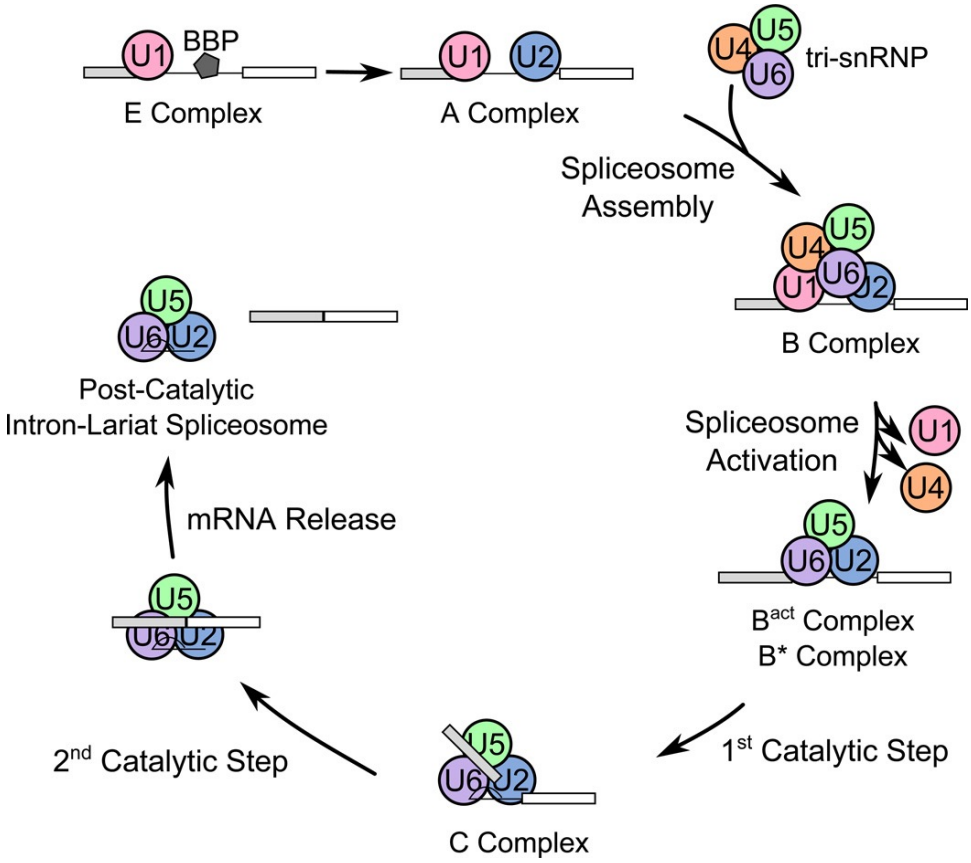

Figure 1.8: ***Spliceosomal assembly cycle and structures of spliceosomal complexes in the cycle.***

U small nuclear ribonucleoproteins (snRNPs) assemble onto a precursor-mRNA (pre-mRNA) transcript and catalyze two transesterification reactions, which result in the splicing of two exons and the release of an intron in the form of a lariat-like structure. Adapted from (Mayerle & Guthrie, 2017).

1.5.2 Exon-definition vs Intron-definition architecture

Two of the main functions of the spliceosomal snRNPs are the recognition and interaction with specific sites at the exon/intron boundaries and the triggering of an efficient splicing reaction. There is ample evidence that exons and introns have not the same length among organisms: vertebrate genes are characterized by short exons separated by considerably longer introns while lower eukaryote genes consists of large exons juxtaposed by small introns (Sakharkar et al., 2005). Interestingly, the size of exons/introns influence the splice sites recognition through sterical hindrance. Nowadays it is known that a minimal distance between splice sites is required to prevent steric blocking of the factors that recognize splice sites bordering an exon.

Indeed, *in vitro* studies led to the proposal of two models based on genome architecture (Figure 1.9): in the first one, called "Intron definition" model, if an intron does not exceed 200–250 nts, the spliceosome assembles across it (splice sites are initially paired across intron). On the other hand, the "Exon definition" model supports the idea that if the intron length exceed 200–250 nts, splicing complexes form across the exon. In human beings, since the vast majority of the exons are shorter than the introns, it is likely that most of the human splice sites are recognized across the exon (De Conti et al., 2013; Will & Luhrmann, 2011).

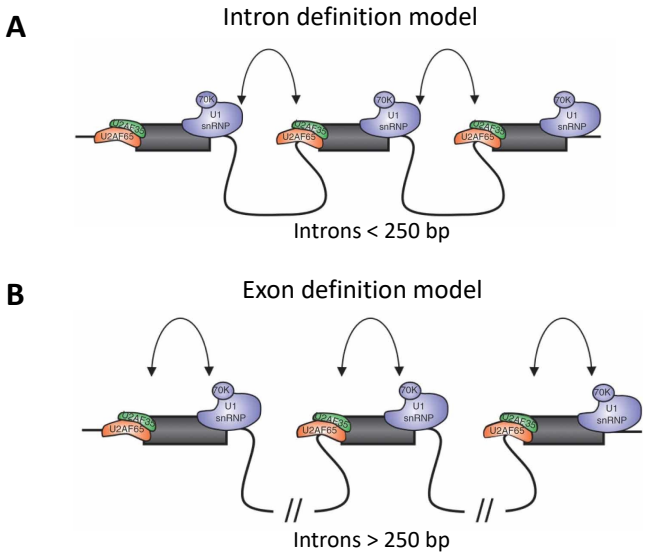

Figure 1.9: ***Intron and Exon definition models.***

A) Schematic representation of the Intron definition model according to which pairing between the splice sites takes place across an intron when long exons are separated by short (<250 bp) introns. **B**) Schematic representation of the Exon definition model where the splice site communication occurs across exons when they are separated by long (>250 bp) introns. Adapted from (De Conti et al., 2013).

1.5.3 Canonical *cis*-acting elements are needed for a correct splicing reaction

Short consensus sequences surrounding the exon/intron boundaries on the pre-mRNA, which are known in literature as 5' (or donor site) and 3' (or acceptor site) are required to proper exon/intron splice site identification (Figure 1.10) (Anna & Monika, 2018). The 5'ss is located at the 5' end of an intron and marks the exon/intron junction. Its consensus sequence consists of 9 partially conserved nucleotides belonging to MAG|GURAGU sequence (M: A or C; R: A or G; |: the exon/intron boundary), located on both sides of the exon/intron boundary and covering from position -3 to +6 (Hoskins & Moore, 2012). The core of the consensus sequence is the GU dinucleotide in position

+1 and +2 since it is almost universally conserved as it is found in more of 98% of human donor splice site. Therefore, mutations affecting the GU dinucleotide often perturb the binding of the U1snRNA and lead to aberrant RNA processing events that result in splicing defects (Langford et al., 1984). The 3'ss defines the border of an intron and its consensus sequence is YAG|G (Y: C or T; |: the exon/intron boundary). In this case, the most conserved nucleotides are the AG since they are necessary for the second splicing transesterification reaction (Roscigno et al., 1993). The branch point site is a highly degenerate sequence defined by the YNYURAC motif (Y: C or T; R: A or G; N: nucleotide) and its relevance relies on the first step of transesterifications reactions because the A provides the nucleophile for 5'ss cleavage and becomes the site of lariat formation (Figure 1.10) (Hoskins & Moore, 2012). In higher eukaryotes, this sequence is located 18-40 nucleotides upstream from the 3'ss and it is followed by the PPT, a sequence that is located between the BS and the AG of the intron/exon junction and it is composed of a stretch of pyrimidines, uridines in particular, that have a role in promoting splicing (Matera & Wang, 2014b; Will & Luhrmann, 2011)

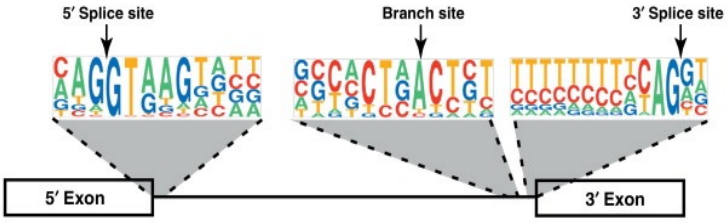

Figure 1.10: ***Schematic representation of exon-intron boundaries and consensus sequences for 5' and 3' splice sites and branch point.***

The two exons and the intron are indicated. To note that the universally conserved nucleotides are the dinucleotide cores of the 5' and 3' splice sites GU (GT on DNA) and AG, respectively, together with the branch point (A). Adapted from (Padgett, 2012).

1.5.4 Splicing Regulatory Elements are additional *cis*-acting elements in splicing

Unsurprisingly, given the high accuracy and fidelity of pre-mRNA splice-site selection *in vivo*, these few essential splicing signals are not sufficient to correctly define exon/intron junctions (Pagani & Baralle, 2004a). Indeed, early experiments in the 80s revealed the existence of exonic and intronic *cis*-acting sequences that are relatively short (usually 4–18 nucleotides) and are recognized by *trans*-acting factors, thus influencing splice-site selection. These additional elements are called Splicing Regulatory Elements (SREs) and they can be located either in exons or introns, even

far kilobases away from the 5'ss and 3'ss (Pagani & Baralle, 2004a). Based on their positions and functions, SREs have been classified as either exonic or intronic splicing enhancers and silencers (ESEs and ISEs versus ESSs and ISSs, respectively (E. Kim et al., 2008; Matera & Wang, 2014b). These elements are often conserved between different species and highly degenerate making them difficult to identify. In mammals, splicing of each gene is controlled by multiple SREs and corresponding splicing factors, whose combinatorial interactions play a pivotal role in the final splicing outcome (Figure 1.11) (Blencowe, 2006; Ramanouskaya & Grinev, 2017).

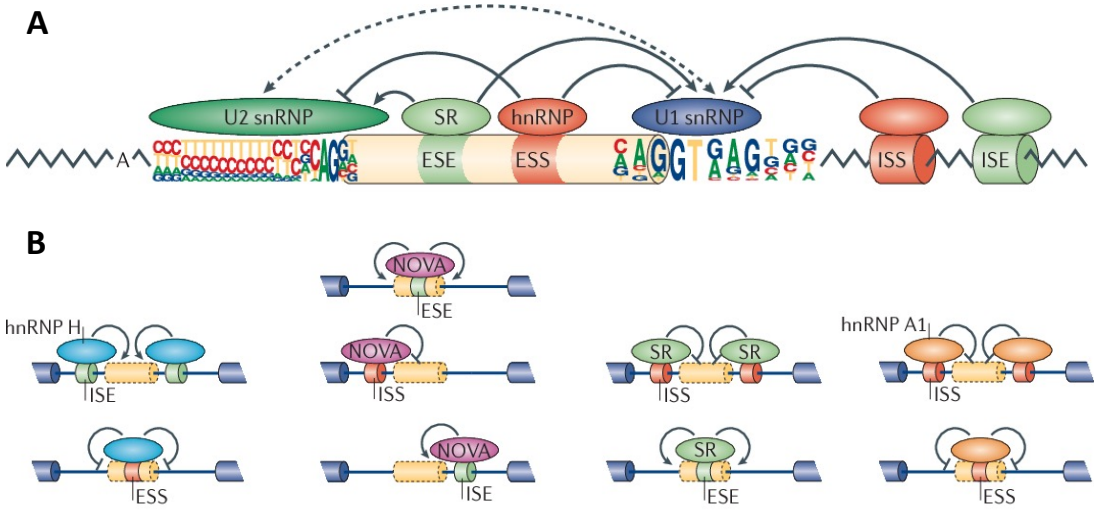

Figure 1.11: ***Auxiliary cis- and trans-acting elements in pre-mRNA splicing.***

A) Splice site choice is regulated through *cis*-acting splicing regulatory elements (SREs) and *trans*-acting splicing factors. SREs are classified as exonic splicing enhancers (ESEs), intronic splicing enhancers (ISEs), exonic splicing silencers (ESSs) or intronic splicing silencers (ISSs). These SREs specifically recruit splicing factors to promote or inhibit recognition of nearby splice sites. Common splicing factors include SR proteins, which recognize ESEs to promote splicing, as well as various heterogeneous nuclear ribonucleoproteins (hnRNPs), which typically recognize ESSs to inhibit splicing. Both often affect the function of U2 and U1 small nuclear RNPs (snRNPs). The consensus motifs of splice sites are shown in the colored pictograph, with the height of each letter representing nucleotide frequency in each position. The dashed arrow represents the formation of the exon definition complex. **B**) The activity of splicing factors and cis-acting SREs is context-dependent. Four well characterized mechanism are shown. Adapted from (Matera & Wang, 2014b).

1.5.5 The importance of being a *trans*-acting element

SREs are recognized and bound by *trans*-acting splicing factors, that are a group of RNA-binding protein (RBP) typically divided into two different categories: small nuclear ribonucleoparticles (snRNPs) and non-snRNPs splicing factors. These splicing factors, independently from their functional characteristics, share some similar

structural features such as the RRM and/or protein binding domains and usually target short sequence elements adjacent to site of regulation (Dreyfuss et al., 2002).

1.5.5.1 Small nuclear ribonucleic particles (snRNPs)

Each snRNP particle is composed of U-rich snRNA molecule (or two in the case of U4/U6), a set of seven Sm (B/B', D3, D2, D1, E, F and G) proteins and several particle-specific factors (Will & Luhrmann, 2011). The Sm proteins, that are the core of every snRNP, are important for snRNPs metabolic stability and they can interact with a conserved sequence present in U1, U2, U4 and U5 thanks to the presence of seven small polypeptides that form a ring shaped heptamer (Staněk, 2017). RNA Pol II transcribes all UsnRNAs except for U6 snRNA that is transcribed by RNA Pol III. After that, U1, U2, U4 and U5 are assembled with the core of the snRNPs in the cytoplasm and their 5' end is modified with a 2,2,7–trimethyl guanosine cap (m^3G-cap) that derives from hypermethylation of the standard 7-methyl guanosine cap. At the end, mature snRNPs are reimported to the nucleus. Concerning the U6 snRNP, there is a structural difference since the Sm proteins are replaced by Sm-like proteins (LSm) and it acquires a ɣ-monomethyl triphosphate at its 5' end remaining in the nucleus. After their biogenesis, U4 and U6 snRNAs create an intermolecular base pairing to form U4/U6 particle, which subsequently forms a tri-snRNP particle thanks to the interaction with the U5 (Pessa et al., 2006; Staněk, 2017; Will & Luhrmann, 2011).

1.5.5.2 Not - snRNPs

This group of *trans*-acting factors are involved in the regulation of general and tissue-specific splicing events. They are composed of SR (Serine-Arginine) proteins and hnRNPs (heterologous nuclear RNPs), two families of proteins that have antagonistic functions, usually promoting (SR proteins) or repressing (hnRNPs) the selection of nearby ss in a concentration dependent manner. Furthermore, they frequently interact with the U1 and U2 snRNP during spliceosomal assembly. Given that, individual exons are often controlled by multiple factors with overlapping RNA-binding specificities that function through the same element at different temporal or cellular contexts (Geuens et al., 2016; Jeong, 2017).

1.5.5.2.1 Serine-arginine rich protein family (SRs)

SR proteins (serine-arginine-rich proteins) are RNA binding proteins involved in the formation of the spliceosome. Previous studies have shown that SR proteins are also involved in other processes of RNA metabolism, from the transport of the transcript into the cytoplasm to translation. Twelve SR proteins has been identified in humans (Figure 1.12 A). From a structural point of view, SR proteins are characterized by the presence of one or two binding domains of the RNA (RRM - RNA recognition motif; RBD - RNA binding domain; RNP - ribonucleoprotein domain), located in the N-terminal and C-terminal RS-rich domains (Howard & Sanford, 2015; Sahebi et al., 2016). Serine residues in the RS domain are subject to intensive phosphorylation by several proteins and it occurs in a relatively narrow region of a serine and arginine rich domain and it is an essential modification for the functioning of the protein. In the process of pre-mRNA splicing, SR proteins function as factors involved in regulation of this process and participate in the formation of spliceosome (Sanford et al., 2005). Specifically, members of this family have a role in enhancing both constitutive and alternative splicing, mediate interactions of the spliceosome components connected to 3'ss and 5'ss in the case of CS and regulating the selection of 3'ss and 5'ss in the case of AS. Indeed, SR proteins can bound to ESEs having a direct role in the recruitment of the splicing machinery or they act antagonizing the action of nearby silencer elements (Blencowe, 2000).

1.5.5.2.2 heterogeneous Ribonucleoproteins (hnRNPs)

The hnRNP protein family is a class of several RNA-binding proteins that associate with nascent pre-mRNA allowing their maturation, export of mRNA from the nucleus to the cytoplasm and translation. Although these factors are predominantly localized in the nucleus, a subset of these proteins shuttles continuously between nucleus and cytoplasm, indicating a role in mRNA export and in other cytoplasm processes (Krecic & Swanson, 1999). These proteins are expressed in all tissues but the relative amount of different hnRNPs vary among cell types and show stage-specific expression pattern: some hnRNPs are extremely abundant while others are present in a lower amount (Kamma et al., 1995). The structure of hnRNPs consists of one or more RRMs associated with auxiliary domains (Figure 1.12 B) that have been shown mediate protein-protein interactions (Martinez-Contreras et al., 2007). The hnRNP proteins usually mediate splicing inhibition, particularly through the interaction with ISS and/or

ESS elements or by steric interference with other splicing factors (Cartegni et al., 2002), antagonizing directly or indirectly SR proteins. Nevertheless, depending on the position of the splicing regulatory elements, hnRNPs can also associate with enhancer elements to help exon inclusion (Caputi & Zahler, 2002), indicating that hnRNPs can have various roles in pre-mRNA splicing.

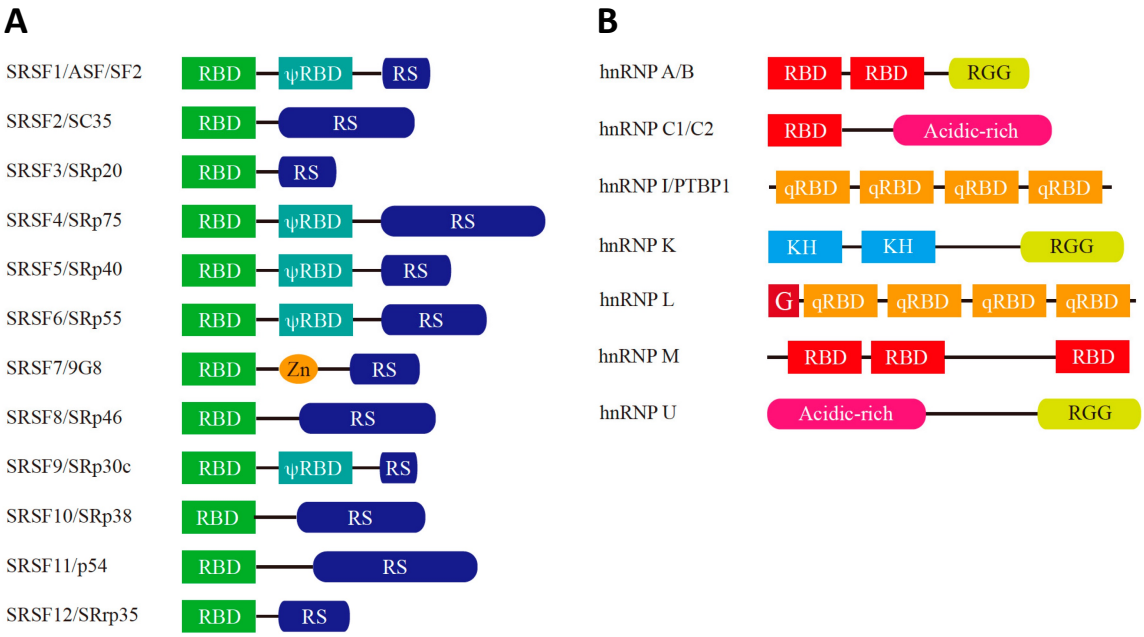

Figure 1.12: ***Molecular structure of human SR and hnRNP proteins.***

A) RBD – RNA binding domain; ψRBD – RBD homology domain; RS – serine/argine rich domain; ZnF – zinc-finger motif. **B)** RBD – RNA binding domain; RGG – arginine-glycine-glycine repeat-rich region; Acidic rich – acidic amino acid residue-rich region; qRBD – non-canonical RBD; G – glycine-rich region; KH – K homology domain. Adapted from (Nakayama & Kataoka, 2019).

1.6 Expanding the proteome diversity: alternative splicing

Alternative splicing (AS) is the process in which different sets of exons from a pre-mRNA are spliced together, leading to different mRNA isoforms starting from a single gene. Consequently, AS leads to the amplification of the number of different translated proteins increasing proteome diversity (E. Kim et al., 2008; F. E. Baralle & Giudice, 2017; Keren et al., 2010a; Ule & Blencowe, 2019). High-throughput sequencing technology revealed that > 90% of human genes undergo AS, strengthen its primary role as the major source for the phenotypic complexity in higher eukaryotes (E. Kim et al., 2008). Indeed, this process explains the discrepancy between the estimated 24,000 protein-coding genes in the human genome and the 100,000 different proteins that are supposed to be synthesized. Splicing in general, and AS in particular, are also important for regulation of spatial/temporal levels and tissue specificity of gene expression and, if disrupted, can lead to disease (F. E. Baralle & Giudice, 2017; Keren et al., 2010b). There are different types of alternative splicing events, classified into five main major subgroups (Ast, 2004; Ramanouskaya & Grinev, 2017). The first case is exon skipping, in which a type of exon is snipped out of the transcript together with its flanking introns. The second and third types are alternative 5′ ss and 3'ss choice, respectively. These types of AS events occur when two or more splice sites are recognized at one end of an exon. The fourth type is intron retention, in which an intron remains in the mature mRNA transcript. The latter one is less frequent compared to the others and consists in exons that are mutually exclusive from the mature transcripts. Besides these AS patterns, other situations can occur: the strength and/or position of promoter may play a role in the skipping or inclusion of 5' or last exon as the presence of alternatively polyadenylation signals (Keren et al., 2010b; Dvinge, 2018; Ule & Blencowe, 2019).

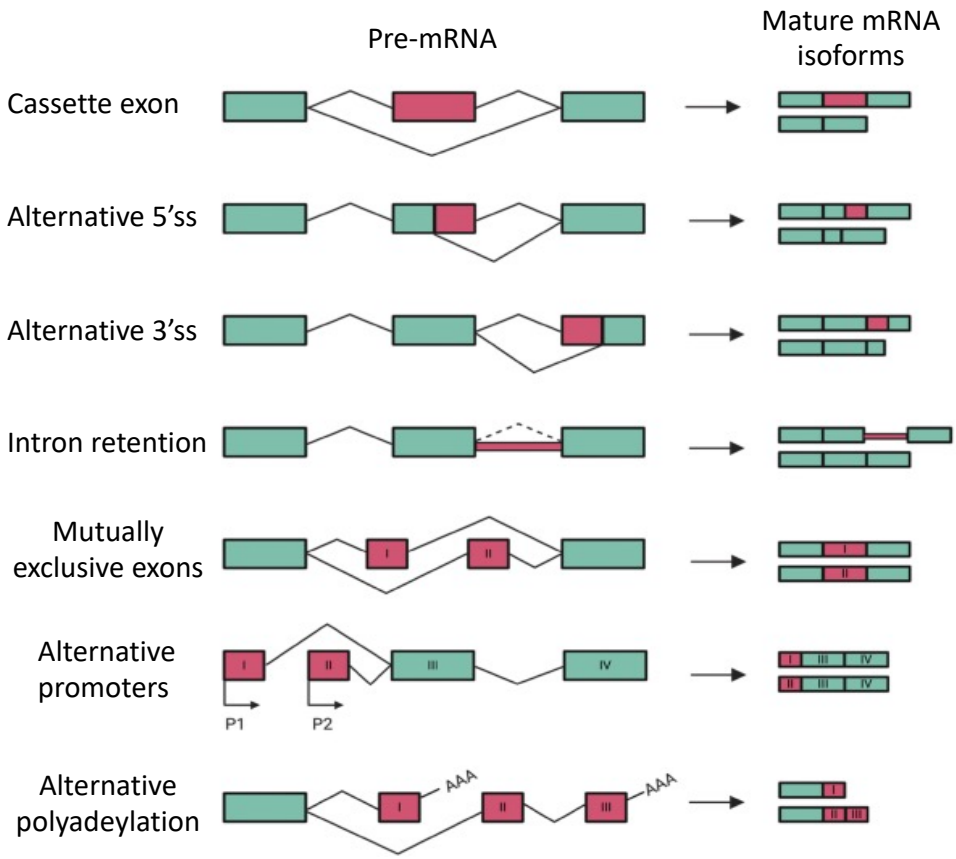

Figure 1.13: ***Schematic representation of different types of splicing events.***

Exons and mRNAs are illustrated as boxes, while introns are represented by solid lines. By alternative splicing, pre-mRNA can encode more than one mRNA isoform. Different isoforms can be generated by exon skipping/inclusion of alternative exons, the selection of alternative 5' or 3' splice sites, the retention of intron(s) or selection of the mutually exclusive exon(s). Extra mRNA isoforms can be generated through the usage of alternative promoters or polyadenylation sites. Constitutive splicing events are depicted in green, alternative splicing events in pink. The lines above and below boxes indicate the alternative splicing event. Adapted from (M et al., 2020).

1.7 An overview on aging process

Over the last decades, the term “aging” has been often redefined but it is generally regarded as a time-dependent functional decline that makes an organism frail, more susceptible to disease and with an increase probability of dying (Deschênes & Chabot, 2017; Harries et al., 2011; López-Otín et al., 2013; Mazin et al., 2013). Even though the causes responsible of aging have been extensively investigated, the full understanding of the mechanisms implicated in this process remains still fragmented. In the past years, scientists that worked in the field aimed to propose a unified theory capable to explain this phenomenon, albeit large body of research set aside this unique view making way for a newer and wider theory. According to this speculation, a network of molecular mechanisms that act in an interconnected manner, often accelerating or aggravating each other, better describes the events that characterized the aging of an organism. Similarly to the hallmarks of cancer established by Hanahan and Weinberg in 2011, Lopez-Otin and co-workers, summarizing the current knowledge about the mechanisms that are affected by aging, proposed nine hallmarks that are still considered to contribute to the aging process and determine its phenotype (Figure 1.14 A) (López-Otín et al., 2013). These include genomic instability, telomere attrition, epigenetic alterations, loss of proteostasis, deregulated nutrient sensing, mitochondrial dysfunction, cellular senescence, stem cell exhaustion, and altered intercellular communication. Besides, the co-occurrence of these hallmarks in aging, their interconnection and hierarchical categorization in primary (the ones that are the primary causes of cellular damage), antagonistic (the ones that are part of the responses to the damage) and integrative (the ones considered to be the felons of the phenotype) strengthen their functional role in the aging-associated decline (Figure 1.14 B) (López-Otín et al., 2013).

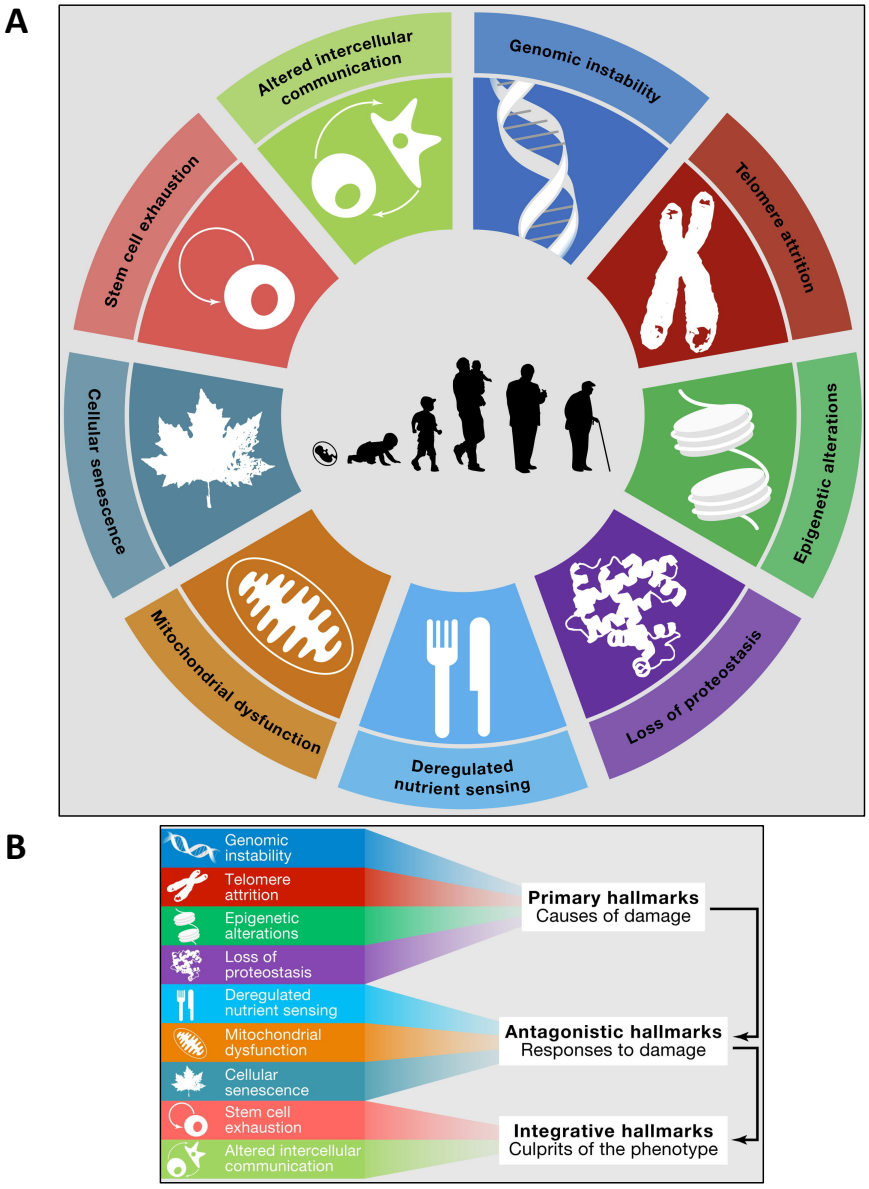

Figure 1.14: ***The nine hallmarks of aging.***

A) The hallmarks proposed by Lopez-Otin and colleagues to define the aging process: genomic instability, telomere attrition, epigenetic alterations, loss of proteostasis, deregulated nutrient sensing, mitochondrial dysfunction, cellular senescence, stem cell exhaustion, and altered intercellular communication. **B**) Functional interconnections in three categories between these hallmarks. Adapted by (Lòpez-Otin et al., 2013).

1.7.1 Gene expression and alternative splicing are subject to changes over development and aging

A growing number of studies suggests that aging is associated with a decrease in the expression of tissue-specific subsets of genes and an induction of those related to stress response and oxidative damage, resulting in a global loss of function (LoF) that occurs at cellular, tissue and organismal level. This LoF is not surprising since aging is characterized by a global functional decline that invest many aspects of gene expression, starting from alteration in the activity of transcription factors to a robust remodeling in the structure and organization of chromatin and DNA methylation along genes (Booth & Brunet, 2016; Stegeman & Weake, 2017). In this scenario, it is fair to expect that splicing process itself is also part of this massive age-related perturbation. Interestingly, only 2-3% of the whole genome shows age-associated changes either in transcript levels or splice isoform usage, with genes that are highly expressed and subject to heavily AS as particularly vulnerable to be mis-spliced with age (Figure 1.15). Splicing misregulation could have detrimental effects on cell physiology because it could lead to changes in protein isoform levels and having an impact on gene expression through NMD of those transcripts that are subject to intron retention (Stegeman & Weake, 2017). It is estimated that more than 50% of all age-associated alteration in AS are due to changes in the expression of tissue-specific splicing factors. The causes of this robust alteration may be found at the transcription level, such as in the decreased expression and modified activity of transcription factors and regulators (TFs), and at the splicing level caused by a decreased efficiency and/or stringency of the RNA splicing machinery. Related to this point, aberrant AS of transcripts encoding for SFs (but also TFs) and epigenetic changes that may perturb the activity and the expression of spliceosome components must be considered as potential players for age-related changes in AS (Deschênes & Chabot, 2017; Mazin et al., 2013; Stegeman & Weake, 2017).

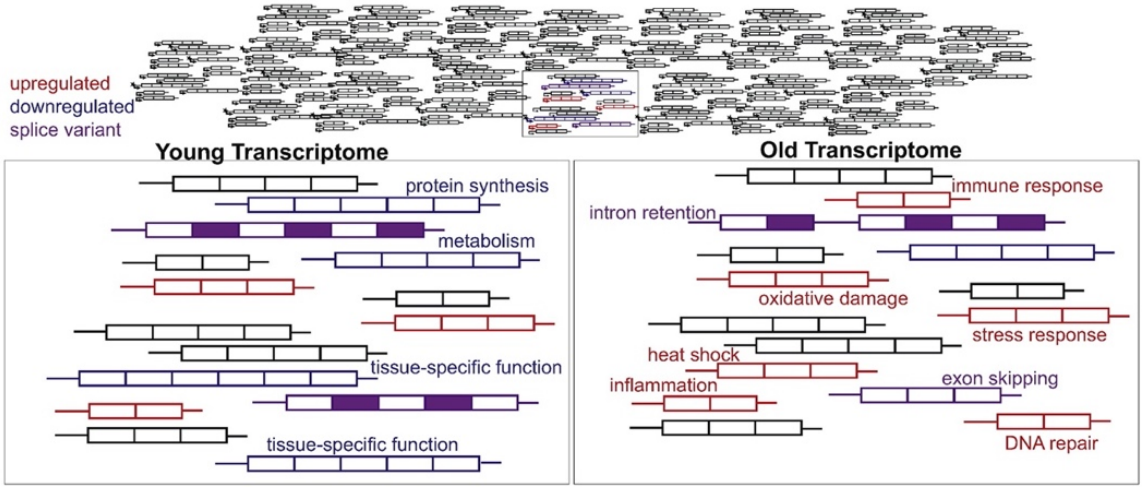

Figure 1.15: ***Transcriptome changes during aging.***

Between young and old cells, transcripts change in terms of either expression or usage of the splice isoform. Adapted from (Stegeman & Weake,2017).

1.8 Key regulators of alternative splicing coordination during development and aging

Although not present in the hallmarks of aging, alternative splicing is now established as a potent contributor in different aspects of cell physiology, from tissue-identity acquisition and maintenance to organ development. During cell differentiation and tissue development, splicing transitions happens in multiple genes at the same time and it is not surprising that these specific AS patterns are determined by a combination of parameters (F. E. Baralle & Giudice, 2017). In this scenario, RBPs play a pivotal role since their expression levels, localization and activity is finely regulated during organ development and cell differentiation. Beside the contribution of a large group of RBPs that are expressed in all tissues, such as members of SR proteins and hnRNPs, cell-type and tissue-specific RBPs expression gives the help necessary to the production of different splicing isoforms. Therefore, in the development as in every stage of cell life, the recruitment of RBPs to their target motifs on pre-mRNA is the ultimate driving factor in the determination of an AS event (F. E. Baralle & Giudice, 2017). Nevertheless, sequence elements present of pre-mRNA and RNA secondary structures together with chromatin and transcriptional machineries act, ultimately, to drive RBPs assemble to the pre-mRNA giving the opportunity to produce thousands of different AS patterns (Figure 1.16) (Ramanouskaya & Grinev, 2017). Although the developmental data regarding the role of the transcriptional machinery or epigenetic modifying-enzymes are much more limited, they all contribute to the regulation of AS, exerting a mechanistic and functional interplay with spliceosomal machinery and related factors (F. E. Baralle & Giudice, 2017; Gómez Acuña et al., 2013; Luco et al., 2011; Naftelberg et al., 2015).

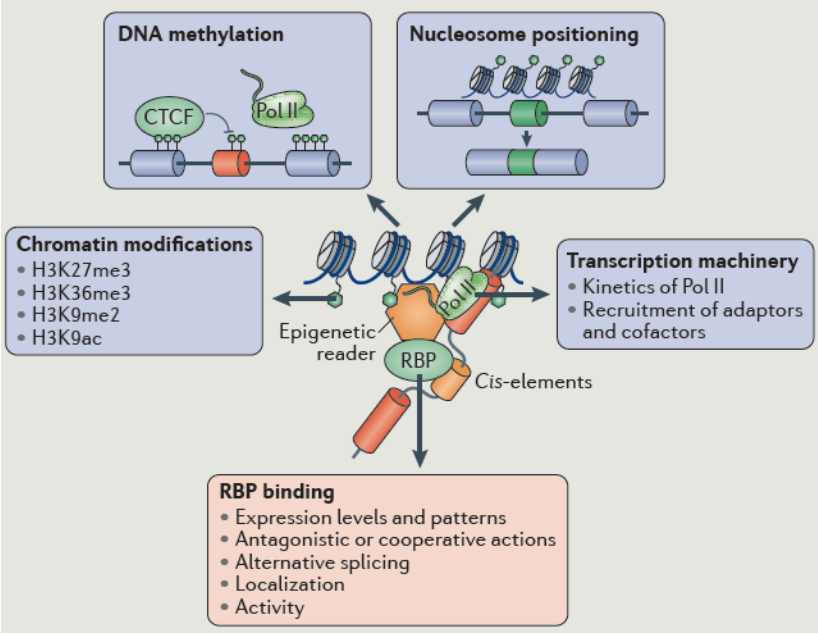

Figure 1.16: ***AS is a coordinated event during development and aging.***

Tissue- and developmental-stage specific AS patterns are determined by a combination of different molecular players: RNA secondary structures, along with RNA regulatory elements and together with the transcriptional machinery and epigenetic properties (DNA methylation and nucleosome sliding/ejecting), regulate the recruitment of RBPs to the pre-mRNA modulating the outcome of thousands of AS outcomes. Adapted from (F. E. Baralle & Giudice, 2020).

1.8.1 RNA secondary structure

RNA molecules have an innate tendency to form stable secondary and tertiary structures via Watson-Crick base pairing in order to assume the shape with the lower free enthalpy possible. *In vivo*, this phenomenon occurs co-transcriptionally and it is influenced by the presence of numerous proteins bounded on the pre-mRNA that impact its ability to fold freely (Mayer et al., 2002) (Buratti & Baralle, 2004). Alterations in RNA secondary structures represent a well-known regulatory mechanism for different cellular processes, including exon-intron definition, AS, proteins' binding to previously buried motif on RNA and others (Hiller et al., 2007b; N. Liu et al., 2015). In the splicing context, intramolecular complementarity-based pairing inside a pre-mRNA creates secondary structures which have been shown to hinder the accessibility of splicing factors to functional sequences, either splice sites or other regulatory motifs, present in the pre-mRNA by sequestering them in stems or looping them out (Hiller et al., 2007b; Ramanouskaya & Grinev, 2017). In addition, RNA secondary structures that do not involve any consensus motifs can affect the

relative distance between functional elements, for example SREs, potentially producing different spliced transcripts (Buratti & Baralle, 2004) (Hiller et al., 2007a).

1.8.2 Nucleosome positioning

The sequence of DNA bases modulates meticulously how and where DNA must be packaged around nucleosomes. Genome-wide mapping of nucleosome density revealed that they are not randomly located but their positioning is higher on internal exons compared to introns, a fact potentially related to the higher GC-content found in exons since nucleosome are preferentially positioned on GC-rich sequences. Furthermore, the stronger intensity of nucleosome occupancy in exons with weak splice sites suggested their intriguing role in the definition of the exon-intron architecture of a gene at the chromatin level (Oesterreich et al., 2011; Schwartz et al., 2009). To explain the role of nucleosome in exon recognition during co-transcriptional splicing, two alternative mechanisms were proposed: the first one assesses that nucleosome may recruit splicing factors through specific histone marks whereas in the second one, nucleosomes themselves may act as “speed bumps” to regulate RNA Pol II elongation kinetics and ultimately the fate of an alternatively spliced exon (Oesterreich et al., 2011).

1.8.3 DNA methylation

DNA methylation refers to an epigenetic modification that is used by mammalian cells to control gene expression and occurs predominantly methylating position 5 of cytosine in CpG dinucleotides. The intriguing role of DNA methylation in AS comes from several studies that showed an enrichment of methylation on exons compared to introns and that there is a difference in the methylation pattern between alternative (lower levels) and constitutive exons (Moore et al., 2013; Shukla et al., 2011).

1.8.4 Chromatin modifications

Despite RBPs and Pol II elongation rate are harshly involved in the regulation of AS, the control of ss choice seems to be far more intricated; indeed, neither the first nor the second player cited above appear sufficient to provide a solid explanation of most AS events. In this doubtful scenario, a striking finding was the discovery that histone marks were differentially distributed according to the gene architecture (for instance, some histone marks such as H3K4me3 are elevated on exons whereas others, such as

H3K9me3 are depleted). Furthermore, certain histone marks can affect AS by recruiting specific splicing factors to pre-mRNA via chromatin-binding protein, a mechanism described as "chromatin-splicing adaptor system" (Figure 1.17) (Kornblihtt et al., 2013; Luco et al., 2011). One example of this system involves the tri-methylation on lysine 36 of histone H3 (H3K36me3), a histone mark present in actively transcribed gene bodies, that influences the choice of two mutually exclusive exons (IIIb and IIIc) of mammalian *FGFR2* gene. Basically, in mesenchymal cells, H3K36me3 creates an anchoring platform for MRG15, a chromodomain protein, which in turn recruit the negative splicing factor PTB to an ISS to induce skipping of exon IIIb. Alternatively, exon IIIb is included in epithelial cells where the levels of this mark are low (Luco et al., 2010). Additionally, other examples of adaptor system regard H3K4me3 and H3K9me3, two functionally opposite marks, which recruit, respectively, a component of the U2snRNP via binding of CHD1 and hnRNP family members via binding of HP1a (Piacentini et al., 2009; Sims et al., 2007).

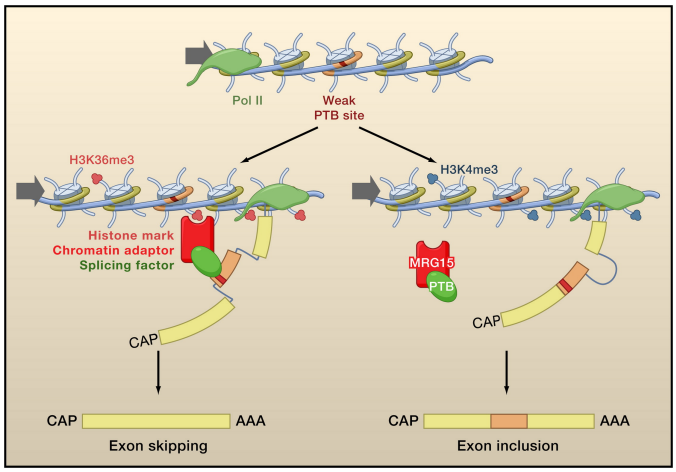

Figure 1.17: ***The chromatin-adaptor model of AS.***

Adapted from (Luco et al., 2011).

1.9 Co-transcriptional models for alternative splicing regulation

Nucleosome positioning, DNA methylation and chromatin modifications can control Pol II elongation rates which in turn impact on splicing of alternatively spliced exons. It is well established that splicing can occur co-transcriptionally, meaning that introns are excised from pre-mRNA before RNA Pol II reaches the end of the gene. Co-transcriptionality of splicing is a prerequisite to the functional coupling between splicing and transcription, in that these two processes influence each other through precise and coordinated mechanisms. Initially, it was suggested that RNA Pol II could regulate splicing through two distinct but non-mutually exclusive mechanisms, known as "recruitment model" and "kinetic model", respectively (Shukla & Oberdoerffer, 2012; Luco et al., 2011; Fong et al., 2014). The first one takes advantage of the capacity of the CTD of RNA Pol II to be phosphorylated and to recruit specific proteins and splicing factors: following to cycles of phosphorylation and dephosphorylation of the five phosphor-acceptor residues, the CTD is capable to act as a "landing pad" for the recruitment of several factors, not only implicated in splicing but also in capping and 3' end processing, that are brought to the proximities of the rising pre-mRNA to act in a specific manner on the splicing event (Figure 1.18 A) (Giono & Kornblihtt, 2020; Shukla & Oberdoerffer, 2012). An example of AS that follows this model is the EDI exon 33, which undergoes splicing thanks to SRSF3 interaction with CTD of RNA Pol II (de la Mata et al., 2003). In the second model proposed, also known as "the window of opportunity" model, the rate of RNA Pol II elongation influences AS by affecting the pace (or speed) at which splice sites and regulatory sequences emerge in the nascent pre-mRNA during transcription (Figure 1.18 B) (Luco et al., 2011; Kornblihtt et al., 2013; Gómez Acuña et al., 2013). Indeed, *in vitro* experiments suggested that a fast elongation exposes weak and strong sites that compete for the splicing decision; however, weak sites are ignored by fast RNA Pol II that favors the recruitment of the spliceosome on the strong ones, resulting in the skipping of the alternatively spliced exon. Accordingly, a slower elongation seems to push the spliceosome components to be recruited to weak sites, resulting in splicing commitment and exon inclusion. Besides these, experiments with slow and fast Pol II mutants lead to propose a novel "Goldilocks" model. This model suggests that at many splice sites, a physiological co-transcriptional AS neither requires a slowed down nor a speeded up Pol II elongation rate, but essentially only an optimal Pol II pace (Figure 1.18 C) (Fong et al., 2014).

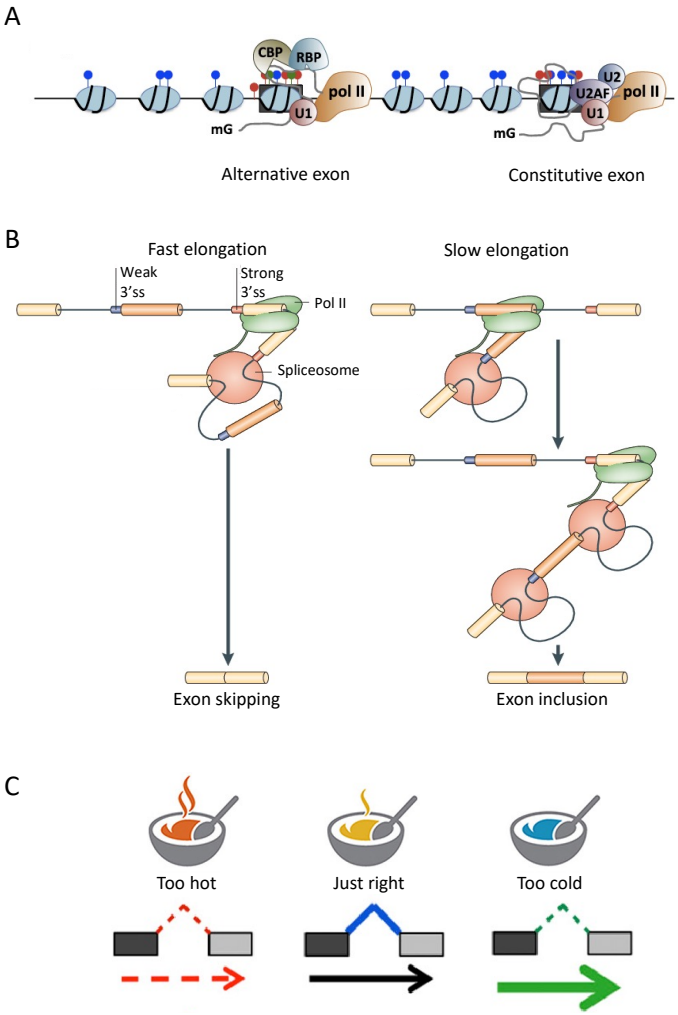

Figure 1.18: ***"Recruitment", "kinetic" and "Goldilocks" models.***

A) The "Recruitment" model proposes that the CTD domain of the largest subunit of Pol II acts as a "landing pad" that recruits different transcriptional and pre-mRNA factors (mRNA capping enzymes, splicing factors and 3'end formation and termination factors) to spatial coupling transcription and pre-mRNA processing. **B**) The "Kinetic" assesses that Pol II elongation pace determines the length of a "window of opportunity" for an upstream event to occur on the nascent pre-mRNA before it must compete with a downstream event. Basically, depending on the 3'ss strength of the AS and CS exon, fast elongation shall favor the recruitment of the spliceosome machinery to the strong 3'ss of downstream intron, resulting in exon skipping. On the other hand, a slow elongation pace shall favour the recruitment of spliceosome to the upstream intron, resulting in exon inclusion. **C**) Like in the "Goldilocks and the three bears" fairy tale in which Goldilocks prefers the porridge bowl that is neither too hot nor too cold, but at the right temperature, this model suggests that many splice sites, neither a slow nor a fast but an optimal Pol II elongation rate is required to achieve a "normal" processing outcome. Adapted from (Fong et al., 2014; Kornblihtt et al., 2013; Shukla & Oberdoerffer, 2012).

1.10 The connection between splicing mutations and disease

Sequence variations occurring in exons or introns may affect the correct processiing of the pre-mRNA in various ways, from the disruption of consensus sequences and/or SREs to the alteration of the secondary structure of the mRNA (D. Baralle & Baralle, 2005). The frequency of splicing-affecting mutations is significantly different among individual genes: it is considered that approximately 15% of pathogenic mutations causes disease through the defect that they introduce in the splicing process (D. Baralle & Buratti, 2017). Although development of fast genome-sequencing is expanding knowledge of genomic variants present in the genome, understanding which mutations are cause of molecular impairment and result in the disease is not always an easy task (Pagani & Baralle, 2004b; Ramanouskaya & Grinev, 2017). While there are a large and growing number of examples of *cis*-acting splicing mutations that cause disease, the examples of *trans*-acting splicing mutations have been relatively limited (E. Kim et al., 2008; Singh & Cooper, 2012). Pathological conditions can arise from mutations that activate cryptic splice sites, disrupt sequences necessary for RNA processing or splicing of an intronic segment, referred to as a pseudoexon, result in inclusion of additional sequence in a spliced mRNA, which causes transcript instability or specific protein isoforms (Dhir & Buratti, 2010).

1.11 Familial Dysautonomia

Familial Dysautonomia (FD), also known as Riley Day syndrome (or hereditary sensory and autonomic neuropathy type III), is a rare autosomal recessive disease resulting from poor development and progressive degeneration of the sensory and autonomic nervous systems (Norcliffe-Kaufmann et al., 2017; Slaugenhaupt et al., 2001). This disease is very common among children that descend from European Jewish (Ashkenazi), where over 99% of patients are direct descendants of a single founder individual with a point mutation in the Elp1 (Elongator Acetyltransferase Complex 1) gene. Previous studies identified three mutations causing FD even if 99.8% of patients is homozygous for a point mutation in intron 20, at position +6 of the 5'ss where T is switched to C; as a result, exon 20 is skipped in a tissue-specific manner (Hims et al., 2007; Norcliffe-Kaufmann et al., 2017). *Elp1* resides on chromosome 9q.31 and codes for ELP1 protein, which is conserved in several organisms (Slaugenhaupt et al., 2001). Although its exact function is not fully understood, in *Saccharomyces cerevisiae* yeast it is used as a scaffold for the six-subunit Elongator complex, which was observed playing a role in transcription elongation, α-tubulin acetylation, tRNA post-transcriptional modifications and intracellular trafficking (Cuajungco et al., 2003; Norcliffe-Kaufmann et al., 2017; Slaugenhaupt & Gusella, 2002). Recently, the lack of Elp1 have been also found to affect a chromatin mark (Cameron et al., 2021)

1.11.1 Molecular pathogenesis of FD

As mentioned above, almost the totality of patients are homozygous for an intronic non-coding point mutation (c.2204 +6T>C), which occurs in the splice donor site consensus of intron 20 causing aberrant skipping of exon 20 in a tissue-specific manner (Slaugenhaupt & Gusella, 2002). Specifically, the 5'ss is mutated from GTAAGT to GTAAGC sequence thus decreasing the potential number of base-pairs between the donor splice site and U1 snRNA (Figure 1.19) (Ibrahim et al., 2007). Since the mutation weakens but does not completely inactivate the 5' ss at the exon-intron boundary, all FD cells express both WT and mutant mRNA that lacks exon 20, resulting in reduced WT protein expression and a variable amount of truncated protein. Furthermore, the mutation introduces a premature termination codon and hence the Elp1 transcripts lacking exon 20 are candidate for degradation by NMD pathway (Bruun et al., 2018).

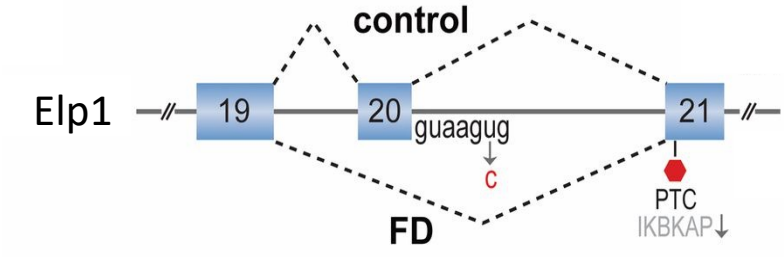

Figure 1.19: ***Graphical representation of normal and abnormal Elp1 exon 20 splicing.***

Alternative splicing path is indicated with dotted lines. IVS20+6T>C represents place of mutation in intron 20 (+6 T→C). Adapted from (Swanson, 2015).

1.11.2 Physiopathology of FD

Clinically, the loss of neuronal function the affects FD patients has many percussions on their physiology: they suffer from gastrointestinal dysmobility, afferent baroreflex failure resulting in extreme blood pressure volatility and abnormal respiratory responses to hypoxic and hypercarbic states. Other symptoms include decreased temperature and pain perception, profuse sweating and vomiting crises (Hims et al., 2007; Slaugenhaupt & Gusella, 2002). However, the most distinctive clinical feature is the absence of overflow tears with emotional crying after 7 months of age (alacrima). Early signs and symptoms appear during infancy; in particular, school-age children may show additional symptoms including episodes of vomiting, bed wetting, poor bone quality and increased risk of bone fractures. Furthermore, about one-third of them have learning difficulties such as short attention span. In the adulthood, patients suffer from vision worsening (optic nerves face atrophy) and they have often increasing difficulties with balance and walking unaided (Norcliffe-Kaufmann et al., 2013; Slaugenhaupt & Gusella, 2002). Affected individuals have also an increased risk of developing tumours (Waszak et al., 2020) and recently Elp1 have been associated to cancers in the general population.

1.12 Spinal Muscular Atrophy

The term Spinal Muscular Atrophy (SMA) refers to a group of genetic diseases affecting the central and peripheral nervous systems (CNS and PNS) and voluntary muscle movement. The features of the disease are the selective loss of lower α-motor neurons in the ventral horn of the spinal cord and the degeneration of motor neurons in brain stem nuclei, resulting in weakness leading to immobility because of a profound muscle atrophy. Besides, in severe cases, patients may suffer of respiratory failure and paralysis that bring them to death (Kolb & Kissel, 2015; Lanfranco et al., 2017). The most common SMA is an autosomal recessive disorder that accounts for over 95% of patients and results from a homozygous deletion or mutation within the Survival of Motor Neuron 1 (Smn1) gene and subsequent loss of functional SMN protein (Kolb & Kissel, 2015; Meijboom et al., 2017). In humans, *Smn1* has been duplicated to create the paralog Smn2 gene, which physiologically produces a low level (~ 10 - 20%) of functional SMN protein (Kashima et al., 2007). The determinant of the disease is *Smn1*, since it is absent or mutated in all patients, whereas *Smn2* is present in all patients and viewed as a modifier of the phenotype (Cartegni et al., 2006).

1.12.1 Molecular pathogenesis of SMA

Smn genes reside within a segmental duplicated region on chromosome 5q.13 as inverted repeats and share > 99% identity at the mRNA level, both encoding SMN, a RNA binding protein of 294 aa (38 kDa). At the level of pre-mRNA splicing Smn1 correctly splices exon 7 but Smn2, because of a single translationally silent transition (c.840 +6C>T) that weakens the recognition of the upstream 3'ss, produces mRNA that significantly skipped this exon. Thus, most Smn2 transcripts lack exon 7 (Smn2Δ7) resulting in a non-functional SMN protein (Hua et al., 2007; Meijboom et al., 2017; Tizzano & Finkel, 2017). In SMA, Smn1 gene is mutated and responsible of the disease and Smn2 largely skips exon 7 producing a quantity of full-length SMN protein not sufficient to compensate for the lack of Smn1 but essential for the survival of SMA patients (Figure 1.20) (Hua et al., 2015). Specifically, the +6C>T transition makes an AS pattern caused by two non-exclusive models: I) the +6 C>T mutation has been attributed to loss of an ESE dependent on the SR protein splicing factor ASF/SF2 (or SRSF1) and/or II) the +6 C>T mutation has been attributed to creation of a ESS element that functions by binding of the splicing repressor hnRNP A1 (Hua et al., 2007;

Kashima et al., 2007). Regarding SMN protein, it is ubiquitously expressed and localized in the cytoplasm and nucleus of all somatic cells and shows high abundance in spinal cord motor neurons (Coovert et al., 1997). Within the nucleus, it is located in "dot like" structures associated with coiled bodies (Cajal) called "gems". This protein is required for the normal function of all cells by impacting various aspects of RNA metabolism such as the biogenesis of snRNPs and most importantly is a key factor in the assembly of splicing machinery (Hua et al., 2015; Lanfranco et al., 2017).

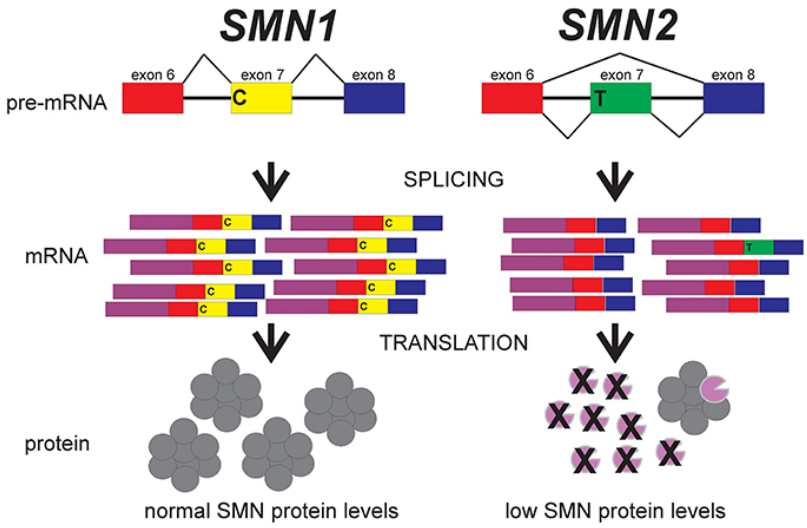

Figure 1.20: ***Smn1 and Smn2 are similar but different.***

The main difference between Smn1 and Smn2 genes is a single substitution in position +6 within exon 7, where a C is converted to T. This conversion causes Smn2 to transcribe the exon 7 in only 10-20% of the total amount of transcripts, instead of 80-90% as Smn1. Translation of these Smn2Δ7 mRNAs produces a truncated protein (shown by the incomplete circles) which is unstable and rapidly degraded by cells. Indeed, in SMA patients, the lack of SMN protein due to the double impairment of Smn1 gene could not be sufficiently compensated due to limited production of Smn2 full-length transcripts. Adapted from (Butchbach, 2016).

1.12.2 Physiopathology of SMA

Based on the clinical severity and age at onset, the multiple described phenotypes were formalized into a classification scheme divided in four types of SMA classified as types one to four, where type four is the least severe and occurs in adult patients (Tosolini & Sleigh, 2017). Nevertheless, a so called "type 0", the worst one, includes patients with prenatal onset and death within weeks. The symptoms vary greatly depending on the SMA type involved, the stage of the disease and individual factors; they commonly include pulmonary complications - so the ultimate cause of death in infants and children with type one and two is usually respiratory failure -, gastrointestinal

worsening and nutritional deficiencies - infants in type one SMA often have prolonged feeding times and tire quickly - and orthopedic and musculoskeletal complications due to weakness and skeletal muscle atrophy (Kolb & Kissel, 2015; Tizzano & Finkel, 2017). SMA types are described in figure 1.21 below.

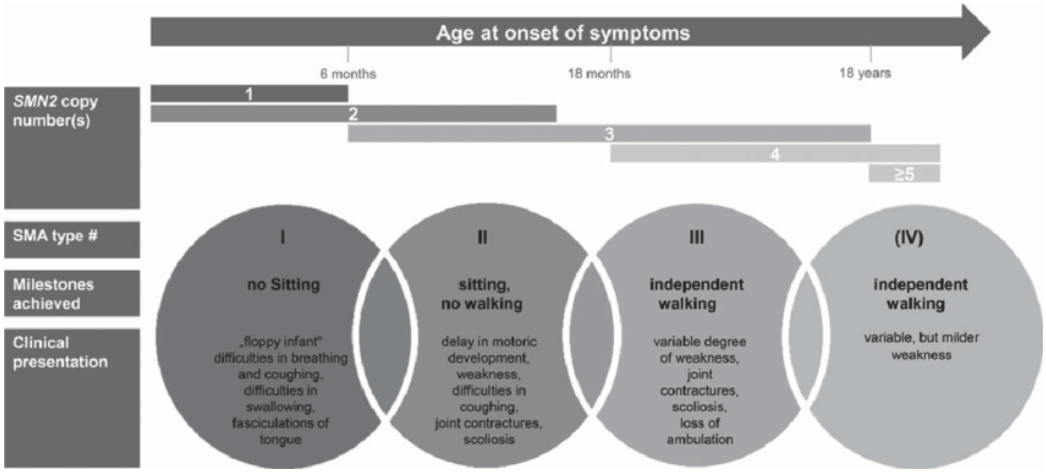

Figure 1.21: ***SMA types.***

Clinical classification of SMA types from type I (the most severe) to the IV (the milder) according to age of onset and clinical presentation. Smn2 copy numbers are displayed. Adapted from (Schorling et al., 2020).

1.13 Familial Dysautonomia and Spinal Muscular Atrophy mouse models

In the last 10-20 years a conspicuous number of FD and SMA mouse models were developed to fully understand the genetic aspects and the pathogenesis of the diseases and to help the development of more comprehensive and efficient therapies (Hims et al., 2007; Hsieh-Li et al., 2000; Lefcort et al., 2017; Perlman, 2016). The first FD model created is a humanized IKBKAP transgenic mouse, that is homozygous for the murine Ikbkap gene and carries the entire human Elp1 gene with the most common mutations affecting FD patients (c.2204 +6T>C). This transgenic mouse recapitulates faithfully the tissue-specific variability of Elp1 exon 20 skipping seen in FD patients and expressing normal levels of endogenous mouse IKAP protein, do not display any phenotypic abnormality of the disease (Hims et al., 2007). Given its features, this model is widely used for studies of tissue-specific splicing regulation and therapeutic development (Dietrich & Dragatsis, 2016). On the contrary, a plethora of mouse models were developed to mimic different types of SMA. In general, these mice express a range of SMN protein levels and extensively cover the severe and mild types of SMA, with neurological and physiological manifestation of disease. One of the models that recapitulates a mild phenotypic aspect of the disease is the "SMA-like" mouse (Hsieh-Li et al., 2000), which does not express the murine Smn gene but carries four copies of the human *Smn2*, exhibiting a molecular and progressive neurodegenerative phenotype similar to Type III SMA. Mice are viable, fertile and their only evident phenotype is tail necrosis that results in short and thickened tail by the 6^{th} week after birth (Hsieh-Li et al., 2000). As reported for FD, the mild SMA mouse model highlighted its usefulness in the development of therapeutic approaches, including antisense oligonucleotides (Hua et al., 2010) and modified U1 spliceosomal particle (Donadon et al., 2019).

Chapter 2 – Aim of the thesis

Spinal Muscular Atrophy (SMA) and Familial Dysautonomia (FD) are two genetic diseases associated with splicing mutations that induce exon skipping. Since the degree of the splicing defects is related to the phenotype of the disease, it is important to study the effect of age on their severity and the underlying regulatory mechanism. Co-transcriptional regulation of alternative splicing is a well-studied phenomenon, but it is not known whether exon skipping defects undergo a similar regulatory mechanism based on RNA Polymerase II (Pol II) transcription and/or chromatin structure and whether this is age-dependent. The major objectives of this thesis are to investigate the temporal changes of two exon skipping defects associated to SMA and FD *in vivo* in transgenic mice and their potential regulation by Pol II and chromatin marks.

The aims of this thesis are:

- To evaluate the age-dependent changes in Smn2 exon 7 and Elp1 exon 20 aberrant splicing *in vivo* in transgenic mouse models;

- To study the temporal changes of chromatin marks and Pol II density in the human Elp1 gene *in vivo* in a transgenic FD mouse model;

- To elucidate the role of Pol II elongation and chromatin modifications on Elp1 exon 20 mis-splicing *in vitro*.

Chapter 3 – Materials & Methods

3.1. Chemical reagents

General chemicals and kits were purchased from Sigma-Aldrich (St. Louis, MO, USA), Merck KGaA (Darmstadt, Germany), Gibco (Thermo Fisher Scientific, Waltham, MA, USA), Boehringer-Mannheim (Roche, Basel, Switzerland), Invitrogen (Thermo Fisher Scientific, Waltham, MA, USA), Fluka (Sigma-Aldrich, St. Louis, MO, USA), Qiagen (Hilden, Germany), Stratagene (Agilent Technologies, Santa Clara, CA, USA), Promega (Madison, WI, USA) and Zymo Research.

Primers used in this study were purchased from Sigma-Aldrich and Eurofins Genomics.

3.2. Standard solutions

All solutions are identified in the text except for the following:
- 5x TBE: 53 g Tris-HCl, 27.5 g Boric acid, 20 ml 0.5 M EDTA, pH 8.0 in 1 l
- 6x DNA sample buffer: 0.25% w/v Bromophenol blue, 0.25% w/v Xylene Cyanol FF, 30% v/v glycerol in H2O
- 1x PBS: 137 mM NaCl, 2.7 mM KCl, 10 mM Na2HPO4, 1.8 mM KH2PO4, pH 7.4
- Luria – Bertani medium (LB): 1% w/v Difco Bactotryptone, 0,5% w/v Oxoid yeast extract, 1% w/v NaCl in dH2O, pH 7.5
- 1x TSS solution: 10% w/v PEG 4000, 5% v/v DMSO, 35 mM MgCl2, pH 6.5 in LB medium
- 10X Blotting buffer: 30 g Tris-HCl, 144 g glycine, 20% methanol in 1 l
- 10X Transfer buffer: 250 mM Tris, 1.92 M glycine in dH2O, pH ~8.3. When diluted to 1x, methanol was added to 20% v/v

3.3. Preparation of bacterial competent cells

Bacterial competent cells were prepared following the method described by Chung et al. (Chung et al., 1989)c. Escherichia coli strains were grown overnight in 10 ml of LB at 37°C. The following day, 150 ml of fresh LB were added and the cells were grown in the shaker at room temperature until the OD600 was 0.3 - 0.4. Cells were then put

on ice to stop the growth and centrifuged at 4°C, 1000 g for 1 hour. The pellet was resuspended in 1/10 volume of cold 1x TSS solution. Cells were aliquoted, rapidly frozen in liquid nitrogen and stored at -80°C. Competence was determined by transformation with 0.1 ng of β-galactosidase-based virgin plasmid (pUC19) control DNA plasmid and was deemed satisfactory if this procedure resulted in more than 100 colonies.

3.4. Bacterial culture

The *E. coli* K12 strain DH5α was transformed with the plasmids described in this study and used for their amplification. Plasmids were incubated with 30 ul of competent cells for 30 minutes on ice, followed by a heat shock at 42°C for 30 seconds. Finally, cells were placed again on ice for 5 minutes and then spread onto agarose plates containing the appropriate antibiotic concentration (100 ug/ml of ampicillin). Plasmids were maintained in the short term as single colonies on agar plates at 4°C. Bacteria were amplified by an overnight incubation in LB medium, 10 g NaCl, pH 7.5 in 1 l. Bacterial growth media were sterilized before use by autoclaving. Then ampicillin was added to the media at a final concentration of 100 ug/ml.

3.5 DNA preparation

3.5.1. Medium scale preparation of plasmid DNA from bacterial cultures

Single bacterial colony was picked and transferred into 50 ml of LB medium containing 100 ug/ml of ampicillin. The culture was incubated overnight at 37°C in a shaking incubator. The Plasmid DNA purification kit (Macherey-Nagel, Düren, Germany) was used according to the manufacturer's instructions to obtain medium amounts of pure plasmid DNA. The final pellet was resuspended in 50 ul of Nuclease-Free water. The quality of extracted plasmid DNA was verified on 0.8% agarose gels. The DNA was stored at -20°C and routinely, 3 ul of such DNA preparations were taken for the restriction enzyme digestion.

3.6 Minigene systems for *in vitro* splicing analysis

Hybrid minigenes are useful construct tools to study *cis*- and *trans*-acting elements that influence splicing process, to understand cell-specific splicing pattern and to identify exonic and intronic elements to determine whether a specific mutation can compromise

the splicing, establishing the role of the splice sites in the exon recognition. This system, after transient or stable transfection and RNA analysis, allowed to study the splicing outcome. The minigene construct used in this thesis was verified by DNA sequencing.

3.6.1 pTB-Elp1 hybrid minigene

pTB-Elp1 minigene was already available in the Human Molecular Genetics laboratory and created by site-directed mutagenesis of Elp1 wt minigene using the QuikChange Sitedirected Mutagenesis Kit II (Agilent Technologies, Santa Clara, CA, USA) according to the manufacturer's instructions. The Elp1 wt minigene genomic region spanning from intron 18 to intron 22 was used as a template for cloning. The PCR product was digested with NdeI and cloned in the NdeI site into previously described pTB-NdeI(-) minigene (Pagani et al., 2003) under the SV40 promoter. A graphical representation of pTB-Elp1 minigene used in the study is shown below (Figure 3.1).

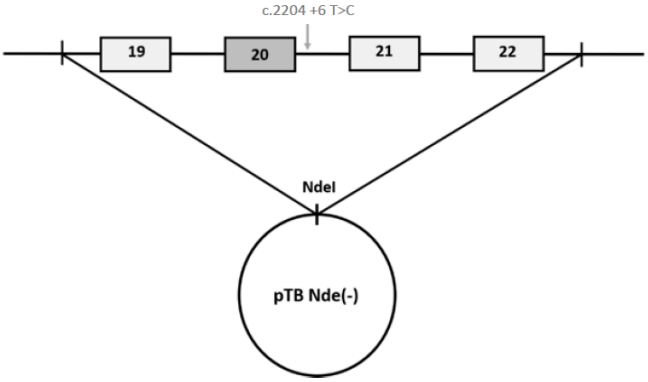

Figure 3.1: ***Schematic representation of the pTB-Elp1 mutant minigene.***

The cassette of expression is cloned in NdeI site; the c.2204 +6T>C is indicated in grey downstream exon 20, the exon alternatively spliced.

3.7 HEK 293T cells maintenance and minigene transfection

3.7.1 Maintenance and analysis of HEK 293T in culture

HEK 293T cells were grown in Dulbecco's Modified Eagle Medium with Glutamax I (Gibco, Life Technologies) (DMEM with glutamine, sodium pyruvate, pyridoxine and 4.5 g/l glucose) supplemented with 10% fetal calf serum (FBS) (Gibco, Life Technologies) and antibiotic antimycotic (Sigma) according to manufacturer's instruction. Cells were kept in humidified incubator at 37°C and 5% of CO_2. A standard 100 mm dish containing a confluent monolayer of cells was washed twice with 1X PBS

solution to remove all medium residues as well as dead cells, treated with 1 ml Trypsin (PBS 1X containing 0.045Mm EDTA and 0,1% trypsin) and incubated at 37°C for 1 minute or until cells were completely detached. After adding 5 ml of medium to block trypsin, cells were precipitated by centrifugation (1500 RPM for 5 minutes) and resuspended in pre-warmed medium. Then, 1 ml of this cellular dilution was added to 9 ml fresh medium and plated in a new 100 mm dish.

3.7.2 Transfection of recombinant DNA

~ 3 x 10^5 HEK 293T cells were plated as described above into 6-well cell culture dishes to reach a final confluence of 50 - 70%. The plasmids DNA used for transfection were prepared with JETSTAR Purification Kit as previously described. Transfection of HEK 293T cells was performed by applying Effectene Transfection Reagent (Qiagen) according to manufacturer's instructions. For 6-wells cell culture plates, 500 - 1500 ng of plasmid DNA were first mixed with 150 - 220 ul of EC buffer and 4 – 24 ul of Enhancer and the mixture was incubated at RT for 5 minutes to allow the condensation of DNA. 5 – 30 ul of Effectene Reagent were then added to the mixture and incubated for 10 minutes to allow Effectene-DNA complexes to form. After the addition of 300 - 500 ul of complete growth medium, the mixture was added to the cells in 1.5 ml of the same medium and incubated at 37°C. After 24 hours, cells were harvested and subjected to further analysis. Each transfection experiment was repeated at least three times in duplicate.

3.7.3 Co-transfection of RNA Polymerase II variants in HEK 293T cells

For co-transfection experiments of α-amanitin-resistant variants of the large subunit of human RNA Polymerase II (hRpb1), that are the wild-type (WT^{res}; pAT7Rpb1αAm^r vector) and the "slow" R749H mutant (pAT7Rpb1αAm^rR749H vector) and the wild-type (WT^{res}; pcDNA5/FRT/TORpb1αAm^r vector) and the "fast" E1126G mutant (pcDNA5/FRT/TORpb1αAm^rE1126G vector), 1500 ng of the pTB-Elp1 minigene have been transfected with 1500 ng or 3000 ng of the expressing plasmids. At the time of transfection, 2.5 ug/ul or 5 ug/ul of α-amanitin were added to cells to block endogenous RNA Pol II transcription and cells were harvested after 24 h for *in vitro* splicing analysis. Each transfection experiment was repeated at least three times in duplicate.

3.7.4 Transfection and addition of chemicals that alter chromatin structure and RNA Polymerase II rate

For transfection experiments followed by the addition of Valproic acid (VPA) or EED-226 chemical, 500 ng of pTB-Elp1 minigene were transfected into cells as previously reported. At the time of transfection, 4 mM of VPA or 100 uM of EED-226 were added to cells. Distilled water (dH_2O) and DMSO were used as control for VPA and EED-226 chemical, respectively. Cells were harvested after 24 h for *in vitro* splicing analysis. Each transfection experiment was repeated at least three times in duplicate. For transfection experiments followed by the addition of (S)-(+) Camptothecin (CPT) or 5,6-Dichloro-1-β-D-ribofuranosylbenzimidazole (DRB), 500 ng of pTB-Elp1 minigene were transfected into cells as previously reported. At the time of transfection, 6 uM or 12 uM of CPT or 50 uM or 75 uM of DRB were added to cells. DMSO was used as control. Cells were harvested after 24 h for *in vitro* splicing analysis. Each transfection experiment was repeated at least three times in duplicate.

3.8 Animal models

Familial Dysautonomia (FD) mouse model was previously described by Hims et al. (Hims et al., 2007). This model is carrying the complete human *Ikbkap* (*Elp1*) locus with the FD IVS20+6T>C splice mutation from a human BAC. Presence of the FD mutation in the BAC causes mis-splicing of human Ikbkap in mice and exon inclusion is seen in a tissue-specific manner that closely represents situation seen in FD patients. Mice do not show any pathological phenotype. Spinal Muscular Atrophy (SMA) mouse model (#005058, jax lab) was previously described by Hsieh-Li et al. (Hsieh-Li et al., 2000). Mice that are homozygous for the Smn1^{tm1Hung} knock-out allele and homozygous for the Tg(SMN2)2Hung transgene display a varied Type III SMA phenotype. They are viable, fertile and exhibit short and thickened tail. Skeletal muscle tissue has fewer myocytes and atrophic muscle bundles and large motor neurons in the anterior horns of the spinal cord degenerate and are lost (www.jax.org). For our purposes, animals were kept in a controlled environment at 25°C with a 12 hours light /dark photoperiod. In general, animals were housed and handled according to institutional guidelines approved by International Centre for Genetic Engineering and Biotechnology (ICGEB) board. The experimental procedures were carried with full respect to the European Union Directive 2010/63/EU for animal experimentation and were approved by the Italian competent authorities and Ethical Committees. Mice were

sacrificed at 10, 90 and 365 post-natal days (P or PND) to collect tissues and organs (brain, spinal cord, dorsal root ganglia, eyes, liver, lung, heart, kidney and muscle).

3.8.1 Animal genotyping

Few days after birth, a small piece of paw was cut to perform genotyping. After genomic DNA extraction, PCR was performed to verify the expression of Elp1 mutant variant with human-specific primers (Hs_sp_ex19_F and Hs_sp_ex22_R). The thermal cycling protocol was: 94°C for 5 minutes, 30 cycles at 94°C for 30 seconds, 58°C for 30 seconds, 72°C for 30 seconds and 72°C for 10 minutes. Primers are listed in the table below (Table 3.1).

Primer name	Sequence 5'-3'
Hs_sp_ex19_F	5'-AGCAGCAATCATGTGTCCCA-3'
Hs_sp_ex22_R	5'-GTGACATCTTCTTCTTTCAA-3'

Table 3.1: ***List of primers used for genotyping.***

3.9 DNA and RNA preparation from cultured cells and mice organs

3.9.1 DNA purification from ChIP experiments

After de-crosslinking (see paragraph 3.12), DNA-containing supernatant was diluted with autoclaved water to a final volume of 200 ul. Next, 1 volume of phenol pH = 7.6 was added followed by a centrifuge at +4°C for 10 minutes at 14.000 RPM. Next, the aqueous phase was transferred to a new tube and 1 volume of phenol pH 7.6: chloroform 1:1 mixture was added followed by a centrifuge at +4°C for 10 minutes at 14.000 RPM. Next, the aqueous phase was transferred to a new tube and 1 volume of chloroform was added followed by a centrifuge at +4°C for 10 minutes at 14.000 RPM. Next, the aqueous phase was transferred to a new tube and 1/10 volume of sodium acetate pH 5.2, 2 volumes of ethanol 100% and 1 ul of 20 mg/ml glycogen (Sigma-Aldrich) were added followed by a centrifuge at +4°C for 10 minutes at 14.000 RPM. Next, supernatant was discarded and the pellet was rinsed in 2 volumes of 70% ethanol and centrifugated at 14.000 RPM for 6 minutes in a microcentrifuge at +4°C. At the end, pellet was air-dried and resuspended in autoclaved dH_2O and stored at -20°C.

3.9.2 RNA preparation from cultured cells and mice organs

Cultured cells were washed twice with 1x PBS and then 750 ul of RNA TRI Reagent (Ambion, now Thermo Fisher Scientific, Waltham, MA, USA) were added. Cells in TRI Reagent were collected into 1.5 ml tubs. Mice tissues were transferred into FastPrep® Lysis Beads & Matrix Tubes for Sample Disruption (MP Biomedicals, Santa Ana, CA, USA). Each impact-resistant tube contains 1.4 mm ceramic spheres. Lysing Matrix D is used primarily for lysis of softer tissues. For tissues homogenization, 1 ml of RNA TRI Reagent was added and MagNA Lyser Instrument (Roche, Basel, Switzerland) was used for automatic disruption. The instrument facilitates the production of a supernatant containing nucleic acids suitable for further extraction. Next, for cells and homogenized tissues 150 ul and 200 ul of chloroform were added, respectively. Samples were vortexed for 15 seconds, left for 10 minutes at room temperature and centrifugated at 13.500 RPM for 15 minutes in a microcentrifuge at + 4°C. Chloroform ensures phase separation of the two liquids, because chloroform is miscible with acid phenol and it has a higher density than phenol; it forces a sharper separation of the organic and aqueous phases thereby assisting in the removal of the aqueous phase. After chloroform extraction, the RNA-containing supernatant (aqueous phases) was precipitated by addition of 1 volume of isopropanol and collected by centrifugation at 13.500 RPM for 30 minutes in a microcentrifuge at +4°C. The pellet was rinsed in 70% ethanol and centrifugated at 13.500 RPM for 6 minutes in a microcentrifuge at +4°C. At the end, pellet was air-dried and resuspended in autoclaved dH_2O and stored at -80°C. Quality of RNA was checked by electrophoresis on a 0.8% agarose gel and quantified using NanoDrop 1000 (Thermo Scientific) spectrophotometer.

3.9.2.1 DNase treatment & RNA clean-up

Depending on the experiment, in the case of DNA contamination, the extracted RNA was treated with RNase-free DNase (Invitrogen) in 1X DNase Buffer, according to manufacturer's instructions. The DNA digestion was performed at 37°C for 30 minutes. The reaction was stopped by adding 1.5 ul of DNase inactivating reagent and incubated at room temperature for 5 minutes. RNA clean-up was performed using RNA Clean & Concentrator-5 (Zymo Research) according to manufacturer's instructions and RNA was resuspend in autoclaved dH_2O and stored at -80°C.

3.10 Estimation of nucleic acid concentration

As both DNA and RNA molecules absorb UV light, this feature is used for measuring the concentration of nucleic acids with NanoDrop spectrophotometer. The nitrogenous bases in nucleotides have an absorption peak at 260 nm, so an optical density of 1.0 at this wavelength is usually taken to be equivalent to a concentration of 50 μg/ml for dsDNA, 40 ug/ml for ssDNA and RNA and approximately 20 ug/ml for ss oligonucleotide sample. The ratio of the absorbance at 260 nm and 280 nm is a measure of the purity of a sample: this ratio should be ~ 1.8 for pure DNA sample and ~ 2.0 for RNA sample. If the ratio is appreciably lower, it may indicate the presence of protein, phenol or other contaminants that absorb strongly at or near 280 nm.

3.11 The mRNA functional splicing assays

3.11.1 cDNA preparation

The first-strand cDNA synthesis was performed with the M-MLV Reverse Transcriptase Kit (Invitrogen) following manufacturer's instructions for experiments performed *in vitro* and with the Superscript VILO MasterMix (Invitrogen) for experiments performed *in vivo*. Briefly, for *in vitro* 250 – 500 ug of total RNA extracted from HEK 293T cells were mixed with 2 ul of random primers (100 ng/ul, Invitrogen) and diluted in sterile water to the final volume of 12 ul. To denature RNA, the mixture was put at 94°C for 2 minutes and quick chilled on ice. After denaturation, 6 ul 5X First-Strand Buffer (250 mM TrisHCl pH 8.3 at RT, 375 mM KCl, 15 mM MgCl2), 3 ul 0.1M DTT, 3 ul dNTPs, 0.5 ul M-MLV RT were added to the reaction. The final mixture was then incubated at 37°C for 90 minutes. 3 ul of the reaction were used as a template for PCR analysis. For *in vivo* 1 ug of total RNA extracted from mice tissues were mixed with 4 ul of Vilo Superscript mixture and diluted in sterile water to the final volume of 20 ul. The mixture was incubated at 25°C for 10 minutes, 42°C for 90 minutes and 85°C for 5 minutes. Samples were then diluted 1:10 and 3 ul were used as a template for PCR and qPCR analysis.

3.11.2 Polymerase Chain Reaction (PCR) analysis

The PCR was performed using cDNA as template and following the basic protocol of Promega Taq DNA polymerase. The volume of the reaction was 25 ul and comprised:

5X Taq buffer, dNTPs mix (100 uM each), oligonucleotide primers (100 ng/ul), Taq DNA polymerase (0.125 ul) and 3ul of cDNA. The synthetic DNA oligonucleotides used for PCR amplification were purchased from Sigma-Aldrich or Eurofins Genomics. For Elp1 exon 20 splicing in mouse tissues specific primers were used (Elp1_ex19_F and Elp1_ex21_R) at the following conditions: 95°C for 2' (initial denaturation), 95°C for 30"(denaturation), 60°C for 30" (annealing), 72°C for 30"(extension) for 40 cycles and 72°C for 5'(final extension); for Smn2 exon 7 splicing in mouse tissues specific primers were used (Smn2_ex6_F and Smn2_ex8_R) at the following conditions: 94°C for 5', 94°C for 45" - 56°C for 45" - 72°C for 45" for 35 cycles and 72°C for 10'; for minigene Elp1 exon 20 specific primers were used (α2_3_F and Elp1_ex21_R) at the following conditions: 94°C for 5', 94°C for 30" - 56°C for 30" - 72°C for 40" for 30 cycles and 72°C for 10'; for minigene HBA exon 2 specific primers were used (HBA_ex1_F and HBA_ex3Edb_R) at the following conditions: 94°C for 5', 94°C for 30" - 60°C for 30" - 72°C for 40" for 30 cycles and 72°C for 10'; for endogenous Elp1 exon 10 specific primers were used (endo_Elp1_ex9_F and endo_Elp1_ex11_R) at the following conditions: 94°C for 5', 94°C for 30" - 58°C for 30" - 72°C for 40" for 30 cycles and 72°C for 10'. PCRs were optimized to be in the exponential phase of amplification. The PCR reactions were performed on a Gene Amp PCR System (Applied Biosystem). Quantification of exon inclusion and exon skipping was performed using ImageJ 1.44o (http://imagej.nih.gov/ij). PCR products were size fractionated by electrophoresis on a 1.5 % agarose gel containing ethidium bromide (0.5 ug/ml) and 1X TBE solution. They were electrophoresed at 90 - 100 V in 1X TBE running buffer for a time depending on the expected fragment length and gel concentration. The results of all transfections are the representative of at least three independent experiments in duplicate. Primers are listed in the table below (Table 3.2).

Primer name	Sequence 5'-3'
Elp1_ex19_F	5'-GGCCGGCCTGAGCAGCAATCATGTGTCC-3'
Elp1_ex21_R	5'-GATTCTCAGCTTTCTCATGCATTC-3'
Smn2_ex6_F	5'-CTCCCATATGTCCAGATTCTCTT-3'
Smn2_ex8_R	5'-CTACAACACCCTTCTCACAG-3'
α2_3_F	5'-CAACTTCAAGCTCCTAAGCCACTGC-3'
HBA_ex1_F	5'-ACGCTGGCGAGTATGGTG-3'
HBA_ex3Edb_R	5'-GCAGGTCACCAGCAGGCAGT-3'
endo_Elp1_ex9_F	5'-GATAAACCCAACCAGCAGGA-3'
endo_Elp1_ex11_R	5'-TTCCAACAGTCCAGAGCTGA-3'

Table 3.2: ***List of primers used in PCR for splicing analysis.***

3.11.3 Real Time Quantitative PCR (qPCR) analysis - SYBR Green

SYBR Green-based quantitative PCR (qPCR) was performed using the iQ SYBR Green Supermix (Bio-Rad Laboratories, Inc., Hercules, CA, USA) in a CFX96 Real-Time PCR system (Bio-Rad Laboratories, Inc., Hercules, CA, USA) following manufacturer's instructions. Briefly, 3 ul of 1:10 diluted cDNA where mixed with the master mix and the forward and reverse primers and filled with water to a final volume of 15 ul. Primers were designed to target an amplicon size of 100 - 150 bp. For qPCR human-specific primers were used: for TgFD9 mice, Elp1_FL_F and Elp1_FL_R for full-length transcripts, Elp1_Δ20_F and Elp1_Δ20_R primers for transcripts lacking the exon 20 and total Elp1 mRNA was quantified with human-specific primers Elp1_TOT_F and Elp1_TOT_R. For SMA mild mice, SMN2_FL_F and SMN2_FL_R for full-length transcripts, SMN2_Δ7_F and SMN2_Δ7_R primers for transcripts lacking the exon 7 and total Smn2 mRNA was quantified with human-specific primers Smn2_TOT_F and Smn2_TOT_R. GAPDH was used as housekeeping for normalization with mouse-specific primers: mGapdh_F and mGapdh_R. At least two replicates per RT reaction were performed. The thermal cycling protocol was: 95°C for 3' (initial denaturation), 95°C for 10" (denaturation), 59°C or 60°C for 45" (annealing/extension + plate read) for 40 cycles and 65°C to 95°C, 0.5°C increment 0.05"/step (Melt Curve analysis). hnrnpA1, Srsf1, Srsf2, Srsf3, Srsf9, Sam68, Tia1, Tra2β, Sfpq, Rbm24, Rbm38 and Fus primers were tested and had the same efficiency of amplification (slope between 3.1 and 3.6; efficiency between 90 – 110%). Fold changes were determined using the 2-ΔΔCt method. Primers are listed in the tables below (Table 3.3).

Primer name	Sequence 5'-3'
mGapdh_F	5'-ATGGTGAAGGTCGGTGTGAA-3'
mGapdh_R	5'-GTTGATGGCAACAATCTCCA-3'
Elp1_FL_F	5'-GCAGCAATCATGTGTCCCA-3'
Elp1_FL_R	5'-ACCAGGGCTCGATGATGAA-3'
Elp1_Δ20_F	5'-CACAAAGCTTGTATTACAGACT-3'
Elp1_Δ20_R	5'-GAAGGTTTCCACATTTCCAAG-3'
Elp1_TOT_F	5'-GCTGTTCCCACACCCTGT-3'
Elp1_TOT_R	5'-AGGGTCAGCACTTGGACAA-3'
Smn2_FL_F	5'-GCTGATGCTTTGGGAAGTATGTTA-3'
Smn2_FL_R	5'-CACCTTCCTTCTTTTTGATTTTGTC-3'
Smn2_Δ7_F	5'-TGGACCACCAATAATTCCCC-3'
Smn2_Δ7_R	5'-ATGCCAGCATTTCCATATAATAGCC-3'
Smn2_TOT_F	5'-AGCGATGATTCTGACATTTGGGATG-3'
Smn2_TOT_R	5'-CTGTTGTAAGGAAGCTGCAGTATTCTT-3'
mhnrnpA1_F	5'-GGTTTGTCACATATGCCACTG-3'
mhnrnpA1_R	5'-CCTTCGTTGAGTTCGAGGAC-3'
mSrsf1_F	5'-CCTTCGTTGAGTTCGAGGAC-3'
mSrsf1_R	5'-CGCTTCGGGGAAACTCTAC-3'
mSrsf2_F	5'-AAAATGATGAATCGGCAAGC-3'
mSrsf2_R	5'-TAGCCAGTTGCTTGTTCCAA-3'
mSrsf3_F	5'-CTGTCCGGGAACTAGATGGA-3'
mSrsf3_R	5'-AGGACTCCTCCTGCGGTAAT-3'
mSrsf9_F	5'-GAACGGGCCTCCTACAAGAC-3'
mSrsf9_R	5'-CCATTCCGTCCTTCTGTACG-3'
mSam68_F	5'-GAATACCTTTGCCTCCCACA-3'
mSam68_R	5'-CTGACTCCCCTTGACTCTGG-3'
mTia1_F	5'-GCACACAGCGTTCACAAGAT-3'
mTia1_R	5'-CCCGGTAGCCATGTCTTTTTA-3'
mTra2β_F	5'-GATGGGCGTCGAATTAGAGT-3'
mTra2β_R	5'-CCGATCGTACCCTCTGTCAT-3'
mSfpq_F	5'-AAAAGCTGGCCCAGAAGAA-3'
mSfpq_R	5'-CATCCAAGGACTTCCATCGT-3'
mRbm24_F	5'-GGCTACGGATTTGTCACCAT-3'
mRbm24_R	5'-GGCTGCATGATTCTTGGTTT-3'
mRbm38_F	5'-GCTGATAGGGCTTGCAAAGA-3'
mRbm38_R	5'-AAGGTGGGGTGTAGTTGCTG-3'
mFus_F	5'-AAGGCCTAGGCGAGAATGTT-3'
mFus_R	5'-CAACTTGCCAGTTTCCCTGT-3'

Table 3.3: ***List of primers used in qPCR to detect changes in the expression level of genes of interest.***

3.12 Chromatin immunoprecipitation (ChIP)

Chromatin immunoprecipitation in TgFD9 mice was performed using EpiQuik Tissue Chromatin Immunoprecipitation (ChIP) kit according to manufacturer's instructions with minor modifications. Briefly, for each age considered in this study, 50 mg of frozen tissue were cut into small pieces with a blade in ice-cold PBS 1X, sucked in 18 G needle syringe for 10 times, cross-linked with 1% formaldehyde for 10 min at room temperature and quenched with 150 ul of PBS 1X-Glycine 1.25M for 10 min at room temperature. Then, lysates were centrifuge for 5 minutes at room temperature at 800 RPM, the supernatant was discarded and an additional round of 10 ml PBS 1X-Glycine was added to the lysate, followed by a wash with 10 ml of ice-cold PBS 1X. Samples were homogenized using a Douncer homogenizer and centrifuged to pellet nuclei at 5000 RPM for 5 minutes at +4°C. After homogenization, lysis buffer was added to nuclei and 18 G needle syringe was used to allow a stronger lysis of the sample. Chromatin was prepared and sonicated using a water bath Bioruptor (Diagenode) (30" ON/30" OFF, High power, 3 x 10 cycles) to a size range of 200 -1000 bp. Sonicated chromatin was centrifuged at 14.000 RPM at +4°C for 10 minutes to pellet nuclei debris and the supernatant was transferred to a new tube. To check the correct sonication, prior to de-crosslinking and DNA purification, a small aliquot was treated with RNase A (20 mg/ml) at 37°C for 30 min and after DNA purification, 500 ng of DNA were added to 2 ul 500 mM NaCl and sterile water to the final volume of 10 ul. Mixture was then put at 99°C for 20 minutes, at 50°C for 20 minutes and chilled in ice. At the end, samples were loaded on 1% agarose gel to see the smear of sonicated DNA. Sonicated chromatin was 1:2 diluted according to manufacturer's instructions and ChIP was performed using antibodies against Rbpd-1 (SantaCruz, 2 ul), H3 total (Abcam, 3,5 ul), H3K4me3 (Abcam, 3,5 ul), H3K36me3 (Abcam, 3,5 ul), H3K9me3 (Abcam, 3,5 ul) and H3K27me3 (Abcam, 3,5 ul). IgG (SantaCruz, 2 ul) was used as negative control in the immunoprecipitation. ChIp reaction was performed using 100 ul of sample at room temperature for 90 minutes on a rotating 96-wells plate. Immunoprecipitated DNA was purified by phenol-chloroform extraction and resuspended in 20 ul. In parallel, 5 ul (5%) were taken to be used as input in the quantification experiments.

3.12.1 ChIP - qPCR – SYBR Green

ChIPs were analyzed by qPCR using iQ SYBR Green in a CFX96 Real-Time PCR system. Briefly, 1.8 ul of 1:3 diluted DNA were mixed with the master mix and the

forward and reverse primers and filled with water to a final volume of 13.2 ul. Primers were designed to target an amplicon size of 80 - 120 bp. Human-specific primers were used: ChIP_Elp1_ex20_F and ChIP_Elp1_ex20_R for exon 20, ChIP_Elp1_ex10_F and ChIP_Elp1_ex10_R for exon 10 ND ChIP_Elp1_ex29_F and ChIP_Elp1_ex29_R for exon 29. The thermal cycling protocol was: 95°C for 3' (initial denaturation), 95°C for 10" (denaturation), 60°C for 45" (annealing/extension + plate read) for 40 cycles and 65°C to 95°C, 0.5°C increment 0.05"/step (Melt Curve analysis). Data at different ages were analyzed relative to input (5%) to include normalization for both background levels and the amount of input chromatin to be used in ChIP. All ChIP experiments were calculated as % DNA immunoprecipitated at the locus of interest relative to the corresponding input samples and normalized to % DNA immunoprecipitated at that locus in the P10 pups. Primers are listed in the table below (Table 3.5).

Primer name	Sequence 5'-3'
ChIP_Elp1_ex20_F	5'-AATTTATTTAAGATGCCAAGGGGAA-3'
ChIP_Elp1_ex20_R	5'-ACAATGGCGCTTACTTGTCC-3'
ChIP_Elp1_ex10_F	5'-GACAGATCTTTTTTCCCTTCTAGG-3'
ChIP_Elp1_ex10_R	5'-GCTGGGGTACTACAGCTGTCTT-3'
ChIP_Elp1_ex29_F	5'-CTGCTGCTTATTGTCTCTACAGG-3'
ChIP_Elp1_ex29_R	5'-AAGGGAGGAATTGAGTTTACCTG-3'

Table 3.4: ***List of primers used in ChIP-qPCR experiments.***

3.13 Protein extraction

Cells treated with EED-226 100 uM or DMSO were washed with 1x PBS, scraped and lysed in 75 ul of RIPA buffer (Sigma-Aldrich, St.Loius, MO, USA) and protease inhibitor cocktail (Roche), in order to inhibit enzymes from degrading proteins. Mice tissues (liver and brain) were lysed in 200 ul of RIPA buffer and protease inhibitor cocktail. Then, cells and mice tissues lysates were sonicated using an ultrasound sonicator (Bandelin Sonopuls) using the following conditions: 10" at 0 cycles, 15% amplitude for 1 time. In order to measure the concentration of total proteins, Bradford assay was performed using Bradford Protein Assay kit (Bio-Rad Laboratories, Inc., Hercules, CA, USA). Standard curve was made using bovine serum albumin (BSA) and spectrophotometer analysis was carried out at 595 nm wavelengths.

3.14 Denaturing polyacrylamide gel electrophoresis (SDS-PAGE)

25 ug of cells' proteins and 20 ug of mice tissues' proteins were mixed with the appropriate volume of 4x Protein loading buffer and 10x of reducing agent and the

mixture was incubated at 94°C for 4 minutes. Protein mixture was separated on NuPAGE 4-12% Bis-Tris precast gels (ThermoFisher) at 120 V in 0,5 L MES Running Buffer 1x for 60 minutes. After running and separating on the gels, proteins were transferred onto a 0.2 um nitrocellulose blotting membrane (Amersham). Sandwich was prepared with 3 pieces of paper, the gel, the membrane (previously washed in 1x Blotting buffer) and other 3 pieces of paper and everything was wet with 1x Blotting buffer. After elimination of air bubbles, the sandwich was closed and put in the blotting support filled with 1x Transfer buffer. The sandwich was blot at 220 mA for 75 minutes at +4°C.

3.15 Western Blotting

After blotted proteins were colored with Red Pounceau staining (Sigma-Aldrich), the membrane was blocked 1 hour RT with TBS buffer supplemented 0.1% Tween-20 (TBS-T) and 3% low fat dry milk for H3K27me3. Membrane was probed with mouse monoclonal primary antibody anti-H3K27me3 (Abcam ab6002, 1:1000) diluted in TBS-T 0.1% buffer supplemented with 3% low fat dry milk overnight at + 4°C. Other primary antibodies that were applied in Western blot analysis are rabbit polyclonal anti-Total H3 antibody (Abcam ab1791, 1:10000) diluted in TBS-T 0.1% buffer supplemented with 5% low fat dry milk and mouse monoclonal anti-GAPDH antibody (Abcam ab8245, 1:5000) diluted in PBS-T 0,1% supplemented with 5% low fat dry milk and used as protein loading control in the experiments. The secondary antibodies are respectively: polyclonal goat anti-mouse immunoglobulins/HRP (Dako P 0447; 1:2000) in PBS-T 0,1% supplemented with 5% low fat dry milk and polyclonal goat anti-rabbit immunoglobulins/HRP (Dako P 0448; 1:2000) in PBS-T 0,1% supplemented with 5% low fat dry milk. Membranes were probed with different primary antibodies and then incubated with secondary antibodies conjugated with horseradish peroxidase (HRP) enzyme and the resulting immunoreactive bands were detected with the Pierce™ ECL Western Blotting Substrate (Thermo Fisher) following by exposure to UVItec (CAMBRIDGE Alliance).

3.16 Statistical analysis

A statistical analysis was performed on the investigated groups of data. In all *in vivo* experiments, One-Way ANOVA was used. The significance levels used were ($p>0.05$: not significant (ns); $p<0.05$*; $p<0.01$**; $p<0.001$***). In all *in vitro* experiments,

Student's t-test (also known as two-samples t-test). ($p>0.05$: not significant (ns); $p<0.05$*; $p<0.01$**; $p<0.001$***). In order to perform these tests, all the experiments were repeated at least three times in duplicate. Data are expressed as mean ± SD or sem as indicated in the figure legend.

Chapter 4 – Results

4.1 Age-dependent changes of Elp1 exon 20 splicing in FD transgenic mouse

To evaluate the temporal changes in Elp1 exon 20 splicing, I used a transgenic mouse model that carries the entire human Elp1 mutant gene (c.2204 +6T>C). As this mouse is homozygous for the murine Ikbkap gene it does not exhibit any pathological phenotype. I sacrificed three mice for each time-point (or age), 10, 90 and 365 days after birth (P10, P90 and P365), respectively, I collected the organs and performed splicing analysis on the following tissues: liver, lungs, muscle, brain, spinal cord, dorsal root ganglia (DRG), eyes, heart and kidney. Following total RNA extraction, I evaluated the aberrant Elp1 exon 20 splicing using semiquantitative RT-PCR assay with specific primers (Elp1_ex19_F and Elp1_ex21_R) and PCR products were separated by electrophoresis on 1.5% agarose gel. During post-natal development (between P10 and P90), several tissues showed a significant decrease in the percentage (%) of exon 20 inclusion. In liver, lung and muscle the percentage of exon 20 inclusion decreased from ~ 60% to ~ 40%, ~ 55% to ~ 40% and ~ 45% to ~ 25%, respectively (Figure 4.1 A, B and C, left and middle panels). Similarly, in brain and spinal cord, the percentage of exon 20 inclusion decreased from ~ 15% to ~ 7.5% and ~ 20% to ~ 15%, respectively (Figure 4.1 D and E). When I looked at the splicing pattern in these five tissues at later time-point P365, I did not observe further alteration in the pattern of splicing (Figure 4.1 A – E). The other tissues analyzed, DRG, eyes, heart and kidney showed no age-dependent differences, neither during post-natal development nor at later time-point (Figure 4.1 F - I). To confirm the semiquantitative RT-PCR data, I analyzed tissues samples by quantitative Real-Time PCR (qPCR) using human specific primers that amplify Elp1 transcripts that include (full-length mRNA) or exclude (Δ20 mRNA) exon 20, respectively, and I expressed the results as Δ20/FL ratio. In each tissue, the level of expression of P10 pups is set to 1. These results well correlated with those obtained with RT-PCR. Indeed, between P10 and P90, I observed a ~ 3- fold increase in the Δ20/FL ratio in liver and ~2- fold increase in lung, muscle and central nervous system (CNS) (Figure 4.1 A – E, right panels). As expected, I did not detect significant differences in the Δ20/FL ratios at later time-point in these tissues (Figure

4.1 A – E). Furthermore, I also checked the Δ20/FL ratios in those tissues in which I did not have any difference in the Elp1 pattern. Consistently with the previous semiquantitative RT-PCR analysis, I did not detect any significant changes in Δ20/FL ratios during the different time-points (Figure 4.1 F – I, right panels). All together, these results indicate that the Elp1 exon 20 inclusion is negatively regulated in a tissue-dependent manner during the post-natal development and then remains unaffected at later age. These age-dependent changes occur in liver, lung, muscle, brain and spinal cord and not in DRG, eyes, heart and kidney.

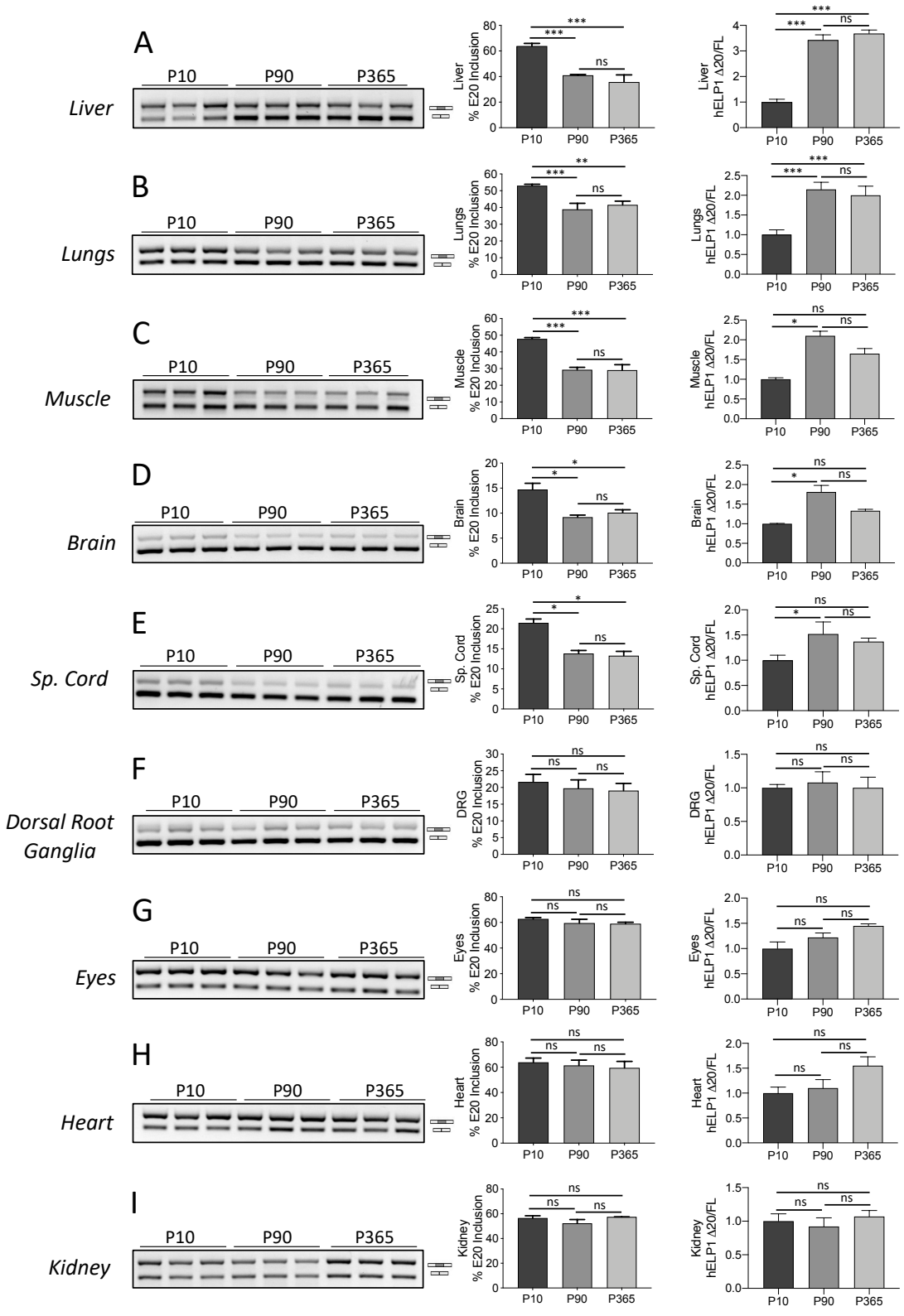

Figure 4.1: ***Human Elp1 exon 20 splicing reveals an age-dependent pattern in some tissues of transgenic FD mice****.*

A-I) *Left*: semiquantitative RT-PCRs (gels) of hELP1 mRNA isoforms in different tissues (liver, lung, muscle, brain, spinal cord, dorsal root ganglia, eyes, heart and kidney) of transgenic FD mice sacrificed at P10, P90 and P365. Total RNA was extracted, mRNAs produced were analyzed through RT-PCR using Elp1_ex19_F1 and Elp1_ex21_R primers. Identity of exon

inclusion (202 bp) and skipping (128 bp) bands are indicated. PCR products were resolved on 1,5% agarose gel and the bands intensity was quantified with ImageJ software. Schematic representation of the splicing pattern is shown on the right of the RT-PCR gel analysis. *Middle*: the histograms represent the quantification of the bands at the indicated age as percentage (%) of Elp1 exon 20 inclusion expressed as mean ± SD. *Right*: Sybr-based qPCRs were performed using human-specific primers Elp1_FL_F and Elp1_FL_R primers for full length (FL) transcripts and Elp1_ Δ20_F and Elp1_ Δ20_R primers for transcripts that skip exon 20 (Δ20). Endogenous GAPDH was used as housekeeping for normalization and amplified with specific primers mGAPDH_F and mGAPDH_R. The histograms represent the quantitative fold change of the ratio of hElp1 Δ20 to FL transcripts in different tissues of transgenic FD mice sacrificed at the indicated age. For each tissue, expression level of P10 pups is set to 1. Data are expressed as mean ± SD of at least 3 mice for each age. Statistical analysis was performed using One-way ANOVA (ns: not significant; * $p<0,05$; ** $p<0,01$; ***$p<0,001$).

4.2 Age-dependent changes of Smn2 exon 7 splicing in a transgenic SMA mouse model

To investigate the temporal changes that affect Smn2 exon 7 splicing during time, I took advantage of a SMA-like transgenic mouse that carries four copies of the human *Smn2*. This mouse does not express the murine Smn gene but shows only a very mild SMA phenotype that is essentially localized in the tail (tail degeneration). As done for FD, I sacrificed three mice at three time points (P10, P90 and P365) and performed Smn2 exon 7 splicing analysis on liver, lung, muscle, kidney, brain, spinal cord and heart. I extracted total RNA and I evaluated Smn2 exon 7 splicing by semiquantitative RT-PCR using specific oligonucleotides (Smn2_ex6_F and Smn2_ex8_R). During post-natal development, liver, lungs, muscle and kidney showed a significant increase in the percentage of exon 7 inclusion. Specifically, in liver exon inclusion increased from ~15% to ~30% (Figure 4.2 A, left and middle panels), in lung, from ~30% to ~40% (Figure 4.2 B), in muscle, from ~25% to ~40% (Figure 4.2 C) and in kidney, from ~20% to ~30% (Figure 4.2 D). In contrast, in brain and spinal cord, I observed a significant decrease in the percentage of exon 7 inclusion, from ~20% to ~10%, in both cases (Figure 4.2 E and F). At P365, in the majority of the tissues splicing remained at the same level observed at P90. The only exception is represented by CNS tissues, brain and spinal cord, in which the percentage of exon 7 inclusion increased, returning to the level observed at P10: exon 7 was more included in mature mRNA going from ~10% to ~25% in brain and from ~10% to ~15% in spinal cord (Figure 4.2 E and F). No changes were observed for heart (Figure 4.2 G). Then, to confirm my results, I analyzed tissues samples by qPCR with human specific primers to amplify Smn2 transcripts that include (full-length mRNA) or exclude (Δ7 mRNA) exon 7, respectively, and I expressed the results as Δ7/FL ratio setting the level of expression of P10 pups to 1. Globally, I observed a good correlation in exon 7 splicing between RT-PCR and qPCR results. In liver, lung, muscle and kidney I detected a ~1.3 – 2-fold decrease in the Δ7/FL ratio within 3 months of age and no further alterations at later time point (Figure 4.2 A – D, right panels). In brain and spinal cord, I observed ~1.2 – 2-fold increase in the Δ7/FL ratio during post-natal development and a slight decrease between P90 and P365 (Fig 4.2 E and F). As expected, in heart I did not observe differences in the Δ7/FL ratio among P10, P90 and P365 (Figure 4.2 G). Collectively, these results show a general increase of Smn2 exon 7 inclusion over time in most tissues, with the greater differences in the splicing happening within 3 months of age.

In brain and spinal cord there is a decrease at post-natal development that is recovered at later age.

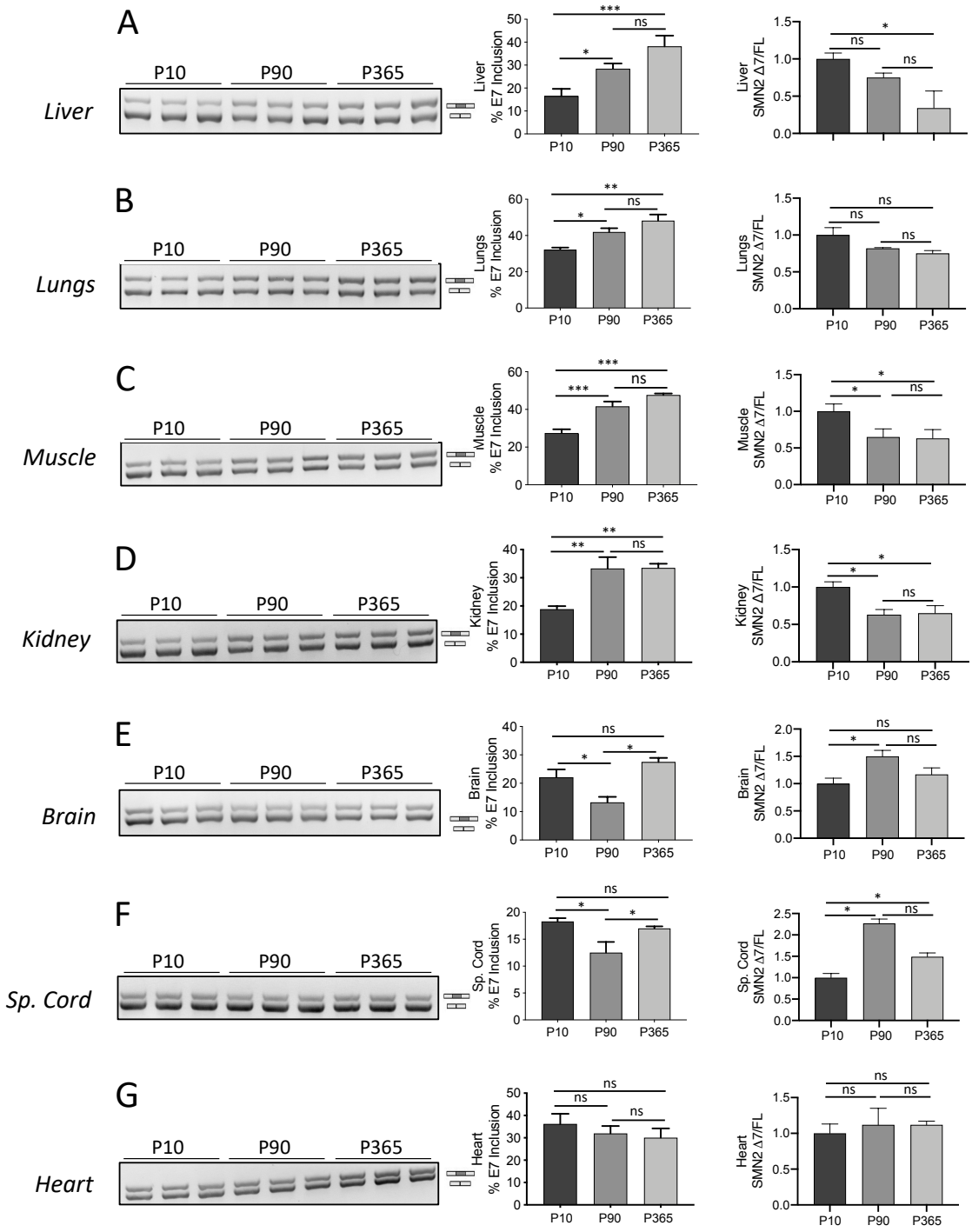

Figure 4.2: ***Human Smn2 exon 7 splicing is age-dependent and tissue-specific in the mild SMA mouse model.***

A-I) *Left*: semiquantitative RT-PCRs (gels) of hSmn2 mRNA isoforms in different tissues (liver, lung, muscle, kidney, brain, spinal cord and heart) of transgenic SMA mice sacrificed at P10, P90 and P365. Total RNA was extracted, mRNAs produced were analyzed through RT-PCR using Smn2_ex6_F and Smn2_ex8_R primers. Identity of exon inclusion (505 bp) and skipping (451 bp) bands are indicated. PCR products were resolved on 2% agarose gel and the bands intensity was quantified with ImageJ software. Schematic representation of the splicing pattern is shown on the right of the RT-PCR gel analysis. *Middle*: The graphs represent the percentage (%) of exon 7 inclusion expressed as mean ± SD at the indicated age. *Right*: Sybr-based qPCRs were performed using human-specific primers Smn2_FL_F and Smn2_FL_R

primers for full length (FL) transcripts and Smn2_ Δ7_F and Smn2_ Δ7_R primers for transcripts that skip exon 7 (Δ7). Endogenous GAPDH was used as housekeeping for normalization and amplified with specific primers mGAPDH_F and mGAPDH_R. The histograms represent the quantitative fold change of the ratio of hSmn2 Δ7 to FL transcripts in different tissues of transgenic SMA mice sacrificed at the indicated age. For each tissue, expression level of P10 pups is set to 1. Data are expressed as mean ± SD of at least 3 mice for each age. Statistical analysis was performed using One-way ANOVA (ns: not significant; * $p<0,05$; ** $p<0,01$; ***$p<0,001$).

4.3 Analysis of the Pattern of Inclusion Ratio (PIR) for Elp1 exon 20 and Smn2 exon 7 in FD and SMA mouse models

To compare the effect that age has on the two splicing events in FD and SMA mouse models, I evaluated the pattern of inclusion ratio (PIR), which is a graphical representation of the age-dependent changes in splicing. To do this analysis, I evaluated the RT-PCR data presented in Figure 4.1 and Figure 4.2 dividing the percentage of exon inclusion obtained at each time-point by the percentage of exon inclusion at P10; considering seven tissues (brain, spinal cord, muscle, liver, lungs, kidney and heart) I identified four different PIRs: down-steady, down-up, up-steady and steady-steady, where the first term refers to the period of time between P10 and P90 and the second one to the period of time between P90 and P365 (Figure 4.3 A). As can be seen in Figure 4.3, in the majority of the tissues analysed, age has a different effect on the two splicing events. In brain and spinal cord, Elp1 exon 20 showed a down-steady PIR whereas Smn2 exon 7 showed a down-up PIR, meaning that both exons inclusion levels went down between P10 and P90 but followed different patterns at later time point (Figure 4.3 B and C). Concerning muscle, liver and lung, Elp1 recapitulated the PIR seen in the CNS (down-steady) but Smn2 showed an up-steady PIR, opposite to the one detected in the CNS (Figure 4.3 D – F). In kidney, I observed a steady-steady PIR for Elp1 exon 20 and an up-steady PIR for Smn2 exon 7 (Figure 4.3 G), whereas in heart both splicing events shared a steady-steady PIR (Figure 4.3 H). Taken together, these results suggest that Elp1 exon 20 and Smn2 exon 7 AS are differently modulated in an age-dependent manner and in a tissue-specific fashion.

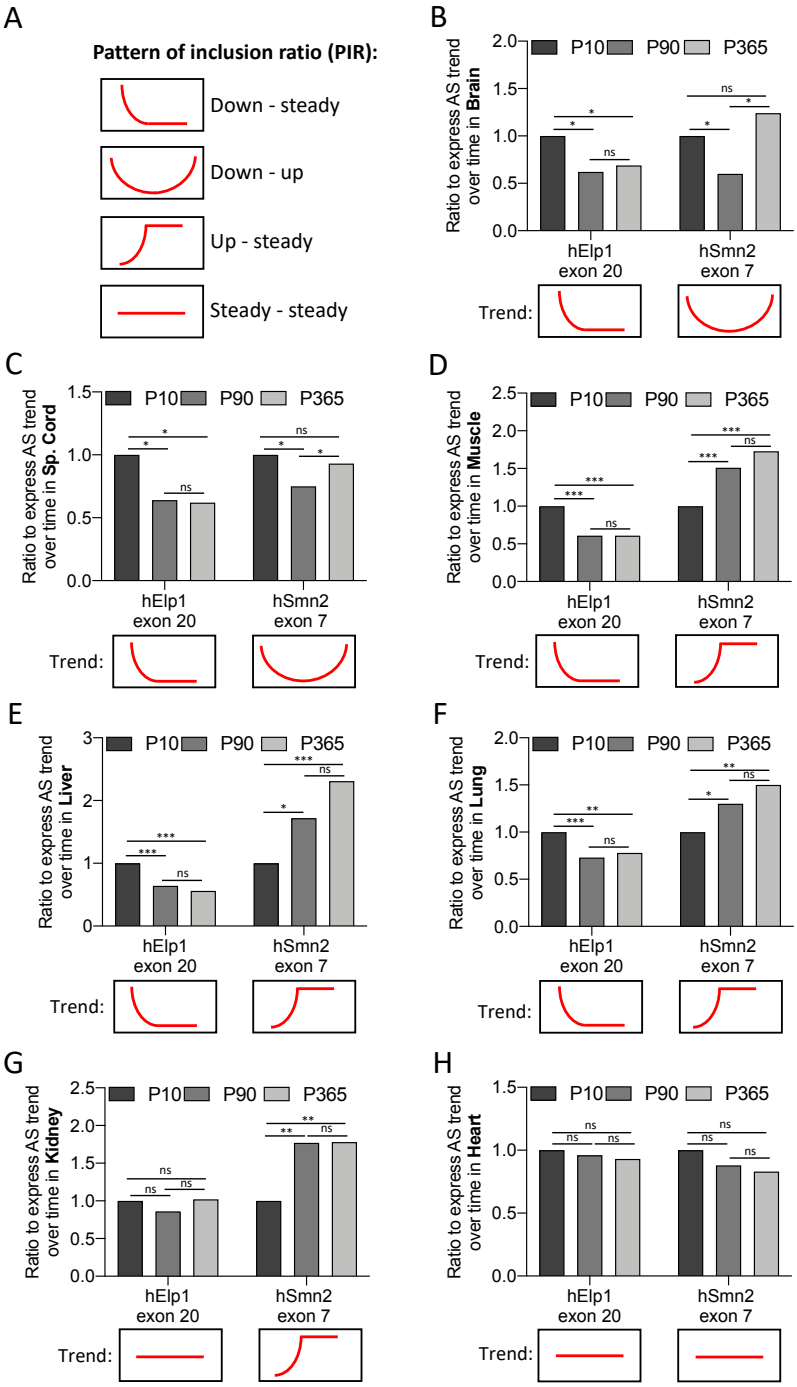

Figure 4.3: ***Elp1 exon 20 and Smn2 exon 7 defective splicing events show a different Patterns of Inclusion Ratio over time.***

A) Schematic representation of the four Pattern of Inclusion Ratio (PIR) that described the trend of Elp1 exon 20 and Smn2 exon 7 splicing events over lifespan. The first term refers to the period between P10 and P90 whereas the second term refers to the period between P90 and P365. **B-H**) For each tissue, the percentage of exon inclusion at P10, P90 and P365 quantified from Figure 4.1 (for FD splicing) and Figure 4.2 (from SMA splicing) was divided by the percentage of exon inclusion at P10 of Elp1 exon 20 (left bars) and Smn2 exon 7 (right bars), respectively. In this manner, for each splicing, the percentage of exon inclusion at P10 is set to 1. Rectangles below graph enclose the PIR (or trend) of the Elp1 exon 20 and Smn2 exon 7 splicing events, respectively, at different time points. Statistics of Figure 4.1 and Figure 4.2 was kept in order to delineate the PIRs.

4.4 Age-dependent effect on the total amount of Elp1 and Smn2 mRNA transcripts

Since the age-dependent severity of the FD and SMA phenotypes may be also due to changes in the total amount of the corresponding Elp1 and Smn2 transcripts, I also assessed the total mRNA expression levels over lifespan. To do so, following total RNA extraction, I analyzed tissues samples by qRT-PCR with human specific primers (Elp1_TOT_F and Elp1_TOT_R for Elp1 and Smn2_TOT_F and Smn2_TOT_R for Smn2) that bind on two exons that are constitutively included in both full-length and Δexon isoforms and I expressed the results as fold change setting to 1 the level of expression of P10 pups. In the FD mouse model, most of the tissue did not show changes in total hElp1 mRNA neither during post-natal development nor at later time point (Figure 4.4 D – I). Only three tissues showed a significant change at post-natal development; I observed a strong ~5-fold and a ~1.8-fold decrease in muscle and eyes, respectively, between P10 and P90 (Figure 4.4 A and B) and a ~1.5 increase of Elp1 mRNA in lung over the same period of time (Figure 4.4 C). In SMA mouse, I detected three tissues with a significant decrease in total Smn2 mRNA during post-natal development and only one tissue that showed an increase over this period of time. Specifically, in muscle and kidney I detected a ~5-fold decrease between P10 and P90 (Figure 4.5 A and B), whereas in lung I observed a ~2-fold decrease (Figure 4.5 C); on the other hand, liver showed a ~1.8-fold increase in Smn2 mRNA level (Figure 4.5 D). Interestingly, this tissue was the only one in which I detected a significant change in the total amount of Smn2 transcripts showing a ~2-fold decrease between P90 and P365. On the other hand, brain, spinal cord and heart did not show changes in total Smn2 mRNA over time (Figure 4.5 E, F and G).

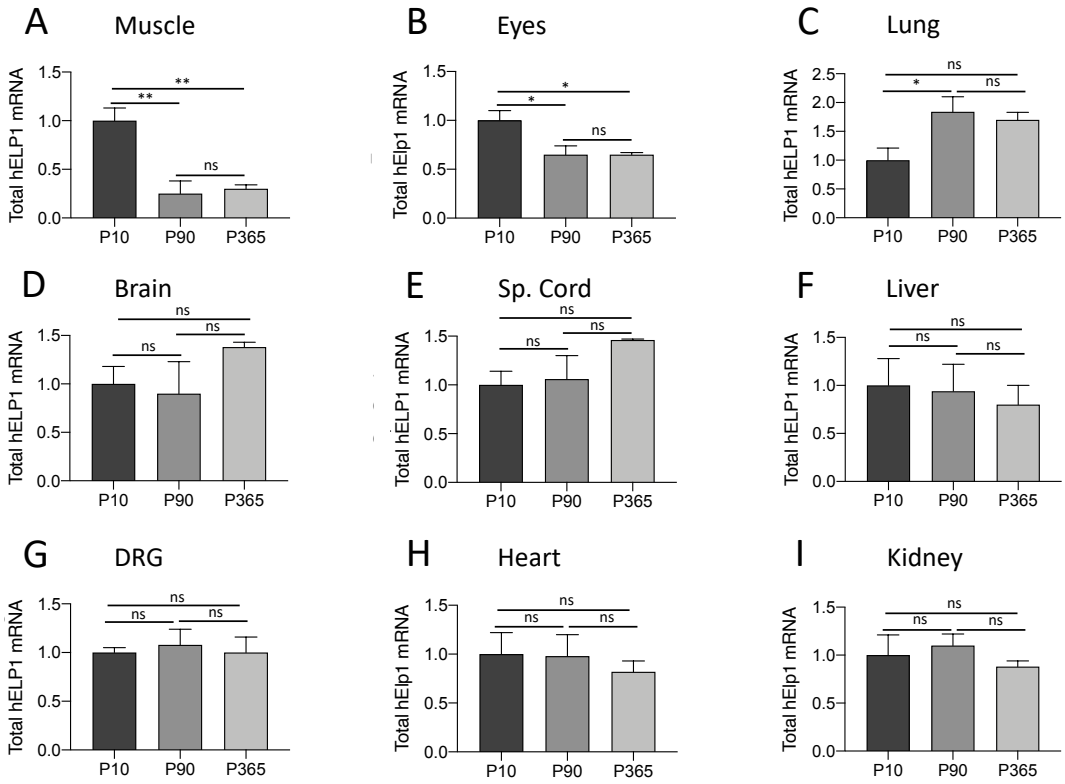

Figure 4.4: ***Total hELP1 mRNA reveals an age-dependent and tissue-specific signature over lifespan in FD model.***

A-I) Sybr-based qPCRs were performed using human-specific primers Elp1_TOT_F and Elp1_TOT_R primers for total Elp1 transcripts. Endogenous GAPDH was used as housekeeping for normalization and amplified with specific primers mGAPDH_F and mGAPDH_R. The histograms represent the quantitative fold change of the total hElp1 transcripts in different tissues (muscle, eyes, lungs, brain, spinal cord, liver, dorsal root ganglia, heart and kidney) of transgenic FD mice sacrificed at P10, P90 and P365. For each tissue, expression level of P10 pups is set to 1. Data are expressed as mean ± sem of 3 mice for each age. Statistical analysis was performed using One-way ANOVA (ns: not significant; * $p<0,05$; ** $p<0,01$; ***$p<0,001$).

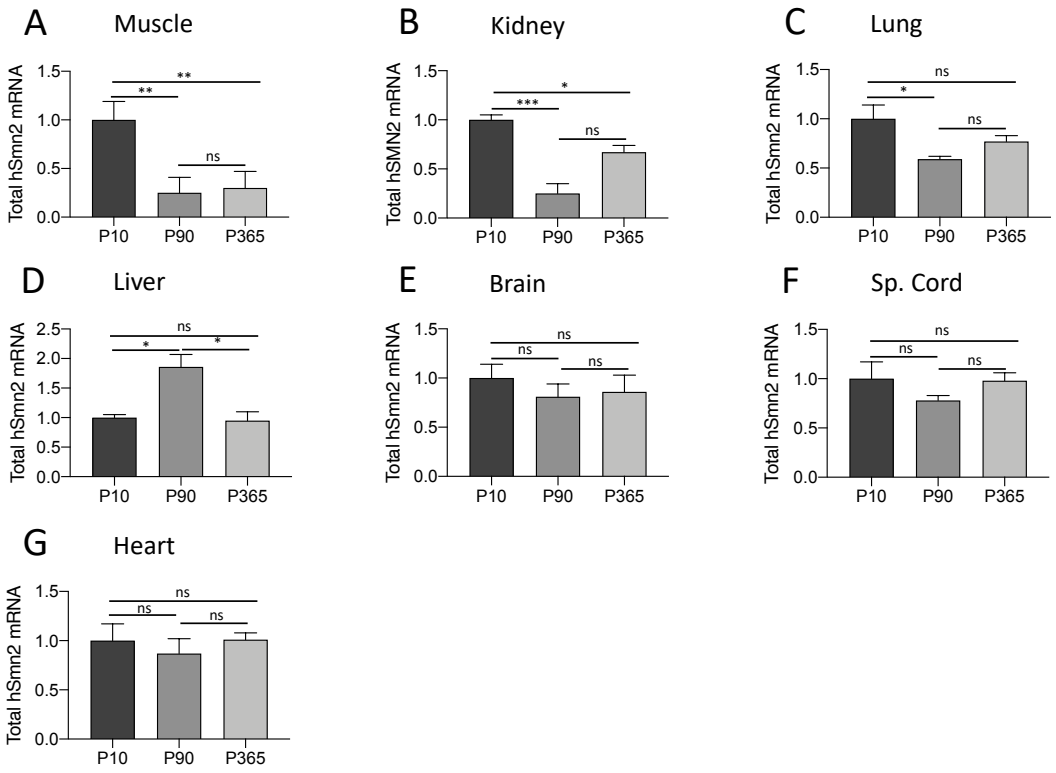

Figure 4.5: ***Total hSmn2 mRNA reveals an age-dependent and tissue-specific signature over lifespan in SMA model.***

A-G) Sybr-based qPCRs were performed using human-specific primers Smn2_TOT_F and Smn2_TOT_R primers for total Smn2 transcripts. Endogenous GAPDH was used as housekeeping for normalization and amplified with specific primers mGAPDH_F and mGAPDH_R. The histograms represent the quantitative fold change of the total hSmn2 transcripts in different tissues (muscle, kidney, lungs, liver, brain, spinal cord and heart) of transgenic SMA mice sacrificed at P10, P90 and P365. For each tissue, expression level of P10 pups is set to 1. Data are expressed as mean ± sem of 3 mice for each age. Statistical analysis was performed using One-way ANOVA (ns: not significant; * $p<0,05$; ** $p<0,01$; ***$p<0,001$).

4.5 Changes in RNA binding proteins mRNA levels in FD and SMA mouse models

To evaluate potential age-dependent changes in expression of RNA Binding Proteins (RBPs), I analyzed by qRT-PCR total RNA from brain, muscle and liver in the FD and SMA mice. For Elp1, I focused on six splicing factors previously described to be involved in regulation of exon 20: three inhibitory (hnRNP A1, SRSF3 and FUS) (Donadon et al., 2018) and three enhancing (RBM24, RBM38 and SFPQ) (Ohe et al., 2017). For SMA, I analyzed a panel of nine RBPs: hnRNP A1, SAM68, SRSF2 and SRSF3, known to be inducer of exon 7 skipping and TIA1, TRA2β, SFPQ, SRSF9 and SRSF1, known to be inducers of exon 7 inclusion (Wee et al., 2014). For each RBP, I evaluated that the amplification efficiency of primers was comparable, and the results of qRT-PCR were expressed as fold change, setting to 1 the level of expression of P10 pups. In brain of FD mice, I observed a strong ~5-fold decrease of hnrnpA1 between P10 and P90 and no further change at later age. Srsf3 showed a ~2-fold decrease between P10 and P90 and then returned to normal levels at P365. Fus levels remained almost unchanged (Figure 4.6 A). Among the enhancing factors, I observed a significant decrease of Rbm38 (~5-fold) and Sfpq (~2-fold) between P10 and P90 and no further change at later age (Figure 4.6 B). Rbm24 showed a not significant progressive age-dependent decrease (Figure 4.6 B). In muscle of Elp1 mice, I observed a decrease of the three inhibiting splicing factors and of Sfpq between P10 and P90 and no further change at later ages. In contrast, Rbm38 and Rbm24 levels remained unmodified, probably because they are regulators of AS in this tissue (Figure 4.6 C and D) (Miyamoto et al., 2009; Yang et al., 2014). In liver of Elp1 mice, I observed an age-dependent decrease of the three inhibiting splicing factors and of Sfpq, a strong ~5-fold decrease of Rbm38 between P10 and P90 and no further change at later ages. Rbm24 was not affected (Figure 4.6 E and F). In brain of SMA mice, among the inhibitory factors, hnrnpA1 (~2.5-fold) and Srsf3 (~1.5-fold) significantly decreased during post-natal development and at later age, whereas Srsf2 showed a ~2-fold decrease between P10 and P365 and Sam68 a steep but not significant decrease overt time (Figure 4.7 A). Enhancing factors Tia1, Tra2β and Sfpq showed a strong decrease, from ~4- to ~5-folds, between P10 and P90 and their levels remained the same at later age. Srsf1 modestly decrease at P365 and Srsf9 did not change over time (Figure 4.7 B). In muscle of SMA mice, I observed a strong and general decrease, from ~3- to ~4- folds, in the expression level of all inhibiting and enhancing factors between P10 and P90 and no

further alterations at P365 (Figure 4.7 C and D). In contrast, in liver of SMA mice, I observed a ~2-fold age-dependent decrease of hnrnpA1 and Srfs3, the latter not showing significant changes at later age (Figure 4.7 E). Among the enhancing factors, all of them showed a robust ~2-fold decrease between P10 and P90; at later age, Tia1, Tra2β and Srsf9 expression levels remained low, Srsf1 did not change significantly and Sfpq returned to normal level (Figure 4.7 F). Collectively, my results suggest that the expression levels of these RBPs show an age- and tissue- dependent changes, with the greater difference occurring between P10 and P90.

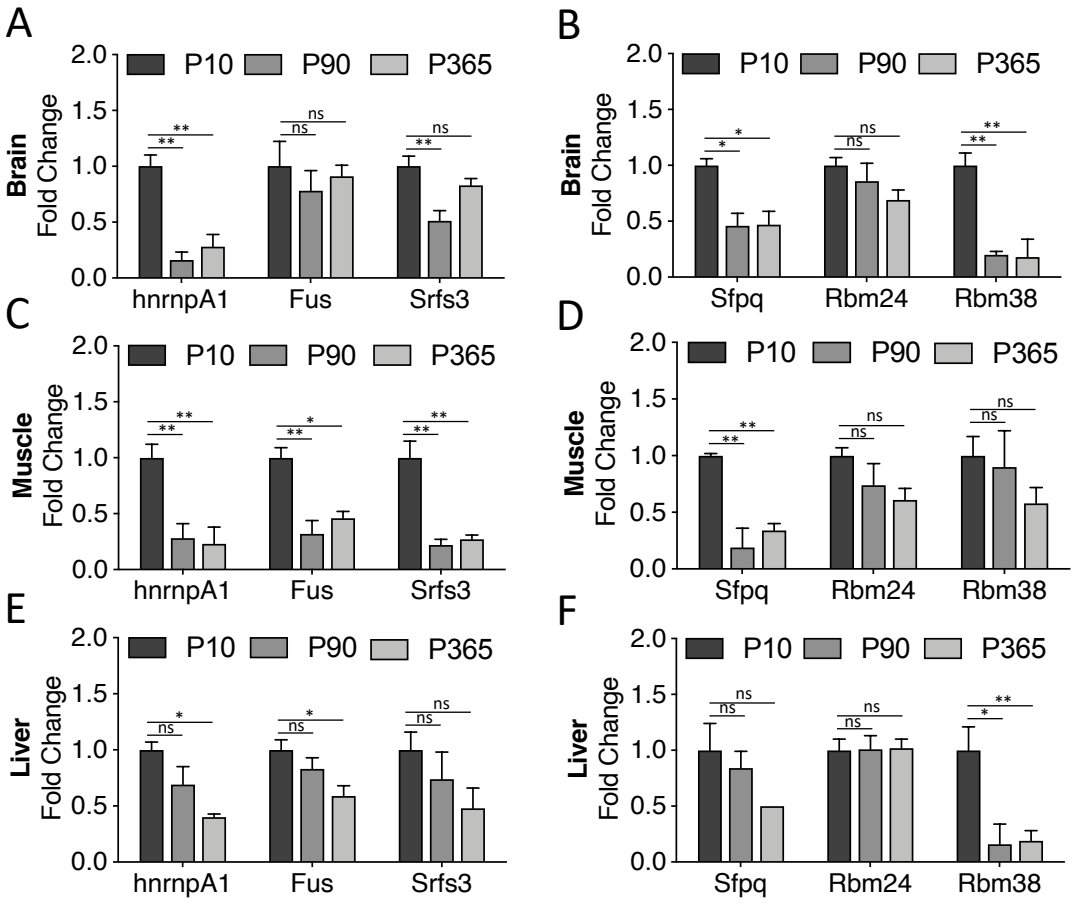

Figure 4.6: ***Age-dependent changes in the expression level of RNA binding protein mRNA in FD model.***

Sybr-based qPCRs were performed using specific primers for each RBP (Table 3.3) and endogenous GAPDH was used as housekeeping for normalization and amplified with specific primers mGAPDH_F and mGAPDH_R. The histograms represent the quantitative fold change of three inhibiting (hnRNPA1, Fus, Srsf3) and three enhancing (Sfpq, Rbm24 and Rbm38) factors that act on Elp1 exon 20 splicing in **A, B**) brain, **C, D**) muscle and **E, F**) liver of transgenic FD mice sacrificed at P10, P90 and P365. In each tissue, expression level of P10 pups is set to 1. Data are expressed as mean ± SD of 3 mice for each age. Statistical analysis was performed using One-way ANOVA (ns: not significant; * $p<0,05$; ** $p<0,01$; *** $p<0,001$).

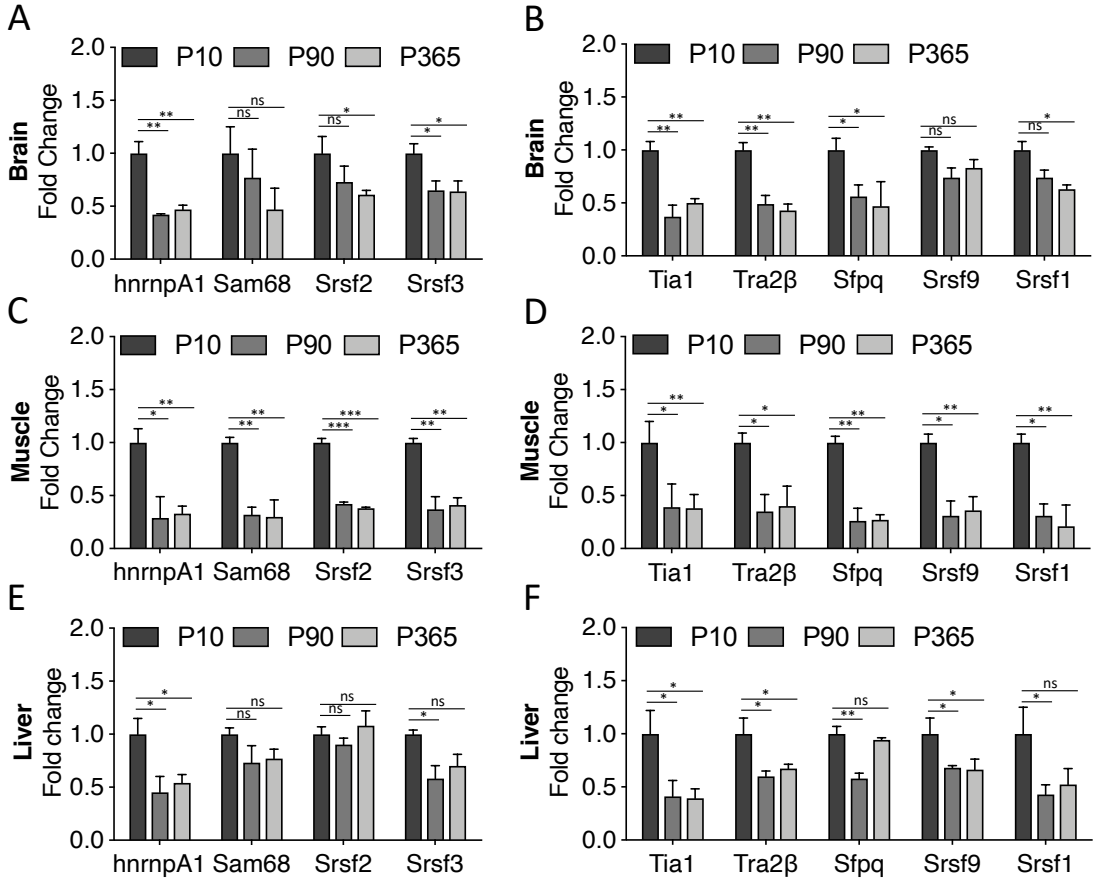

Figure 4.7: ***Age-dependent changes in the expression level of RNA binding protein mRNA in SMA model.***

Sybr-based qPCRs were performed using specific primers for each RBP (Table 3.3) and endogenous GAPDH was used as housekeeping for normalization and amplified with specific primers mGAPDH_F and mGAPDH_R. The histograms represent the quantitative fold change of four inhibiting (hnRNPA1, Sam68, Srsf2, Srsf3) and five enhancing (Tia1, Tra2β, Sfpq, Srsf9 and Srsf1) factors that act on Smn2 exon 7 splicing in **A, B**) brain, **C, D**) muscle and **E, F**) liver of transgenic SMA mice sacrificed at P10, P90 and P365. In each tissue, expression level of P10 pups is set to 1. Data are expressed as mean ± SD of 3 mice for each age. Statistical analysis was performed using One-way ANOVA (ns: not significant; * $p<0,05$; ** $p<0,01$; *** $p<0,001$).

4.6 Analysis of RNA Polymerase II density profile and histone H3 lysine tri-methylation in FD mouse model

To understand the possible contribution of RNA Polymerase II (Pol II) and chromatin in regulating defective splicing I focused on the FD mouse model performing Chromatin Immunoprecipitation assay. This analysis was performed against the main subunit of Pol II (RPB1) and four tri-methylated lysines. By qPCR (ChIP-qPCR) I evaluated with human-specific primers the density profile of these targets on three regions of human Elp1 mutated gene: exon 10, exon 20 and exon 29. I chose these three genomic regions to cover most of the Elp1 gene: exons 10 and 29 are two constitutive spliced exons that lay ~16.5 kb and ~10.8 kb upstream and downstream, respectively, from the alternative spliced exon 20 (Figure 4.8 A). The specific pair of primers were design on the intron-exon boundary to selectively amplify human Elp1 gene (Figure 4.8 B). Next, I extracted genomic DNA (gDNA) from the liver of FD and I evaluated the specificity of my set of primers separating PCR products by electrophoresis on 1.5% gel. Liver from SMA mice and HEK 293T cells were used as negative and positive controls for the human specific primers. The presence of amplification in samples derived from FD mouse and HEK 293T cells, but not from SMA mouse, confirmed that my sets of primers correctly amplified only the human Elp1 gene and not the mouse homolog (Figure 4.8 C). Next, I evaluated the amplification efficiency for each set of primers; as shown in Figure 4.8 D, each graph represents calibration curves on Cyles – RFU cartesian coordinate system. The values of Slope and Efficiency calculated on calibration curves are included in the respective ranges, showing that these set of primers amplified exon 10, exon 20 and exon 29 with the same efficiency (Slope between 3.1 and 3.6 and Efficiency between 90 and 110%).

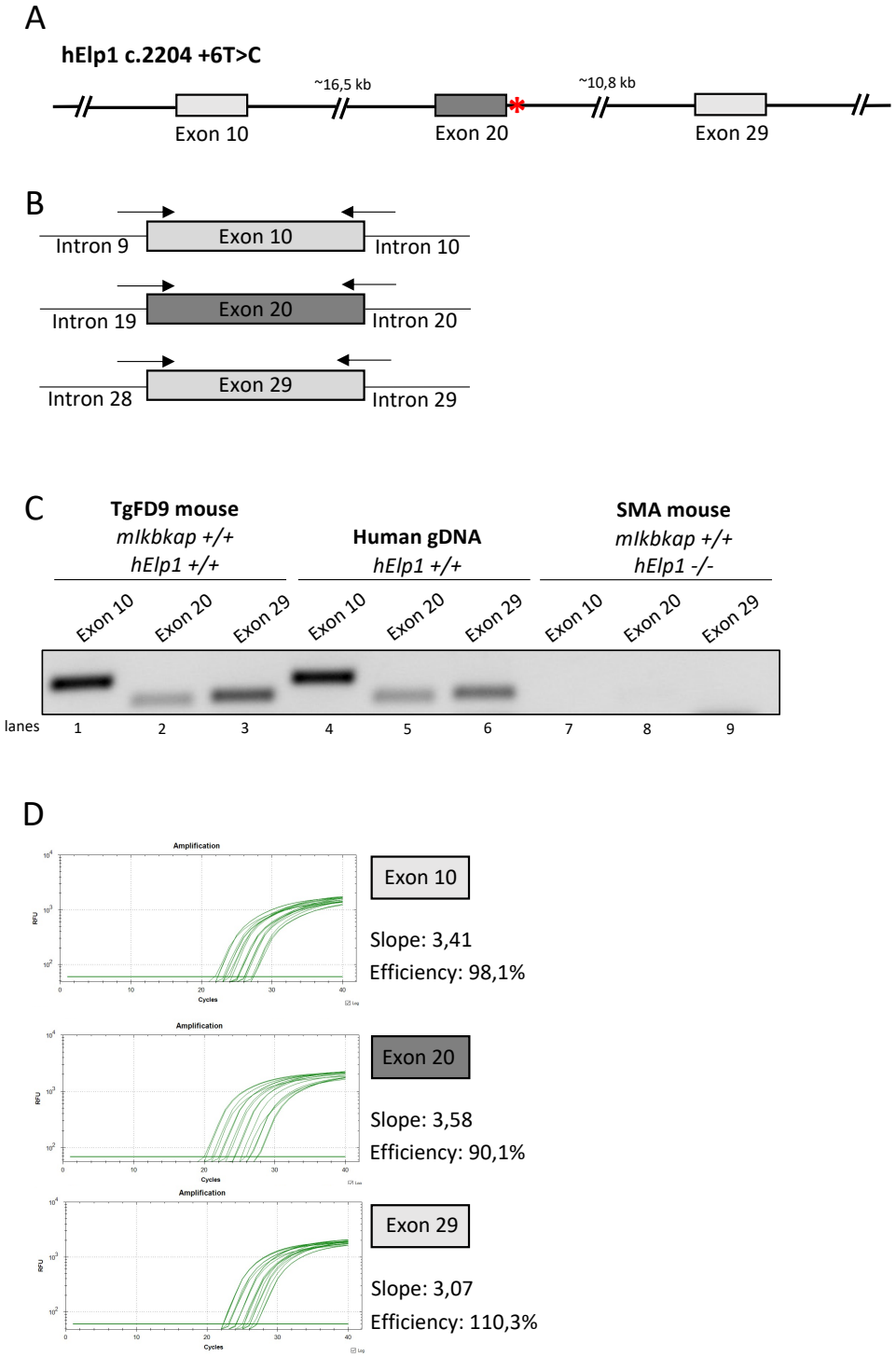

Figure 4.8: ***ChIP-qPCR primers amplify specifically hElp1 exon 10, exon 20 and exon 29 with comparable efficiency.***

A) Schematic representation of the human Elp1 gene: boxes represent exons whereas lines represent the sequence of the gene. The distance between exon 10 and exon 20 and exon 20 and exon 29, respectively, is indicate above. The c.2204 +6T>C mutation is indicated as a red asterisk. **B**) Schematic representation of the genomic DNA (gDNA) boundaries intron 9-exon 10-intron 10, intron 19-exon 20-intron 20 and intron 28-exon 29-intron 29. Arrows upon the boundaries indicate the position of the primers used for qPCR amplification:

ChIP_Elp1_ex10_F and ChIP_Elp1_ex10_R for exon 10, ChIP_Elp1_ex20_F and ChIP_Elp1_ex20_R for exon 20 and ChIP_Elp1_ex29_F and ChIP_Elp1_ex29_R for exon 29. **C**) gDNA extracted from TgFD9 mouse, human HEK 293T cells and SMA mouse was amplified with primers for exon 10, exon 20 and exon 29. Bands corresponds to exon 10 (142 bp), exon 20 (100 bp) and exon 29 (104 bp). As expected, only human Elp1 gDNA was amplified (lanes 1, 2, 3, 4, 5 and 6). **D**) Levels of exon 10, exon 20 and exon 29 on gDNA were determined by three qPCR reactions to show their equivalent efficiencies. gDNA 1:2 dilutions were used as template to determine the efficiencies of qPCR reactions. Primers used for the amplification are the ones reported above. Calibration curves show that slope and efficiency values lie between ranges, thus allowing to compare them directly. Data are expressed as mean of two independent experiments.

4.7 RNA Polymerase II density profile along human Elp1 gene shows an age-dependent decrease in liver and brain of FD mouse

Once the protocol to perform ChIP-qPCR analysis was set, I performed Pol II ChIP-qPCR on liver and brain in the FD animal model; I decided to focus on these two tissues since they showed the most relevant and interesting changes in splicing over time. At P10, P90 and P365 samples were cross-linked with formaldehyde, quenched with Glycine, homogenized and centrifuged to pellet nuclei. After the lysis of nuclei membranes, chromatin was sonicated to a size range of 200-1000 bp. Then, I performed the ChIP using the antibody against Pol II and an IgG as negative control. After, the ChIP IP DNA was de-crosslinked, purified and amplified by qPCR. I normalized IP DNA on the % of input and expressed data as fold change, where I set to 1 Pol II density profile at P10. Interestingly, the density profile of Pol II showed a consistent age-dependent decrease on the three genomic regions considered: exon 10, exon 20 and exon 29. In liver, within 3 months of age, I observed from ~ 2.5- to ~5-folds decrease in the density profile of Pol II in the regions surrounding exon 10, exon 20 and exon 29, whose level remained steady at later time point along human Elp1 gene (Figure 4.9 A, B and C). Interestingly, I found a similar trend in the brain, in which Pol II density profile significantly decreased from ~ 2.5- to ~ 4-folds between P10 and P90 and remained at the same low level between P90 and P365 (Figure 4.9 D, E and F). Only exon 20 showed a small enrichment of Pol II at P365, although this level is ~ 2-fold lower compared to the one at P10 (Figure 4.9 E). Taken together, these results indicate that there is an age-dependent decrease in the total amount of Pol II in the body of the Elp1 gene. Interestingly, this age-dependent decrease in Pol II density occurs both on constitutive (exon 10 and 29) and alternative spliced exons (exon 20). As alterations in Pol II density profile have been shown to impact alternative splicing of different genes (Fong et al., 2014), my results suggest that the age-dependent changes in Pol II elongation I have observed might affect the alternatively spliced exon 20 but not the other constitutive exons 10 and 29.

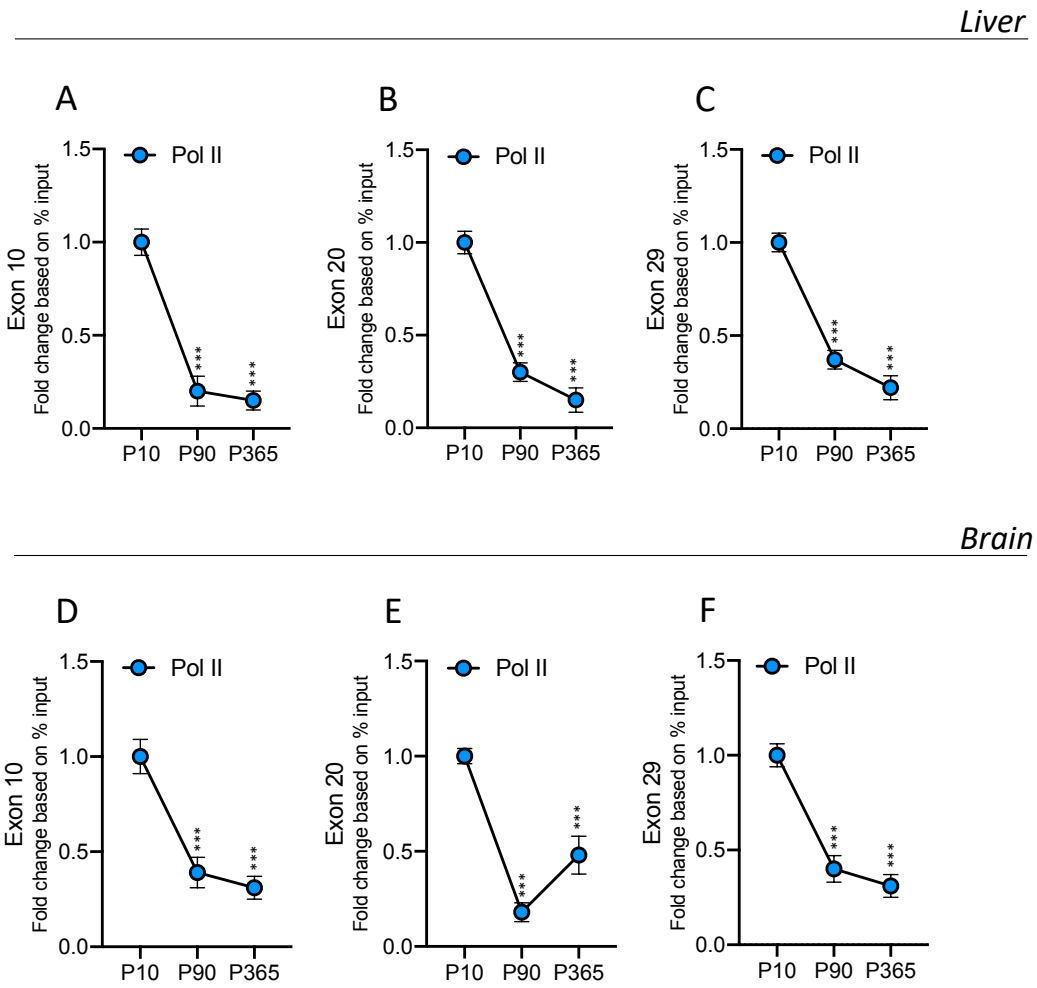

Figure 4.9: ***Pol II-ChIP-qPCR analysis on Elp1 exon 10, exon 20 and exon 29 reveals an age-dependent drop in Pol II density profile in liver and brain in FD mouse model.***

Mice were sacrificed at P10, P90 and P365 and liver (**A**, **B** and **C**) and brain (**D**, **E** and **F**) were harvested. The cross-linked and shared chromatin was immunoprecipitated with the indicated antibodies: IgG and anti-RBP1 Pol II. After reversal of the cross-linking and purification of the DNA, qPCR was used to detect the sequences corresponding to exon 10, exon 20 and exon 29 with specific primers: ChIP_Elp1_ex10_F and ChIP_Elp1_ex10_R for exon 10, ChIP_Elp1_ex20_F and ChIP_Elp1_ex20_R for exon 20 and ChIP_Elp1_ex29_F and ChIP_Elp1_ex29_R for exon 29. 5% input was used to normalization. For exon 10 (left panels), exon 20 (middle panels) and exon 29 (right panels), the graphs represent the fold change based on the % of input of P10 pups set to 1. Data are expressed as mean ± sem of at least 3 mice for each age. Statistical analysis was performed using One-way ANOVA (ns: not significant; ***p<0,001).

4.8 Age-dependent changes in the histone H3 lysines methylation status in liver and brain of FD mouse model

As changes in the Pol II density profile may be due to alteration in the chromatin status (Giono & Kornblihtt, 2020), I have evaluated four different histone modifications that have been associated with permissive or repressive gene expression. Specifically, I focused on tri-methylation of lysine 4, 36, 9 and 27 of histone H3 (H3K4me3, H3K36me3, H3K9me3 and H3K27me3), those clusters that alter chromatin structural organization and are associated with active (H3K4me3 and H3K36me3) or repressive (H3K9me3 and H3K27me3) transcription (Weaver et al., 2017). In the FD mouse model, I evaluated the density profile of these 4 histone marks on human Elp1 in two representative tissues, liver and brain, at P10, P90 and P365. ChIPs were performed on exon 10, exon 20 and exon 29 using the antibody against total histone H3, my four targets and an IgG as negative control. IP DNA was normalized on the % of input and total histone H3 and data were expressed as fold change relative to P10 for the three exons. In liver, the H3K4me3 density profile on the three exons showed slight but not significant decrease between P10 and P90, followed by minimal variations between P90 and P365; H3K36me3 density profile slightly increased during post-natal development and slightly decreased at later time point (Figure 4.10 A, B and C). When I looked at the density profiles of the repressive marks, H3K9me3 did not undergo any significant variation over lifespan along hElp1 gene whereas H3K27me3 constantly increased over time along the three exons analyzed. Indeed, in liver I observed a ~2- ~3-folds increase in H3K27me3 density profile within 3 months of age followed by a further ~2.5- ~3.5-folds increase between P90 and P365 in exons 10, 20 and 29 (Figure 4.10 A, B and C). ChIP-qPCR experiments performed in brain revealed similar results. Specifically, density profiles of the permissive chromatin marks (H3K4me3 and H3K36me3) displayed the same increasing trend on all exons over lifespan, whereas H3K9me3 enrichment increased within 3 months to then decrease at later age slightly (Figure 4.10 D, E and F). H3K27me3 showed a striking age-dependent change: H3K27me3 increased from ~10- to ~15-folds between P10 and P90 and from ~25- to ~30-folds between P10 and P365 (Figure 4.10 D, E and F). All together, I observed a significant age-dependent increase in the H3K27me3 repressive mark in both liver and brain of the FD mice both on the constitutive (exon 10 and exon 29) and alternative (exon 20) spliced Elp1 exons. Interestingly, as the age-dependent increase of the H3K27me3 mark in liver and brain correlates with a decrease of the RNA polymerase

II density (Figure 4.9) and with a decrease in exon 20 inclusion (Figure 4.1 A and D), it is possible that this chromatin modification, affecting the Pol II elongation, might negatively regulate exon 20 alternative splicing.

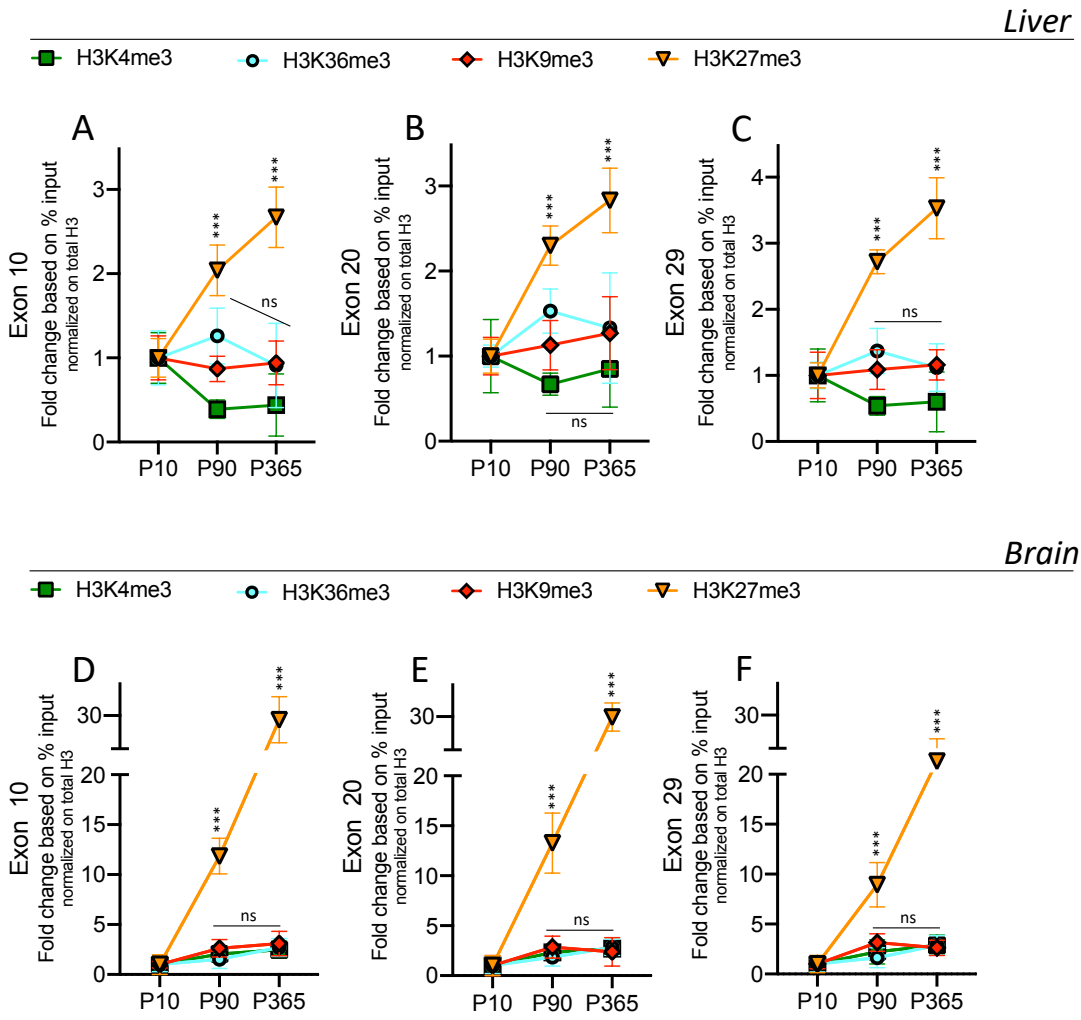

Figure 4.10: ***ChIP-qPCR on H3Ks tri-methylation show age-dependent changes along Elp1 gene in liver and brain in FD mouse model.***

Mice were sacrificed at P10, P90 and P365 and liver (**A**, **B** and **C**) and brain (**D**, **E** and **F**) were harvested. The cross-linked and shared chromatin was immunoprecipitated with the indicated antibodies: IgG, anti-total H3, anti-H3K4me3, anti-H3K36me3, anti-H3K9me3 and anti-H3K27me3. After reversal of the cross-linking and purification of the DNA, qPCR was used to detect the sequences corresponding to exon 10, exon 20 and exon 29 with specific primers: ChIP_Elp1_ex10_F and ChIP_Elp1_ex10_R for exon 10, ChIP_Elp1_ex20_F and ChIP_Elp1_ex20_R for exon 20 and ChIP_Elp1_ex29_F and ChIP_Elp1_ex29_R for exon 29. 5% input and total H3 were used to normalization. For exon 10 (left panels), exon 20 (middle panels) and exon 29 (right panels) the graphs represent the fold change based on the % of input of P10 pups set to 1 for each histone lysine modification. Data are expressed as mean ± sem of at least 3 mice for each age. Statistical analysis was performed using One-way ANOVA (ns: not significant; ***p<0,001).

4.9 H3K27me3/H3 ratio globally increases in liver and brain of FD model in an age-dependent manner

To understand if the age-dependent increase in the H3K27me3 mark on the hElp1 gene is related to a global change in H3K27me3, I analyzed the ratio between H3K27me3 and H3 (H3K27me3/H3) on total liver and brain protein extracts. Protein extracts from liver and brain of FD mice sacrificed at P10, P90 and P365 were analyzed in immunoblot experiments with one antibody against total H3 and another specific for the K27 trimethylation. The H3K27me3 and total H3 levels were evaluated using mouse monoclonal and rabbit polyclonal antibodies, respectively, and GAPDH was used as housekeeping loading control. I quantified the bands with ImageJ software and data expressed the H3K27me3/H3 ratio as fold change, setting to 1 the P10 samples. In liver, I observed an approximately 1.7-fold increase in the H3K27me3/H3 ratio between P10 and P90 and a slight decrease at the later time point (Figure 4.11 A and B). Interestingly, the same analysis in brain revealed a ~2.5 times increase in the H3K27me3/H3 ratio during post-natal development and a robust ~5.5 times increase when I compared P365 to P10 enrichment (Figure 4.11 C and D). The P365 increase in the H3K27me3/H3 ratio is mainly due to a relative decrease in the total amount of histone H3. Collectively, these results indicate that in liver and brain the age-dependent increase of the H3K27me3 mark occurs both on the Elp1 gene and in the entire tissue.

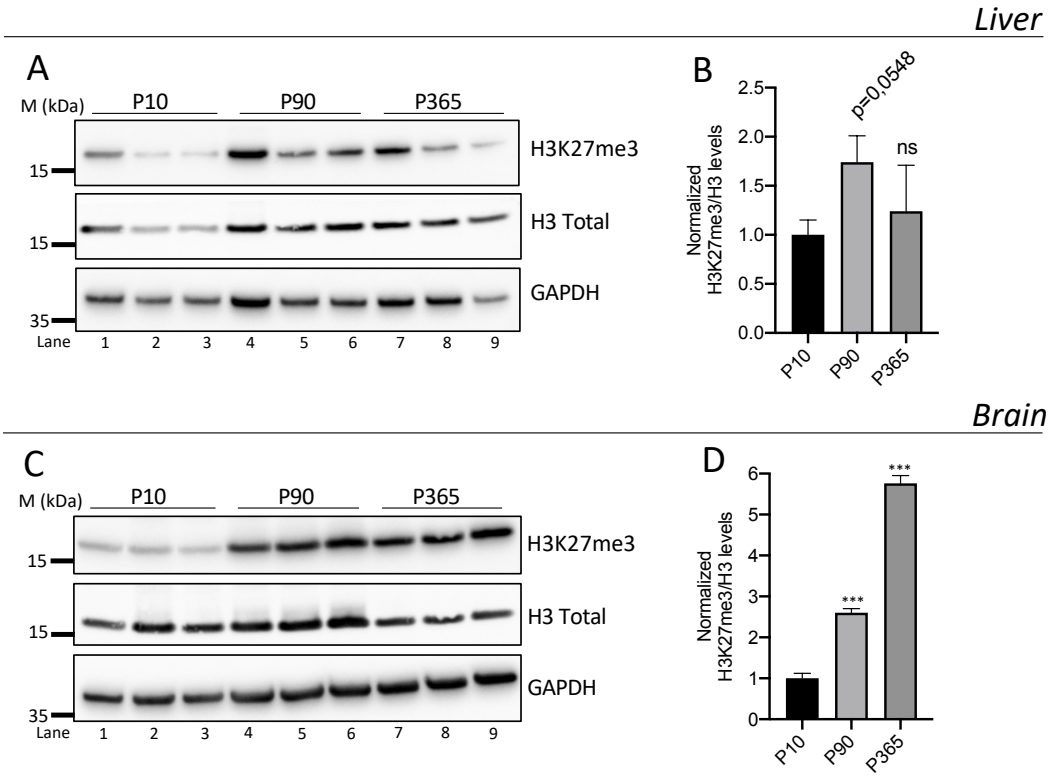

Figure 4.11: ***The global H3K27me3/H3 ratio increases in an age-dependent manner in liver and brain protein extracts of FD mouse.***

Western blot analysis of H3K27me3 and total H3 in (**A**) liver and (**C**) brain of FD mice sacrificed at P10 (lane 1-3), P90 (lane 4-6) and P365 (lane 7-9). For H3K27me3 monoclonal antibody was used; for total H3 polyclonal antibody was used. GAPDH was used as housekeeping loading control. The graph represents the quantification analysis obtained with ImageJ software of the Western blot in (**B**) liver and (**D**) brain, respectively. The abundance of H3K27me3/H3 ratio of P10 pups is set to 1. Data are expressed as mean ± SD of 3 mice for each age. Statistical analysis was performed using One-way ANOVA (ns: not significant; ***p<0,001).

4.10 EED-226-mediatd inhibition of PRC2 reduces H3K27me3 and induces Elp1 exon 20 inclusion

To understand if the chromatin structure can influence Elp1 exon 20 splicing, I initially focused on H3K27me3, the modification that showed the most important age-dependent changes in liver and brain of the FD mouse model. To this aim, I tested the effect of a small molecule known to affect H3K27me3 status of chromatin in an *in vitro* minigene splicing assay. Tri-methylation of K27 on H3 is performed by the Polycomb Repressive Complex 2 (PRC2), whose core consists of three components: EZH2, which represents the catalytic subunit and deposits all three methylation states of K27 on H3 (H3K27me1/me2/me3), EED, a protein that binds the H3K27me3 deposited by EZH2 and ensures its propagation on adjacent nucleosomes and SUZ12, a zinc-finger protein. EED-226 is an allosteric and selective PRC2 inhibitor that binds to the H3K27me3 pocket of EED, leading to loss of PRC2 activity and causing a global H3K27me1/me2/me3 reduction (Lavarone et al., 2019; Qi et al., 2017). To test the contribution of H3K27me3, HEK 293T cells were transiently transfected with the Elp1 exon 20 minigene, in the presence or absence of EED-226. RNA was extracted and minigene splicing pattern was analyzed by RT-PCR. Interestingly, upon H3K27me3 reduction, exon 20 increased its inclusion by ~1.5-fold compared to DMSO-treated cells (Figure 4.12 A). In parallel, I also evaluated the effect of the drug on two constitutive spliced exons, the α-globin (HBA gene) exon 2 in the hybrid minigene and the endogenous Elp1 exon 10. Using specific primers (HBA_ex1_F1 and HBA_ex3edb_R2 for α-globin exon 2 and Ex9_F1 and Ex11_R1 for Elp1 exon 10), I performed RT-PCR analysis and PCR products were separated by electrophoresis on 1.5% agarose gel. The reduction in H3K27me3 status caused by EDD-226 addition did not alter their splicing pattern (Figure 4.12 B and C). To confirm the efficacy of the chemical, after 24 hours I isolated total proteins and performed immunoblot to check the reduction of H3K27me3 in treated cells. Upon the EED-226 addition, the H3K27me3/H3 ratio decreased of ~ 60% compared to DMSO-treated cells (Figure 4.12 D and E). Collectively, these results demonstrate that a reduction in H3K27me3 levels mediated by the specific EED-226 inhibitor induces an increased inclusion of the alternative spliced Elp1 exon 20 but has no effect on other constitutive exons.

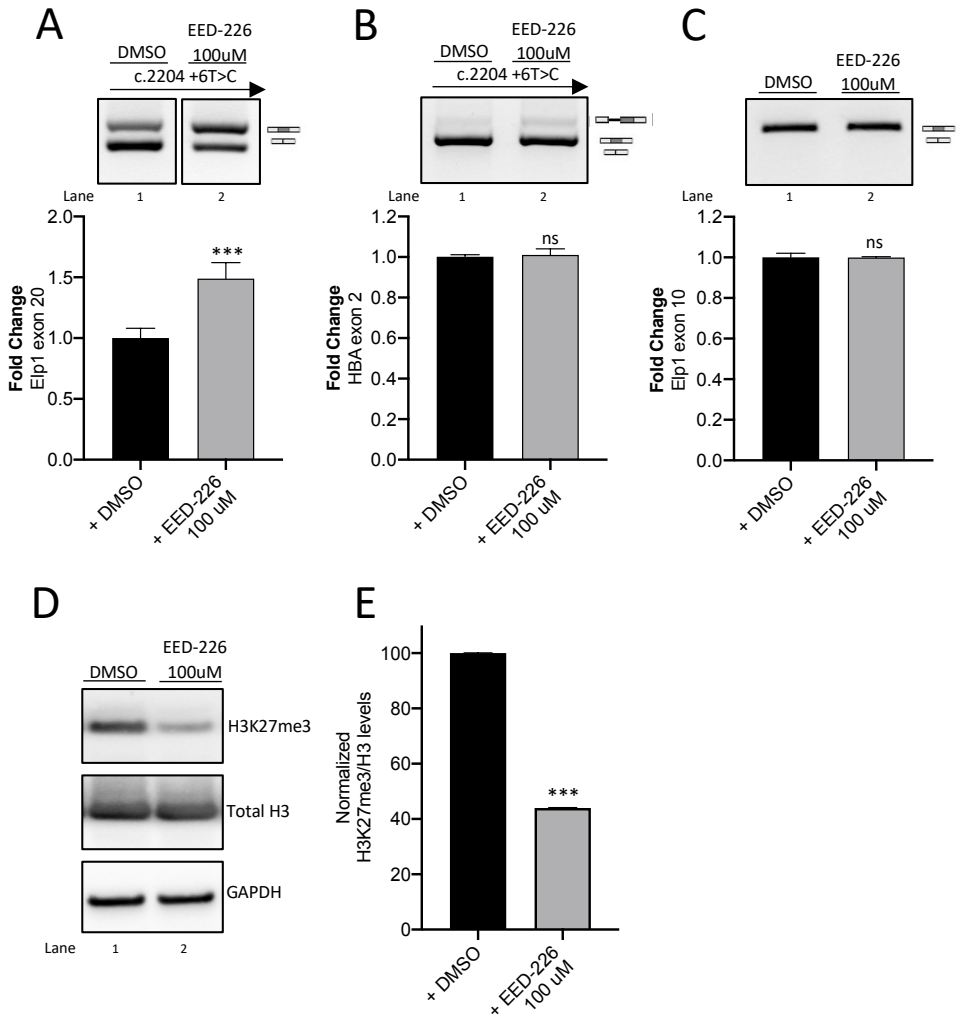

Figure 4.12: ***EED-226-mediated reduction of H3K27me3 increases Elp1 exon 20 inclusion in splicing assay.***

(**A**) HEK 293T cells were transfected with Elp1 mutant minigene and treated with DMSO or 100 uM of EED-226. After 24 hours total RNA was extracted, mRNAs produced were analysed through RT-PCR using α2,3_F and Elp1_ex21_R primers for Elp1 exon 20. The upper band of 349 bp corresponds to transcripts including the exon 20; the lower band of 275 bp to exon 20 skipping. PCR products were resolved on 1,5% agarose gel and the bands intensity was quantified with ImageJ software. Schematic representation of the splicing pattern is shown on the right of the RT-PCR gel analysis. Histogram below gel displays the % of Elp1 exon 20 inclusion expressed as fold change (DMSO-treated cells are set to 1). (**B**) HEK 293T cells were transfected with Elp1 mutant minigene and treated with DMSO or 100 uM of EED-226. After 24 hours total RNA was extracted, mRNAs produced were analysed through RT-PCR using HBA_ex1_F1 and HBA_ex3edb_R2 primers for HBA exon 2. The upper band of 386 bp corresponds to transcripts retaining intron 1; the lower band of 269 bp to spliced transcripts that include exon 2. PCR products were resolved on 1,5% agarose gel and the bands intensity was quantified with ImageJ software. Schematic representation of the splicing pattern is shown on the right of the RT-PCR gel analysis. Histogram below gel displays the % of HBA exon 2 inclusion expressed as fold change (DMSO-treated cells are set to 1). (**C**) After 24 hours from EED-226 (or DMSO) treatment, total RNA was extracted from HEK 293T cells, mRNAs produced were analysed through RT-PCR using Ex9_F1 and Ex11_R1 primers for endogenous Elp1 exon 10. The band of 202 bp corresponds to transcripts including exon 10. PCR products

were resolved on 1,5% agarose gel and the bands intensity was quantified with ImageJ software. Schematic representation of the splicing pattern is shown on the right of the RT-PCR gel analysis. Histogram below gel displays the % of Elp1 exon 10 inclusion expressed as fold change (DMSO-treated cells are set to 1). (**D**) Western blot analysis of H3K27me3 and total H3 in HEK 293T cells treated with DMSO (lane 1) or with EED-226 100 uM (lane 2). For H3K27me3, monoclonal antibody was used; for total H3, polyclonal antibody was used. GAPDH were used as reference for internal normalization. Representative samples are shown. (**E**) The graph represents the quantification analysis obtained with ImageJ software of the Western blot. The abundance of H3K27me3/total H3 ratio in DMSO-treated cells is set to 100. Data are expressed as mean ± SD of three independent experiments performed in triplicate. Statistical analysis was performed using Student t-test (ns: not significant; *** p<0,001).

4.11 The histone deacetylase inhibitor VPA induces Elp1 exon 20 inclusion

Next, to further dissect the relationship between Elp1 exon 20 splicing regulation and chromatin structure, I decided to evaluate the effect of a chemical that affects global acetylation levels. I transiently transfect HEK 293T cells with the Elp1 mutant minigene in the presence of Valproic acid (VPA), a histone deacetylase (HDAC) inhibitor known to create a more open chromatin structure that in turn promotes Pol II elongation (Jimeno-González & Reyes, 2016). After 24 hours RNA was extracted and minigene splicing pattern was analyzed by RT-PCR. Interestingly, in cells treated with VPA, exon 20 inclusion significantly increased by ~1.5-fold compared to untreated cells (Figure 4.13 A); furthermore, when I checked the splicing of α-globin exon 2 and Elp1 exon 10, I did not detect any changes in their patterns (Figure 4.13 B and C), suggesting that VPA-induced changes in chromatin affect the Elp1 alternative exon 20 but not other constitutive exons.

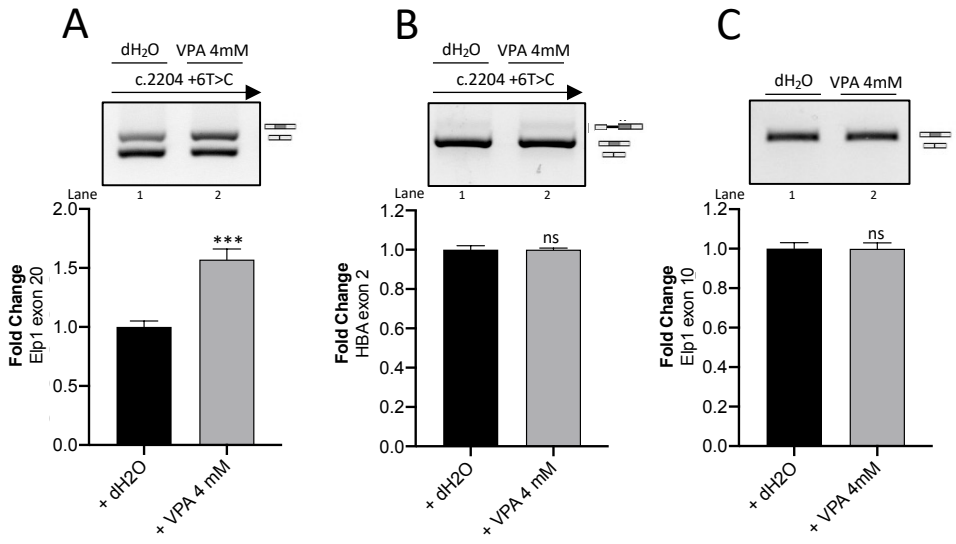

Figure 4.13: ***Valproic acid (VPA) increases Elp1 exon 20 inclusion in an in vitro splicing assay.***

(**A**) HEK 293T cells were transfected with Elp1 mutant minigene and treated with dH_2O or VPA 4 mM. After 24 hours total RNA was extracted, mRNAs produced were analysed through RT-PCR using α2,3_F and Elp1_ex21_R primers for Elp1 exon 20. The upper band of 349 bp corresponds to transcripts including the exon 20; the lower band of 275 bp to exon 20 skipping. PCR products were resolved on 1,5% agarose gel and the bands intensity was quantified with ImageJ software. Schematic representation of the splicing pattern is shown on the right of the RT-PCR gel analysis. Histogram below gel displays the % of Elp1 exon 20 inclusion expressed as fold change (dH_2O-treated cells are set to 1). (**B**) HEK 293T cells were transfected with Elp1 mutant minigene and treated with dH_2O or VPA 4mM. After 24 hours total RNA was extracted, mRNAs produced were analysed through RT-PCR using using HBA_ex1_F1 and HBA_ex3edb_R2 primers for HBA exon 2. The upper band of 386 bp corresponds to transcripts retaining intron 1; the lower band of 269 bp to spliced transcripts that include exon 2. PCR products were resolved on 1,5% agarose gel and the bands intensity was quantified with ImageJ software. Schematic representation of the splicing pattern is shown on the right of the RT-PCR gel analysis. Histogram below gel displays the % of HBA exon 2 inclusion expressed as fold change (dH_2O-treated cells are set to 1). (**C**) After 24 hours from VPA (or dH_2O) treatment, total RNA was extracted from HEK 293T cells, mRNAs produced were analysed through RT-PCR using Ex9_F1 and Ex11_R1 primers for endogenous Elp1 exon 10. The band of 202 bp corresponds to transcripts including exon 10. PCR products were resolved on 1,5% agarose gel and the bands intensity was quantified with ImageJ software. Schematic representation of the splicing pattern is shown on the right of the RT-PCR gel analysis. Histogram below gel displays the % of Elp1 exon 10 inclusion expressed as fold change (dH_2O-treated cells are set to 1). Data are expressed as mean ± SD of three independent experiments performed in triplicate. Statistical analysis was performed using Student t-test (ns: not significant; *** $p<0,001$).

4.12 Pol II transcription elongation rate regulates Elp1 exon 20 splicing

To understand the role of Pol II elongation rate on Elp1 exon 20 regulation, I performed minigene experiments with human Pol II variants. Human Pol II mutants, R749H and E1126G, have been shown to slow down (~ 4 times slower) or speed up (~ 0.88 times faster) Pol II speed, respectively, and have an effect on alternative splicing (Fong et al., 2014). These Pol II variants also contain another mutation that makes them resistant to α-amanitin inhibition. Elp1 minigene was co-transfected with different Pol II variants in the presence of different concentrations of α-amanitin to block endogenous Pol II (Dujardin et al., 2014; Fong et al., 2014) and after 24 hours total RNA was extracted and minigene splicing pattern analyzed by RT-PCR using specific primers. Notably, I found an α-amanitin dose-dependent decrease of exon 20 inclusion, from ~1.6- to ~ 2.5-folds, when transcription is carried out by the slow Pol II (Figure 4.14 A) but it remained unchanged after that Elp1 elongation was carried out by the fast Pol II mutant (Fig 4.14 B). Furthermore, in the presence of a slow Pol II, I observed the presence of a 24 nt cryptic exon localized approximately 650 nt downstream the 5'ss of exon 20 in the mature mRNA (Fig. 4.14 A, lanes 3 and 5, # mark). Next, to assess whether a sub-optimal Pol II elongation rate may affect the splicing of constitutive spliced exons, I looked at the splicing of α-globin exon 2 and endogenous Elp1 exon 10; interestingly the two Pol II mutants did not alter the splicing pattern of neither α-globin exon 2 (Figure 4.14 C and D) nor Elp1 exon 10 (Figure 4.14 E and F). This indicate, as previously reported (Kornblihtt, 2004) that alterations in Pol II elongation pace do not affect the splicing of constitutive spliced exons. Taken together, these results demonstrate that the speed of the Pol II regulates aberrant Elp1 splicing of exon 20 co-transcriptionally: a slow Pol II induces exon skipping while a fast Pol II has no apparent effect. The lack of effect by the fast Pol II might be due to the relative low speed increase of this variant (only ~ 0.88 times faster) compared to the slow Pol II (~ 4 times slower).

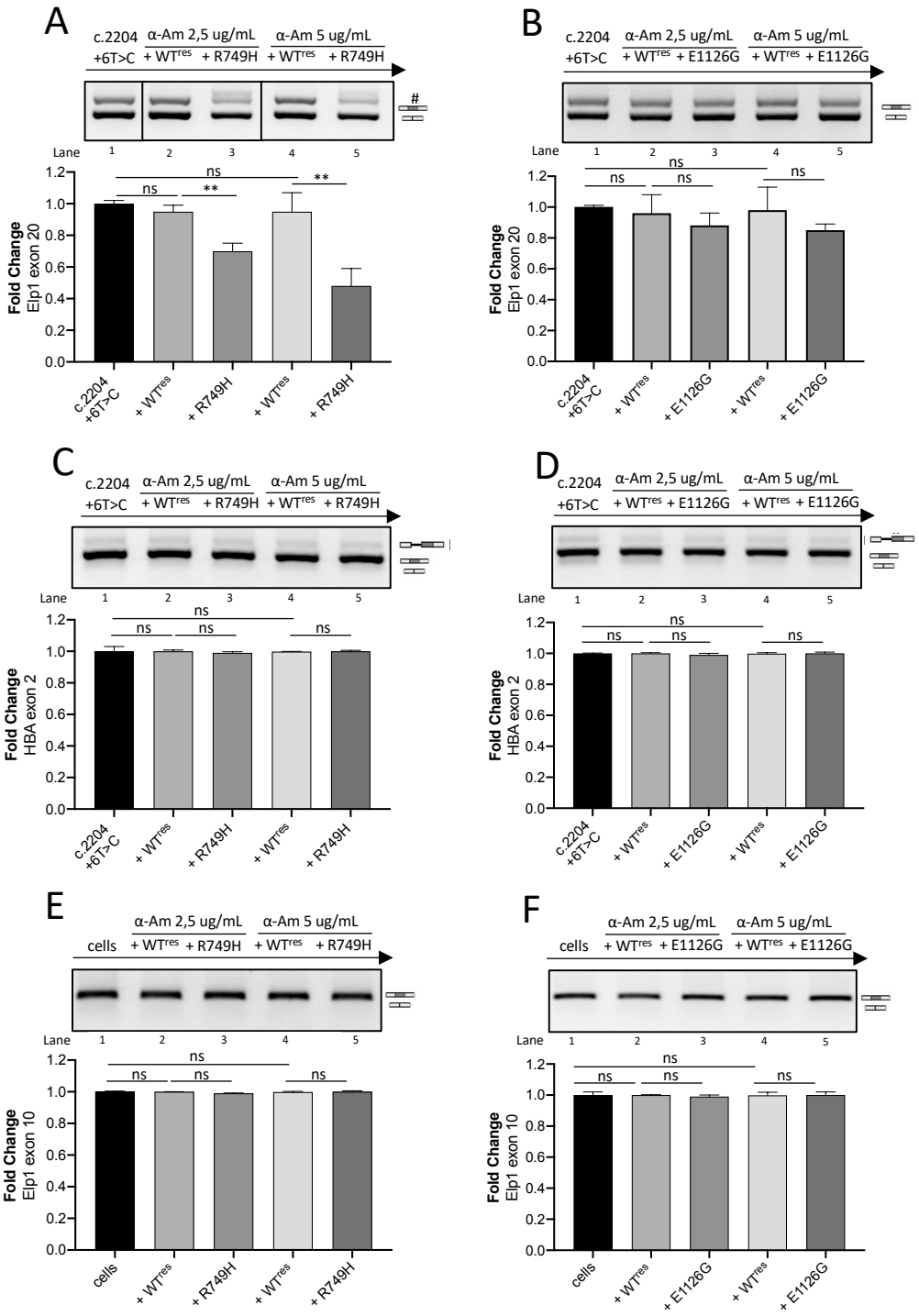

Figure 4.14: ***Pol II elongation rate influences Elp1 exon 20 inclusion in an in vitro splicing assay.***

HEK 293T cells were co-transfected with Elp1 mutant minigene (c.2204 +6T>C) and the expression vectors for $WT^{res\ Pol\ II}$, R749H slow mutant Pol II and E1126G fast mutant Pol II, respectively, followed by the addition of 2.5 ug/mL or 5 ug/mL of α-amanitin for 24h. After 24 hours total RNA was extracted, mRNAs produced were analyzed through RT-PCR using (**A**, **B**) α2,3_F and Elp1_ex21_R primers for Elp1 exon 20, (**C**, **D**) HBA_ex1_F1 and HBA_ex3edb_R2 primers for HBA exon 2 and (**E**, **F**) Ex9_F1 and Ex11_R1 primers for endogenous Elp1 exon 10. PCR products were resolved on 1,5% agarose gel and the bands intensity was quantified with ImageJ software. Schematic representation of the splicing pattern

is shown on the right of the RT-PCR gel analysis. In panels **A**) and **B**) the upper band of 349 bp corresponds to transcripts including the exon 20; the lower band of 275 bp to exon 20 skipping; in panel **A**) # represents transcripts including a cryptic exon downstream the 5'ss of exon 20. Graph below gels displays the % of Elp1 exon 20 inclusion expressed as fold change (this % in lane 1 is set to 1). In panels **C**) and **D**) the upper band of 386 bp corresponds to transcripts retaining intron 1; the lower band of 269 bp to spliced transcripts that include exon 2. Graph below gels displays the % of HBA exon 2 inclusion expressed as fold change (this % in lane 1 is set to 1). In panels **E**) and **F**) the band of 202 bp corresponds to transcripts including exon 10. Graph below gels displays the % of Elp1 exon 10 inclusion expressed as fold change (this % in lane 1 is set to 1). Dividing lines indicate cropping and annealing of the same agarose gel. Data are expressed as mean ± SD of three independent experiments performed in triplicate. Statistical analysis was performed using Student t-test (ns: not significant; * $p<0,05$; ** $p<0,01$).

4.13 Inhibition of transcription elongation by CPT and DRB decreases Elp1 exon 20 inclusion

Next, to strengthen the results regarding the connection between slow Pol II elongation and Elp1 exon 20 regulation, I assessed the effect of Camptotechin (CPT) and 5,6-Dichloro-1-β-D-ribofuranosylbenzimidazole (DRB), two chemicals known to inhibit endogenous transcription elongation through different mechanisms (Ip et al., 2011). I transiently transfected HEK 293T cells with the mutant Elp1 minigene in the presence of different concentrations of CPT or DRB. After 24 hours, I evaluated the splicing pattern by RT-PCR. Both chemicals induced a significant dose-dependent decrease in exon 20 inclusion, from ~1.5- to ~2.5-folds, in comparison to control cells (Figure 4.15 A and B). This mimics the changes previously observed with the slow Pol II mutant. Furthermore, also after the addition of these chemicals, the 24 nt cryptic exon in the middle of intron 20 was spliced in a subset of transcripts (Fig. 4.15 A and B, lane 3, # mark), as previously detected when transcription was carried out with slow Pol II. α-globin exon 2 and endogenous constitutive Elp1 exon 10 were not affected by CPT (Figure 4.15 C and D) or DRB treatments (Figure 4.15 E and F). Taken together, these results further reinforce the concept that a reduced elongation rate negatively affects Elp1 exon 20 defective splicing, leaving unmodified other constitutive exons.

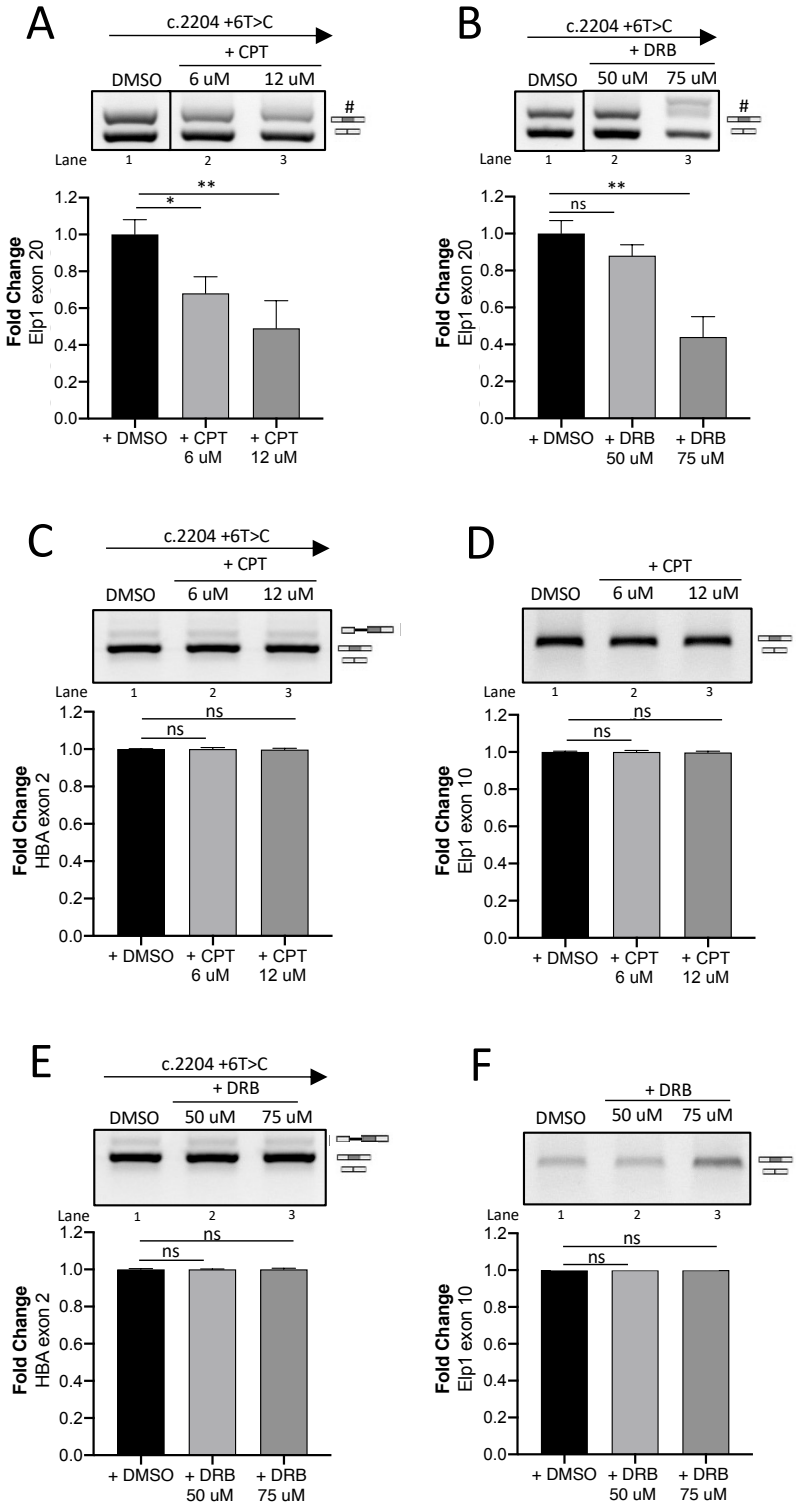

Figure 4.15: ***CPT and DRB decreases Elp1 exon 20 inclusion in an in vitro splicing assay.***

A, **B**) HEK 293T cells were transfected with Elp1 mutant minigene or treated with DMSO or 6 uM or 12 uM of Camptothecin (CPT) and with 50 uM or 75 uM of 5,6-Dichloro-1-β-D-ribofuranosylbenzimidazole (DRB), respectively. After 24 hours total RNA was extracted, mRNAs produced were analyzed through RT-PCR using α2,3_F and Elp1_ex21_R primers for Elp1 exon 20. The upper band of 349 bp corresponds to transcripts including the exon 20; the lower band of 275 bp to exon 20 skipping; # represents transcripts including a cryptic exon

downstream the 5'ss of exon 20. PCR products were resolved on 1,5% agarose gel and the bands intensity was quantified with ImageJ software. Schematic representation of the splicing pattern is shown on the right of the RT-PCR gel analysis. Histogram below gel displays the % of Elp1 exon 20 inclusion expressed as fold change (this % in DMSO-treated cells is set to 1). HEK 293T cells were transfected with Elp1 mutant minigene or treated with DMSO or (**C**) 6 uM or 12 uM of Camptothecin (CPT) and (**E**) with 50 uM or 75 uM of 5,6-Dichloro-1-β-D-ribofuranosylbenzimidazole (DRB), respectively. After 24 hours total RNA was extracted, mRNAs produced were analyzed through RT-PCR using HBA_ex1_F1 and HBA_ex3edb_R2 primers for HBA exon 2. The upper band of 386 bp corresponds to transcripts retaining intron 1; the lower band of 269 bp to spliced transcripts that include exon 2. PCR products were resolved on 1,5% agarose gel and the bands intensity was quantified with ImageJ software. Schematic representation of the splicing pattern is shown on the right of the RT-PCR gel analysis. Histogram below gel displays the % of HBA exon 2 inclusion expressed as fold change (this % in DMSO-treated cells is set to 1). After 24 hours from the treatment with DMSO or (**D**) 6 uM or 12 uM of Camptothecin (CPT) and (**F**) 50 uM or 75 uM of 5,6-Dichloro-1-β-D-ribofuranosylbenzimidazole (DRB), respectively, total RNA was extracted from HEK 293T cells, mRNAs produced were analyzed through RT-PCR using Ex9_F1 and Ex11_R1 primers for endogenous Elp1 exon 10. The band of 202 bp corresponds to transcripts including exon 10. PCR products were resolved on 1,5% agarose gel and the bands intensity was quantified with ImageJ software. Schematic representation of the splicing pattern is shown on the right of the RT-PCR gel analysis. Histogram below gel displays the % of Elp1 exon 10 inclusion expressed as fold change (this % in DMSO-treated cells is set to 1). Data are expressed as mean ± SD of three independent experiments performed in triplicate. Statistical analysis was performed using Student t-test (ns: not significant; * $p<0,05$; ** $p<0,01$).

Chapter 5 – Discussion

5.1 Aberrant splicing events associated to Familial Dysautonomia and Spinal Muscular Atrophy show a tissue-specific and age-dependent regulation

It is well established that alternative splicing greatly contributes to various physiological processes, such as the tissue-identity acquisition and organ development (F. E. Baralle & Giudice, 2017) and that its derangement is implicated in several diseases including cancer (Gebauer et al., 2021). A series of not yet completely clarified genetic programs that operate through t*rans*-acting factors, epigenetic modifications, co-transcriptional regulation mediated by Pol II and DNA methylation act in a combinatorial manner on alternative splicing during embryonic and post-natal development to define the tissue and cellular identity. How these genetic programs operate on alternative splicing in physio-pathological context is the objective of several studies but the temporal effect of these programs on genes that contain splicing mutations it is still largely unexplored. This is particularly important for disease-causing mutations that do not completely disrupt splicing, such as those that induce partial exon skipping, in which the extend of the splicing defect (and the corresponding therapeutic rescue) is directly related to the tissue- and phenotypic- severity. In this study, I focused on two rare diseases, Spinal Muscular Atrophy (SMA) and Familial Dysautonomia (FD), both associated to an exon skipping defect: the first due to mutation in an Exonic Regulatory Element and the second to a variant in the donor site consensus. To address how the genetic programs act in a temporal manner on these two aberrant splicing events, I used *in vivo* animal models: transgenic mice that contain the corresponding defective human Smn2 or Elp1 genes for SMA and FD disease, respectively. As these mice are asymptomatic (only the SMA mouse develops a mild phenotype localized to the tail), they can be considered useful and powerful models to explore the age-dependent regulation of Smn2 exon 7 and Elp1 exon 20 defects and the underlying regulatory mechanisms. The first interesting result I have obtained is that these aberrant splicing events are both temporally regulated in a tissue-specific manner. In the central nervous system (CNS) (brain and spinal cord) of SMA mouse,

Smn2 exon 7 inclusion decreases within 3 months of age to then return to its basal level at next time point (P365), whereas in muscle, liver, lung and kidney exon 7 shows a general increase in inclusion over time, with the greater changes occurring at post-natal age (between P10 and P90). No changes occur in heart (Figure 4.2). In FD model, Elp1 exon 20 inclusion is negatively regulated in the CNS, liver, muscle and lung between 10 and 90 post-natal days, remaining constant at one year of life. No changes are observed in Dorsal Root Ganglia (DRG), eyes, kidney and heart (Figure 4.1). These data indicate that age has different effect on the two splicing events according to the tissue considered. Indeed, the Pattern of Inclusion Ratio (PIR) show different slopes according to the tissue: in the CNS, exon 20 and exon 7 follow a down-steady and down-up PIRs, respectively, meaning that Elp1 and Smn2 share a decrease in their exon inclusion levels between P10 and P90, but showed opposite changes at later age (Figure 4.3 B and C). On the contrary, in muscle, liver and lung, Elp1 exon 20 shows a down-steady PIR whereas Smn2 exon 7 an up-steady PIR; this means that in these tissues exon 20 goes toward skipping, as previously observed in the CNS, but exon 7 results more included in the mRNA within 3 months of age with no further changes for both events at one year of life (Figure 4.3 D, E and F). Kidney shows an up-steady PIR in SMA whereas in FD I have not detected any difference in splicing (Figure 4.3 G). In heart of SMA model and in eyes, heart and dorsal root ganglia (DRG) of FD mouse, splicing does not change over time. For both Smn2 exon 7 and Elp1 exon 20, the most significant changes in splicing occur within 3 months of age. The only age-dependent change I have observed between P90 and P365 occurs in Smn2 exon 7 in brain and spinal cord. This is not unexpected as during the post-natal growth, animals go toward important changes in their physiology, going from the embryo phase, in which tissues form and begin functioning, to the post-natal, in which animals incorporates nutrition for anabolic processes, grown in size and tissues mature and function to sustain the new basic needs of the body (Charizanis et al., 2012; Kadota et al., 2020). Assuming that the temporal program that affects splicing (and also transcription) is conserved in humans, the age-dependent changes in Elp1 exon 20 and Smn2 exon 7 I have observed in mice might have functional consequences on affected individuals and help in understanding the progression of the disease. Even if SMA is now considered a multi-systemic disease, the CNS and the muscle are the major tissues affected and in particular motor neurons located in the ventral horn of the spinal cord where their progressive degeneration leads to weakness and muscle atrophy (Kolb & Kissel, 2015). Brain and spinal cord of SMA mice showed the lowest level of exon 7 inclusion at P90

whereas no changes were observed in the amount of total Smn2 transcript (Figure 4.5 E and F). Thus, post-natal development might represent a critical period where affected cells in the CNS have a reduced amount of normally spliced transcripts and thus are more susceptible to pathological degeneration. Even if the effect on splicing is relatively small (from ~20% to ~10% between P10 and P90, respectively) it accounts for a significant ~2-fold reduction in the residual amount of functionally active Smn2 transcript. It is interesting to note that the typical presentation of SMA symptoms in the most severe form (type 1) occurs during post-natal development, prior to 6 months of age (Kolb & Kissel, 2015). Muscle and in particular the neuromuscular junctions are also involved in SMA pathology. In muscle, post-natal development has a positive effect on Smn2 exon 7 as its percentage increase from ~25% to ~40% (~2-fold increase). However, this positive effect on splicing is counterbalanced by a significant decrease (~5-fold reduction) in the total amount of Smn2 transcript (Figure 4.5 A), suggesting that the most severe age-dependent changes in this tissue affect transcription. FD is also considered a multi-systemic disease but its major symptoms are due to a severe sensory and autonomic neuropathy that affects mainly the CNS and the peripheral ganglia including the DRG (Dietrich & Dragatsis, 2016). I observed that brain and spinal cord of FD mice have the lowest level of exon 20 inclusion at P90, with no changes in the amount of Elp1 transcript (Figure 4.4 D and E). Similar to SMA, the percentage of exon 20 inclusion shows a ~1-2-fold reduction between P10 and P90 (from ~15% to ~7.5% in brain and ~20% to ~15% in spinal cord), suggesting that, even in the case of FD, post-natal development might represent a critical period for the CNS. However, in DRG, I did not observe any temporal change in splicing or transcript abundance, indicating that age-dependent programs in this organ have no effect on processing of defective Elp1. Interestingly, Weyn-Vanhentenryck and colleagues, investigating temporal splicing switches of transcriptome profiles of developing mouse cortices and subtypes of neurons, have identified that sensory neurons exhibit a distinct splicing program from CNS neurons. This may arise from the different embryonic origin of these cell types or from the necessity to accommodate unique cellular properties, such as the ability to adapt to new environmental stimuli (Weyn-Vanhentenryck et al., 2018). Thus, in FD temporal programs during post-natal development negatively impact exon 20 splicing in CNS but not DRG.

5.2 Expression of RNA binding proteins (RBPs) shows a general lack of correlation with FD and SMA splicing over lifespan

RNA binding proteins (RBPs), such as those belonging to SR and HNRNP families, are important regulators of alternative splicing and are implicated in development and cell differentiation (F. E. Baralle & Giudice, 2017). In some cases, specific splicing factors have been found to orchestrate multiple change in AS in a tissue specific manner. For example, during brain development NOVA2 regulates the skipping of two exons from adaptor protein DAB1, allowing the production of a shorter and functional isoform (Yano et al., 2010) and RBFOX3 induces skipping of an alternatively spliced exon in the adaptor protein Numb, allowing the progression of neuronal differentiation (K. K. Kim et al., 2013). Alternative splicing transitions occur also in other tissues: in liver ESPR2, a key hepatocyte RBP, controls a highly conserved splicing regulatory network to govern terminal differentiation and maturation of hepatocytes (Bhate et al., 2015) whereas in heart development, tissue-specific factor RBM20 regulates the splicing of titin, a protein acting as a spring, whose long isoforms (N2BA) are expressed in neonates and a shorter isoform (N2B) in adults (Guo et al., 2012; S. Li et al., 2013; Linke & Krüger, 2010). Since these and others RBPs are responsible for the regulation of tissue-specific splicing networks, I reasoned that one (or more) RBPs may explain the age-dependent changes of Elp1 exon 20 and Smn2 exon 7 splicing. In order to find a potential splicing factor(s) that might orchestrate the age-dependent changes, I focused on the most important RBPs that have been shown to affect splicing of Elp1 exon 20 and Smn2 exon 7. For FD, I considered three positive splicing factors (RBM24, RBM38 and SFPQ) and three negative regulators (hnRNP A1, SRSF3 and FUS). For SMA, I tested five enhancing factors (TIA1, TRA2β, SFPQ, SRSF9 and SRSF1) and four inhibiting ones (hnRNP A1, SAM68, SRSF2 and SRSF3). In general, I did not observe a clear correlation between the changes in splicing and the expression of RBPs. For example, in SMA brain the significant decrease at P90 of the negative regulators hnRNPA1 and SRSF3 (Figure 4.7 A) should increase the Smn2 exon 7 inclusion which instead decreases (Figure 4.2 E). However, at P90 there is also a concomitant reduction in the expression of enhancing splicing factors that can potentially counteract the negative effect of hnRNPA1/SRSF3. In FD brain, the reduction in Elp1 exon 20 inclusion that I have observed between P10 and P90 may correlate with the decrease of SFPQ and RBM38 enhancing factors (Figure 4.6 B), but

it does not relate with the concomitant decrease in hnRNPA1 and SRSF3 levels within the same period of time (Figure 4.6 A). Similar observations can be made analyzing the other tissues in the mouse models. Thus, the study of the expression of the most important splicing factors does not lead to the identification for the two defective exons of a main factor that explain the age- and tissue- dependent changes in splicing. However, I cannot exclude that other tissue-specific factors, not yet known to modulate these two aberrant splicing events, might be implicated in their age-dependent regulation.

5.3 Age-dependent changes in Elp1 exon 20 splicing are associated to changes in RNA Polymerase II elongation rate and chromatin signatures *in vivo*

To explore the potential age-dependent co-transcriptional regulation of Elp1 exon 20 splicing *in vivo*, I have evaluated the Pol II density in chromatin immunoprecipitation experiments. This analysis was performed in the FD model on two representative tissues, liver and brain. To my knowledge this is the first time that a study evaluates *in vivo* the age-dependent changes in Pol II density in a gene. Typically, Pol II density has been analysed on promoters and connected to transcriptional activation and its density has been studied in embryonic stem cells (Williams et al., 2015), in mouse embryonic fibroblasts (Min et al., 2011), in *Drosophila melanogaster*'s mid-blastula transition (Chen et al., 2013) and in early phases of embryo development (Lagha et al., 2013). My analysis shows a strong reduction in the density of Pol II in both liver (from ~ 2.5- to ~5-folds) and brain (from ~ 2.5- to ~4-folds) between P10 and P90, but not at P365 (Figure 4.9). As the genomic region analysed (between exon 10 and 29) includes both constitutive (exons 10 and 29) and alternative exons (exon 20) spanning approximately 27.3 kb, the age-dependent reduction in Pol II density profile in Elp1 does not seem a specific feature of the alternative spliced exon but probably occurs along the entire gene. Alterations in Pol II density have been associated to changes in transcription or elongation rates. As I did not detect any differential expression of Elp1 transcript over time (Figure 4.4 D and F), the age-dependent reduction in Pol II density profile is probably due to alterations in its kinetics (that, in turn, affect alternative splicing). As the structural status of chromatin is an important modulator of the Pol II kinetics (Giono & Kornblihtt, 2020), I have evaluated four important modifications that affect lysines of H3: H3K4me3, H3K9me3, H3K27me3 and H3K36me3. H3K4me3 and H3K36me3 act as "permissive" modifications that promote a more loosed chromatin structure and are associated with foci of active transcription, whereas H3K9me3 and H3K27me3 work as "repressive" methylations, being mainly deposited on heterochromatin and associated with chromatin packaging and transcriptional silencing (Naftelberg et al., 2015). Of the chromatin modifications analysed, H3K27me3 showed the most significant variation. H3K27me3 increased ~2-3 fold in liver and ~10-15 fold in brain between P10 and P90 in genomic Elp1 regions corresponding to both constitutive (exons 10 and 29) alternative exons (exon 20). A

further but less pronounced increase is observed at P365 (~1-2-folds in both tissues) (Figure 4.10). Interestingly, in both liver and brain of FD mice, the most relevant changes in H3K27me3 occur within 3 months of age, a timing similar to what observed for the decrease of the Pol II density profile, suggesting a possible functional connection between these two events. Furthermore, the changes of H3K27me3 on the Elp1 gene correlates with the abundance of this chromatin mark in the corresponding tissues, as evaluated by western blotting with specific antibodies. In liver, H3K27me3 increases ~1.7-fold between P10 and P90 and slight decreases at P365 whereas in brain this mark shows a steep increase during post-natal development (~2.5-folds) that further increase at P365 (~5.5-folds) (Figure 4.11). H3K27me3 is a fundamental repressive mark that is dynamically modified during development and differentiation to allow the repression (or derepression) of specific subsets of genes (Bracken & Helin, 2009). The Polycomb Repressive Complex 2 (PRC2), once recruited to its target genes, coordinates the deposition and propagation of H3K27me3 (Lavarone et al., 2019). Age-associated changes in H3K27me3 expression profile have been previously observed in several model organisms and have been also associated to longevity. Several *in vitro* and *in vivo* studies reported an age-dependent increase in H3K27me3; this has been observed in human peripheral blood mononuclear cells (Cheung et al., 2018), in human adipose-derived mesenchymal stem cells (L. Liu et al., 2013; Noer et al., 2009) and in quiescent mouse muscle stem cells (Schwörer et al., 2016). An increase in H3K27me3 also occurs in brain and skeletal muscle of the killfish torquoise *Nothobranchius furzeri* (Baumgart et al., 2014; Cencioni et al., 2019) and in the brain of SAMP8 mice, a strain of mice that displays a phenotype of accelerated aging (Wang et al., 2010). H3K27me3 has been also associated with longevity. In *Drosophila melanogaster*, decrease in the total H3K27me3 levels through mutation of E(Z), the fly homolog of PRC2-subunit EZH1/2, or mutation of its targeting partner ESC protein, increases the flies' longevity (Siebold et al., 2010). In contrast, in *Caenorhabditis elegans*, a global decrease in H3K27me3 levels is associated with premature aging. Indeed, an age-dependent increase in UTX-1 activity, the H3K27me3 demethylase, leads to a decrease of this mark with negative downstream effects on worms' lifespan (Maures et al., 2011). The correlation between H3K27me3, a chromatin repressive mark, and Pol II present *in vivo* in the FD transgenic mice, suggests an age-dependent kinetic model of co-transcriptional regulation of Elp1 exon 20 splicing.

5.4 Elp1 exon 20 defective splicing is subject to co-transcriptional regulation

As Pol II kinetics and chromatin dynamics show interesting age-dependent changes *in vivo,* I reasoned that part of the FD exon 20 splicing regulation may occur co-transcriptionally and is mechanistically modulated by these events. To investigate this possibility, I performed a series of minigene experiments where I tested on Elp1 exon 20 alternative splicing and on constitutive exons the effect of different chemical compounds that either alter the chromatin structure or affect the Pol II elongation rate. In addition, I also evaluated on these exons the effect of mutants of Pol II with a slow or a fast elongation rate. The chemicals I have used that act on chromatin are specific inhibitor of the H3K27me3 mark (EED-226) (Qi et al., 2017) or inhibitor of the Histone DeACetylases (HDAC) (VPA) (Göttlicher et al., 2001). Both EED-226 and HDAC inhibitors will result with two different mechanisms in a more relaxed chromatin structure. Chemicals that slow down the Pol II elongation rate act on the proximities of the transcription bubble by creating Topoisomerase I-DNA adducts which physically interfere with elongating Pol II (CPT) or on inhibiting the kinase activity of positive transcription factor P-TEFb (DRB). All these compounds have been previously used to demonstrate that coupling of transcription and splicing regulates some alternative spliced exons (de la Mata et al., 2003; Dujardin et al., 2014; Ip et al., 2011). The results I have obtained on FD *in vitro* clearly show that the chromatin composition and Pol II elongation rate regulates Elp1 exon 20 alternative splicing. In fact, the treatments that provoke a chromatic relaxation (EED-226 and VPA) induce an increase in exon 20 inclusion (Figure 4.12 and 4.13) whereas the two treatments that slow down the Pol II (CPT and DRB) (Figure 4.15) or experiments with a slow Pol II mutant (Figure 4.14) decrease the exon 20 inclusion. Interestingly, none of these treatments affect constitutive splicing events neither in the minigene (α-globin exon 2) nor in the endogenous context (Elp1 exon 10) (Figure 4.12, 4.13, 4.14 and 4.15). The absence of splicing variation in the fast Pol II mutant experiment (Figure 4.14) is probably due to its relatively small effect on the elongation rate (~ 0.88-fold increase) compared to the slow counterpart (~ 4 fold decrease) (Fong et al., 2014). Of particular interest is the effect of EED-226, as this molecule is a potent and specific inhibitor of H3K27me3, the chromatin modification that increases during post-natal development in liver and brain. EED-226 selectively binds to the H3K27me3 binding pocket of EED protein, a

subunit of PRC2, and allosterically inhibits PRC2 complex resulting in a loss of its activity (Qi et al., 2017). For this reason, it is a first-in-class EED inhibitor and has been shown to possess a strong antitumor activity in xenograft mice model (Kosti et al., 2020). Interestingly, its analogue MAK683 it is actively tested in clinical settings against lymphoma and different solid tumors (Zhu et al., 2020). The improved inclusion of exon 20 induced by EED-226-mediated inhibition of H3K27me3 *in vitro* well correlates with the *in vivo* observations where an age-dependent increase of H3K27me3 (Figure 4.10 and 4.11) is associated with exon 20 skipping (Figure 4.1). All together, these results support the hypothesis that the selective loss of H3K27me3 and/or the acetylation of core histones would facilitate the passage of the transcribing Pol II, which would move faster since it finds a more open chromatin structure, inducing Elp1 exon 20 inclusion. Collectively, my results indicate that Elp1 exon 20 aberrant splicing is a co-transcriptional event, whose splicing is regulated by coupling chromatin dynamics and Pol II kinetics.

5.5 A model for the age-dependent regulation of co-transcriptional Elp1 exon 20 splicing based on chromatin marks and Pol II kinetics

The kinetic model of co-transcriptional splicing originally proposed by Alberto Kornblihtt links Pol II elongation rate, modulated by promoter architecture and/or chromatin signatures, to alternative splicing regulation. In the first proposal, as inferred by experiments on the mouse alternative spliced EDI exon of fibronectin (also known as EDA in humans), on the adenovirus exon E1a and on Ncam exon 18 (de la Mata et al., 2003; Schor et al., 2013) the speed of the polymerase is inversely related to the degree of exon inclusion: a slow Pol II elongation induces a greater exon inclusion while a fast Pol II elongation exon skipping. This relationship is based on the assumption that during transcription, the Pol II kinetic affects the timing of presentation of splice sites and regulatory sequences gradually emerging from the transcribing pre-mRNA. Thus, a slow Pol II would favor the usage of a weak 3'ss of the upstream intron instead of using the stronger 3'ss of the downstream intron, resulting in splicing commitment and exon inclusion. On the contrary, a fast-elongating Pol II shall favor the assembly of the spliceosome to the strong 3'ss of a downstream intron and not on the weak 3'ss of the upstream intron, giving as a result exon skipping. This model was also valid for Ncam exon 18 where an increase in the repressive marks H3K9me2 and H3K27me3 throughout the gene correlated with a slow Pol II elongation in the region surrounding exon 18, inducing its inclusion in the mature mRNA (Schor et al., 2013). However, analysis of another alternative splicing event (Cftr exon 9) showed that the speed of the polymerase has the oppose effect on splicing as the speed is directly correlated to the degree of exon inclusion. This effect is explained by the peculiar architecture of this exon with the critical contribution of ETR-3, a negative splicing factor. In the Cftr exon 9, a slow Pol II elongation rate would provide a "window of opportunity" to a negative *trans*-acting factor to be recruited on pre-mRNA, preventing the assembly of the spliceosome on the exon, resulting in its skipping. Specifically, the ETR-3 splicing factor, that binds to a UG stretch at the end of intron 8 is involved in the Pol II-mediated effect on exon 9 skipping (Dujardin et al., 2014). A further implementation of the model comes from experiments with Pol II mutants with different kinetics (Fong et al., 2014). This analysis led to the classifications of alternative exons in two types depending on the effect that a fast or a slow Pol II have on splicing. In type I exons, slow elongation promotes inclusion and fast elongation promotes skipping whereas in type II exons, exon inclusion is promoted by fast

elongation and exon skipping by slow elongation (Fong et al., 2014). Interestingly, genome-wide studies demonstrated that ~20% of the alternative splicing event in cells are Pol II elongation-sensitive: type I exons account for ~50% - ~80% while type II are between ~20% to ~50% (Fong et al., 2014; Ip et al., 2011; Maslon et al., 2019; Muñoz et al., 2009). Furthermore, an additional group of alternative splicing events responded in a not predictable manner to the Pol II rate (i.e. both fast and slow Pol II have the same effect on splicing or only one was active). In this group, coupling of splicing with transcription is considered a "Goldilocks"-like phenomenon in the sense that proper elongation speed seems critical to achieve an adequate processing outcome (Fong et al., 2014). Based on the *in vitro* minigene experiment with the slow Pol II (Figure 4.14), chemical compounds that modulate the Pol II elongation (Figure 4.15) or drugs that open the chromatin (Figure 4.12 and 4.13), Elp1 exon 20 should belong to the type II group. In the exons that belong to this type, like the Cftr exon 9, negative *trans*-acting factors play a major role: their recruitment on pre-mRNA regulates co-transcriptionally the assembly of the spliceosome. Few years ago, Bruun and colleagues demonstrated the presence of an ISS downstream the 5'ss of exon 20 and that negative factor HNRNPA1 was able to bind to this element and to two ESS (ESS1 and ESS2) in Elp1 exon 20 (Bruun et al., 2018). Further investigations are needed to uncover the mechanistic aspects that govern this splicing event and its role in kinetic coupling. Based on *in vivo* and *in vitro* experiments I propose the following co-transcriptional model for the regulation of Elp1 exon 20 through kinetic coupling: during post-natal development and at later age, in the liver and brain there is a general increase in the repressive mark H3K27me3 that induces a compaction in the chromatin structure along the human Elp1 gene body. This new-packaged chromatin conformation slows down Pol II elongation rate, causing a reduction in its density profile that results in skipping of the alternative spliced exon 20 (Figure 5.1). This change in Pol II elongation due to H3K27me3 does not affect the other constitutive nearby Elp1 exons. Even if my experiments point to H3K27me3 as a chromatin mark involved in the regulation of Elp1 exon 20 splicing other modification can be involved. I have evaluated the deployment of four histone marks that are known to loosen (H3K4me3 and H3K36me3) or compact (H3K9me3 and H3K27me3) chromatin structure. It is possible that also other histone marks cooperate to regulate Elp1 splicing over lifespan *in vivo*. Agirre and colleagues have recently identified eleven chromatin modifications, including H3K27me3, that act in a combinatorial and position-dependent manner to impact the outcome of a subgroup of alternative spliced exons. A precise splicing-

associated chromatin signatures (SACS) differentially mark alternatively spliced exon depending on the level of exon inclusion and also on the presence of regulatory elements on pre-mRNA, such as RNA splice sites strength and exon length or on positioning of the nucleosomes (Agirre et al., 2021). Based on these assumptions, it is highly possible that H3K27me3, by itself or in combination with other histone modifications, cooperatively affect co-transcriptionally exon 20 splicing through Pol II-mediated elongation. However, I cannot exclude that H3K27me3 or other chromatin marks might also facilitate co-transcriptional recruitment of specific splicing factors on Elp1 pre-mRNA. In this sense, some histone marks have been shown to bind adaptor proteins that, in turn, interact with the recruitment of splicing factors to their specific motifs on nascent RNA to regulate alternatively spliced exons (Luco et al., 2010; Sims et al., 2007).

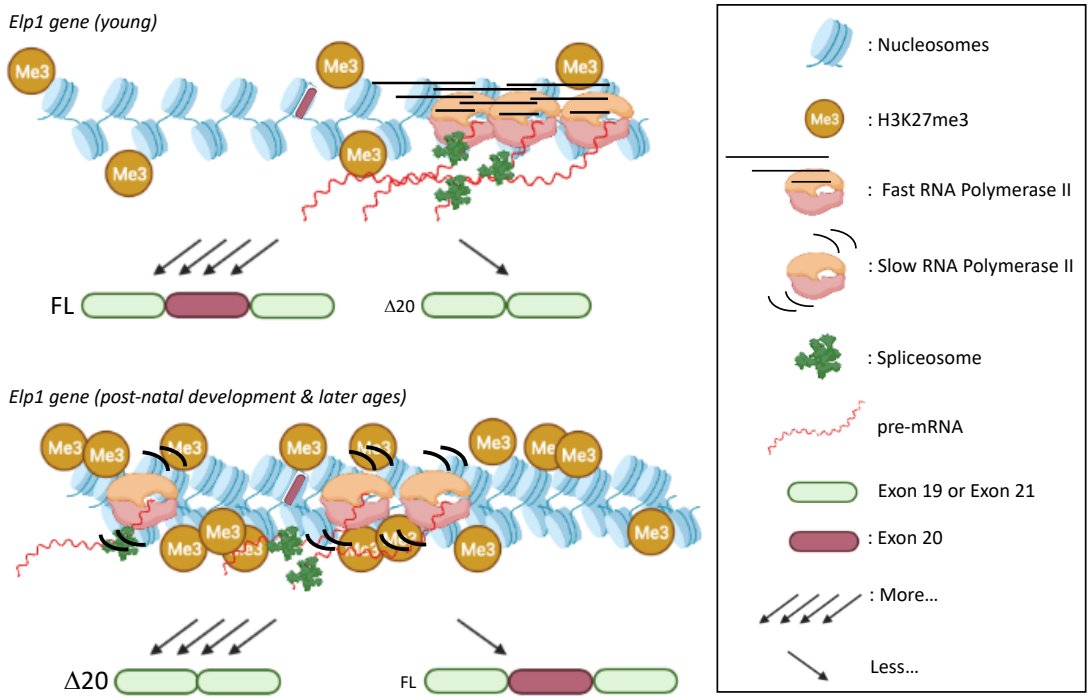

Figure 5.1: ***Model of Elp1 exon 20 kinetic coupling.***

In liver and brain of FD young model (upper panel), faster Pol II-mediated elongation is carried out throughout the entire Elp1 gene within a relaxed chromatin landscape, resulting in an increased production of Elp1 transcripts that include exon 20 in the mature mRNA (FL) compared to those that skip this exon (Δ20). During post-natal development and at later age (lower panel), a robust increase in the density profile of H3K27me3 repressive mark on Elp1 gene body slows down Pol II elongation pace, inducing a strong and general reduction of Pol II enrichment; this, in turn, affects the splicing of this event, leading to an increased production of Elp1 transcripts that skipped exon 20 compared to those that include it. The legend of each element is indicated on the right (Created by Biorender.com).

Chapter 6 – Bibliography

Agirre, E., Oldfield, A. J., Bellora, N., Segelle, A., & Luco, R. F. (2021). Splicing-associated chromatin signatures: A combinatorial and position-dependent role for histone marks in splicing definition. *Nature Communications*, *12*(1), 682. https://doi.org/10.1038/s41467-021-20979-x

Anna, A., & Monika, G. (2018). Splicing mutations in human genetic disorders: Examples, detection, and confirmation. *Journal of Applied Genetics*, *59*(3), 253–268. https://doi.org/10.1007/s13353-018-0444-7

Ast, G. (2004). How did alternative splicing evolve? *Nature Reviews Genetics*, *5*(10), 773–782. https://doi.org/10.1038/nrg1451

Baralle, D., & Baralle, M. (2005). Splicing in action: Assessing disease causing sequence changes. *Journal of Medical Genetics*, *42*(10), 737–748. https://doi.org/10.1136/jmg.2004.029538

Baralle, D., & Buratti, E. (2017). RNA splicing in human disease and in the clinic. *Clinical Science (London, England: 1979)*, *131*(5), 355–368. https://doi.org/10.1042/CS20160211

Baralle, F. E., & Giudice, J. (2017). Alternative splicing as a regulator of development and tissue identity. *Nature Reviews Molecular Cell Biology*, *18*(7), 437–451. https://doi.org/10.1038/nrm.2017.27

Baumgart, M., Groth, M., Priebe, S., Savino, A., Testa, G., Dix, A., Ripa, R., Spallotta, F., Gaetano, C., Ori, M., Terzibasi Tozzini, E., Guthke, R., Platzer, M., & Cellerino, A. (2014). RNA-seq of the aging brain in the short-lived fish N. furzeri—Conserved pathways and novel genes associated with neurogenesis. *Aging Cell*, *13*(6), 965–974. https://doi.org/10.1111/acel.12257

Bhate, A., Parker, D. J., Bebee, T. W., Ahn, J., Arif, W., Rashan, E. H., Chorghade, S., Chau, A., Lee, J.-H., Anakk, S., Carstens, R. P., Xiao, X., & Kalsotra, A. (2015). ESRP2 controls an adult splicing programme in hepatocytes to support postnatal liver maturation. *Nature Communications*, *6*, 8768. https://doi.org/10.1038/ncomms9768

Biterge, B., & Schneider, R. (2014). Histone variants: Key players of chromatin. *Cell and Tissue Research*, *356*(3), 457–466. https://doi.org/10.1007/s00441-014-1862-4

Blencowe, B. J. (2000). Exonic splicing enhancers: Mechanism of action, diversity and role in human genetic diseases. In *Trends in Biochemical Sciences*. https://doi.org/10.1016/S0968-0004(00)01549-8

Blencowe, B. J. (2006). Alternative splicing: New insights from global analyses. *Cell*, *126*(1), 37–47. https://doi.org/10.1016/j.cell.2006.06.023

Boesler, C., Rigo, N., Anokhina, M. M., Tauchert, M. J., Agafonov, D. E., Kastner, B., Urlaub, H., Ficner, R., Will, C. L., & Lührmann, R. (2016). A spliceosome intermediate with loosely associated tri-snRNP accumulates in the absence of Prp28 ATPase activity. *Nature Communications*, *7*, 11997. https://doi.org/10.1038/ncomms11997

Booth, L. N., & Brunet, A. (2016). The Aging Epigenome. *Molecular Cell*, *62*(5), 728–744. https://doi.org/10.1016/j.molcel.2016.05.013

Bracken, A. P., & Helin, K. (2009). Polycomb group proteins: Navigators of lineage pathways led astray in cancer. *Nature Reviews. Cancer*, *9*(11), 773–784. https://doi.org/10.1038/nrc2736

Bruun, G. H., Bang, J. M. V., Christensen, L. L., Brøner, S., Petersen, U. S. S., Guerra, B., Grønning, A. G. B., Doktor, T. K., & Andresen, B. S. (2018). Blocking of an intronic splicing silencer completely rescues IKBKAP exon 20 splicing in familial

dysautonomia patient cells. *Nucleic Acids Research*, *46*(15), 7938–7952. https://doi.org/10.1093/nar/gky395

Buratti, E., & Baralle, F. E. (2004). Influence of RNA Secondary Structure on the Pre-mRNA Splicing Process. *Molecular and Cellular Biology*. https://doi.org/10.1128/mcb.24.24.10505-10514.2004

Butchbach, M. E. R. (2016). Copy Number Variations in the Survival Motor Neuron Genes: Implications for Spinal Muscular Atrophy and Other Neurodegenerative Diseases. *Frontiers in Molecular Biosciences*, *3*, 7. https://doi.org/10.3389/fmolb.2016.00007

Calado, A., & Carmo-Fonseca, M. (2000). Localization of poly(A)-binding protein 2 (PABP2) in nuclear speckles is independent of import into the nucleus and requires binding to poly(A) RNA. *Journal of Cell Science*, *113 (Pt 12)*, 2309–2318.

Cameron, B., Lehrmann, E., Chih, T., Walters, J., Buksch, R., Snyder, S., Goffena, J., Lefcort, F., Becker, K. G., & George, L. (2021). Loss of Elp1 perturbs histone H2A.Z and the Notch signaling pathway. *Biology Open*, *10*(9), bio058979. https://doi.org/10.1242/bio.058979

Caputi, M., & Zahler, A. M. (2002). SR proteins and hnRNP H regulate the splicing of the HIV-1 tev-specific exon 6D. *The EMBO Journal*, *21*(4), 845–855. https://doi.org/10.1093/emboj/21.4.845

Cartegni, L., Chew, S. L., & Krainer, A. R. (2002). Listening to silence and understanding nonsense: Exonic mutations that affect splicing. *Nature Reviews. Genetics*, *3*(4), 285–298. https://doi.org/10.1038/nrg775

Cartegni, L., Hastings, M. L., Calarco, J. A., de Stanchina, E., & Krainer, A. R. (2006). Determinants of Exon 7 Splicing in the Spinal Muscular Atrophy Genes, SMN1 and SMN2. *The American Journal of Human Genetics*, *78*(1), 63–77. https://doi.org/10.1086/498853

Cencioni, C., Heid, J., Krepelova, A., Rasa, S. M. M., Kuenne, C., Guenther, S., Baumgart, M., Cellerino, A., Neri, F., Spallotta, F., & Gaetano, C. (2019). Aging Triggers H3K27 Trimethylation Hoarding in the Chromatin of Nothobranchius furzeri Skeletal Muscle. *Cells*, *8*(10), E1169. https://doi.org/10.3390/cells8101169

Charizanis, K., Lee, K.-Y., Batra, R., Goodwin, M., Zhang, C., Yuan, Y., Shiue, L., Cline, M., Scotti, M. M., Xia, G., Kumar, A., Ashizawa, T., Clark, H. B., Kimura, T., Takahashi, M. P., Fujimura, H., Jinnai, K., Yoshikawa, H., Gomes-Pereira, M., … Swanson, M. S. (2012). Muscleblind-like 2-mediated alternative splicing in the developing brain and dysregulation in myotonic dystrophy. *Neuron*, *75*(3), 437–450. https://doi.org/10.1016/j.neuron.2012.05.029

Chen, K., Johnston, J., Shao, W., Meier, S., Staber, C., & Zeitlinger, J. (2013). A global change in RNA polymerase II pausing during the Drosophila midblastula transition. *ELife*, *2*, e00861. https://doi.org/10.7554/eLife.00861

Cheung, P., Vallania, F., Warsinske, H. C., Donato, M., Schaffert, S., Chang, S. E., Dvorak, M., Dekker, C. L., Davis, M. M., Utz, P. J., Khatri, P., & Kuo, A. J. (2018). Single-Cell Chromatin Modification Profiling Reveals Increased Epigenetic Variations with Aging. *Cell*, *173*(6), 1385-1397.e14. https://doi.org/10.1016/j.cell.2018.03.079

Chung, C. T., Niemela, S. L., & Miller, R. H. (1989). One-step preparation of competent Escherichia coli: Transformation and storage of bacterial cells in the same solution. *Proceedings of the National Academy of Sciences of the United States of America*, *86*(7), 2172–2175. https://doi.org/10.1073/pnas.86.7.2172

Clerici, M., Faini, M., Muckenfuss, L. M., Aebersold, R., & Jinek, M. (2018). Structural basis of AAUAAA polyadenylation signal recognition by the human CPSF complex. *Nature Structural & Molecular Biology*, *25*(2), 135–138. https://doi.org/10.1038/s41594-017-0020-6

Coovert, D. D., Le, T. T., McAndrew, P. E., Strasswimmer, J., Crawford, T. O., Mendell, J. R., Coulson, S. E., Androphy, E. J., Prior, T. W., & Burghes, A. H. (1997). The

survival motor neuron protein in spinal muscular atrophy. *Human Molecular Genetics*, *6*(8), 1205–1214. https://doi.org/10.1093/hmg/6.8.1205

Cuajungco, M. P., Leyne, M., Mull, J., Gill, S. P., Lu, W., Zagzag, D., Axelrod, F. B., Maayan, C., Gusella, J. F., & Slaugenhaupt, S. A. (2003). Tissue-Specific Reduction in Splicing Efficiency of IKBKAP Due to the Major Mutation Associated with Familial Dysautonomia. *The American Journal of Human Genetics*, *72*(3), 749–758. https://doi.org/10.1086/368263

De Conti, L., Baralle, M., & Buratti, E. (2013). Exon and intron definition in pre-mRNA splicing: Exon and intron definition in pre-mRNA splicing. *Wiley Interdisciplinary Reviews: RNA*, *4*(1), 49–60. https://doi.org/10.1002/wrna.1140

de la Mata, M., Alonso, C. R., Kadener, S., Fededa, J. P., Blaustein, M., Pelisch, F., Cramer, P., Bentley, D., & Kornblihtt, A. R. (2003). A Slow RNA Polymerase II Affects Alternative Splicing In Vivo. *Molecular Cell*, *12*(2), 525–532. https://doi.org/10.1016/j.molcel.2003.08.001

Deschênes, M., & Chabot, B. (2017). The emerging role of alternative splicing in senescence and aging. *Aging Cell*, *16*(5), 918–933. https://doi.org/10.1111/acel.12646

Dhir, A., & Buratti, E. (2010). Alternative splicing: Role of pseudoexons in human disease and potential therapeutic strategies. *The FEBS Journal*, *277*(4), 841–855. https://doi.org/10.1111/j.1742-4658.2009.07520.x

Dietrich, P., & Dragatsis, I. (2016). Familial Dysautonomia: Mechanisms and Models. *Genetics and Molecular Biology*, *39*(4), 497–514. https://doi.org/10.1590/1678-4685-gmb-2015-0335

Donadon, I., Bussani, E., Riccardi, F., Licastro, D., Romano, G., Pianigiani, G., Pinotti, M., Konstantinova, P., Evers, M., Lin, S., Rüegg, M. A., & Pagani, F. (2019). Rescue of spinal muscular atrophy mouse models with AAV9-Exon-specific U1 snRNA. *Nucleic Acids Research*, *47*(14), 7618–7632. https://doi.org/10.1093/nar/gkz469

Donadon, I., Pinotti, M., Rajkowska, K., Pianigiani, G., Barbon, E., Morini, E., Motaln, H., Rogelj, B., Mingozzi, F., Slaugenhaupt, S. A., & Pagani, F. (2018). Exon-specific U1 snRNAs improve ELP1 exon 20 definition and rescue ELP1 protein expression in a familial dysautonomia mouse model. *Human Molecular Genetics*, *27*(14), 2466–2476. https://doi.org/10.1093/hmg/ddy151

Dreyfuss, G., Kim, V. N., & Kataoka, N. (2002). Messenger-RNA-binding proteins and the messages they carry. *Nature Reviews Molecular Cell Biology*, *3*(3), 195–205. https://doi.org/10.1038/nrm760

Dujardin, G., Lafaille, C., de la Mata, M., Marasco, L. E., Muñoz, M. J., Le Jossic-Corcos, C., Corcos, L., & Kornblihtt, A. R. (2014). How Slow RNA Polymerase II Elongation Favors Alternative Exon Skipping. *Molecular Cell*, *54*(4), 683–690. https://doi.org/10.1016/j.molcel.2014.03.044

Dvinge, H. (2018). Regulation of alternative mRNA splicing: Old players and new perspectives. *FEBS Letters*, *592*(17), 2987–3006. https://doi.org/10.1002/1873-3468.13119

Even-Faitelson, L., Hassan-Zadeh, V., Baghestani, Z., & Bazett-Jones, D. P. (2016). Coming to terms with chromatin structure. *Chromosoma*, *125*(1), 95–110. https://doi.org/10.1007/s00412-015-0534-9

Fong, N., Kim, H., Zhou, Y., Ji, X., Qiu, J., Saldi, T., Diener, K., Jones, K., Fu, X.-D., & Bentley, D. L. (2014). Pre-mRNA splicing is facilitated by an optimal RNA polymerase II elongation rate. *Genes & Development*, *28*(23), 2663–2676. https://doi.org/10.1101/gad.252106.114

Gebauer, F., Schwarzl, T., Valcárcel, J., & Hentze, M. W. (2021). RNA-binding proteins in human genetic disease. *Nature Reviews. Genetics*, *22*(3), 185–198. https://doi.org/10.1038/s41576-020-00302-y

Geuens, T., Bouhy, D., & Timmerman, V. (2016). The hnRNP family: Insights into their role

in health and disease. *Human Genetics*, *135*(8), 851–867. https://doi.org/10.1007/s00439-016-1683-5

Giono, L. E., & Kornblihtt, A. R. (2020). Linking transcription, RNA polymerase II elongation and alternative splicing. *The Biochemical Journal*, *477*(16), 3091–3104. https://doi.org/10.1042/BCJ20200475

Gómez Acuña, L. I., Fiszbein, A., Alló, M., Schor, I. E., & Kornblihtt, A. R. (2013). Connections between chromatin signatures and splicing: Connections between chromatin signatures and splicing. *Wiley Interdisciplinary Reviews: RNA*, *4*(1), 77–91. https://doi.org/10.1002/wrna.1142

Göttlicher, M., Minucci, S., Zhu, P., Krämer, O. H., Schimpf, A., Giavara, S., Sleeman, J. P., Lo Coco, F., Nervi, C., Pelicci, P. G., & Heinzel, T. (2001). Valproic acid defines a novel class of HDAC inhibitors inducing differentiation of transformed cells. *The EMBO Journal*, *20*(24), 6969–6978. https://doi.org/10.1093/emboj/20.24.6969

Guo, W., Schafer, S., Greaser, M. L., Radke, M. H., Liss, M., Govindarajan, T., Maatz, H., Schulz, H., Li, S., Parrish, A. M., Dauksaite, V., Vakeel, P., Klaassen, S., Gerull, B., Thierfelder, L., Regitz-Zagrosek, V., Hacker, T. A., Saupe, K. W., Dec, G. W., … Gotthardt, M. (2012). RBM20, a gene for hereditary cardiomyopathy, regulates titin splicing. *Nature Medicine*, *18*(5), 766–773. https://doi.org/10.1038/nm.2693

Harries, L. W., Hernandez, D., Henley, W., Wood, A. R., Holly, A. C., Bradley-Smith, R. M., Yaghootkar, H., Dutta, A., Murray, A., Frayling, T. M., Guralnik, J. M., Bandinelli, S., Singleton, A., Ferrucci, L., & Melzer, D. (2011). Human aging is characterized by focused changes in gene expression and deregulation of alternative splicing: Gene expression changes in human aging. *Aging Cell*, *10*(5), 868–878. https://doi.org/10.1111/j.1474-9726.2011.00726.x

Herzel, L., Ottoz, D. S. M., Alpert, T., & Neugebauer, K. M. (2017). Splicing and transcription touch base: Co-transcriptional spliceosome assembly and function. *Nature Reviews. Molecular Cell Biology*, *18*(10), 637–650. https://doi.org/10.1038/nrm.2017.63

Hiller, M., Zhang, Z., Backofen, R., & Stamm, S. (2007a). Pre-mRNA secondary structures influence exon recognition. *PLoS Genetics*. https://doi.org/10.1371/journal.pgen.0030204

https://doi.org/10.1371/journal.pgen.0030204

Hims, M. M., Shetty, R. S., Pickel, J., Mull, J., Leyne, M., Liu, L., Gusella, J. F., & Slaugenhaupt, S. A. (2007). A humanized IKBKAP transgenic mouse models a tissue-specific human splicing defect. *Genomics*, *90*(3), 389–396. https://doi.org/10.1016/j.ygeno.2007.05.012

Horowitz, D. S. (2012). The mechanism of the second step of pre-mRNA splicing. *Wiley Interdisciplinary Reviews. RNA*, *3*(3), 331–350. https://doi.org/10.1002/wrna.112

Hoskins, A. A., & Moore, M. J. (2012). The spliceosome: A flexible, reversible macromolecular machine. *Trends in Biochemical Sciences*, *37*(5), 179–188. https://doi.org/10.1016/j.tibs.2012.02.009

Howard, J. M., & Sanford, J. R. (2015). The RNAissance family: SR proteins as multifaceted regulators of gene expression: The RNAissance family. *Wiley Interdisciplinary Reviews: RNA*, *6*(1), 93–110. https://doi.org/10.1002/wrna.1260

Hsieh-Li, H. M., Chang, J. G., Jong, Y. J., Wu, M. H., Wang, N. M., Tsai, C. H., & Li, H. (2000). A mouse model for spinal muscular atrophy. *Nature Genetics*, *24*(1), 66–70. https://doi.org/10.1038/71709

Hua, Y., Liu, Y. H., Sahashi, K., Rigo, F., Bennett, C. F., & Krainer, A. R. (2015). Motor neuron cell-nonautonomous rescue of spinal muscular atrophy phenotypes in mild and severe transgenic mouse models. *Genes & Development*, *29*(3), 288–297. https://doi.org/10.1101/gad.256644.114

Hua, Y., Sahashi, K., Hung, G., Rigo, F., Passini, M. A., Bennett, C. F., & Krainer, A. R.

(2010). Antisense correction of SMN2 splicing in the CNS rescues necrosis in a type III SMA mouse model. *Genes & Development*, *24*(15), 1634–1644. https://doi.org/10.1101/gad.1941310

Hua, Y., Vickers, T. A., Baker, B. F., Bennett, C. F., & Krainer, A. R. (2007). Enhancement of SMN2 Exon 7 Inclusion by Antisense Oligonucleotides Targeting the Exon. *PLoS Biology*, *5*(4), e73. https://doi.org/10.1371/journal.pbio.0050073

Hyun, K., Jeon, J., Park, K., & Kim, J. (2017). Writing, erasing and reading histone lysine methylations. *Experimental & Molecular Medicine*, *49*(4), e324–e324. https://doi.org/10.1038/emm.2017.11

Ibrahim, E. C., Hims, M. M., Shomron, N., Burge, C. B., Slaugenhaupt, S. A., & Reed, R. (2007). Weak definition of IKBKAP exon 20 leads to aberrant splicing in familial dysautonomia. *Human Mutation*, *28*(1), 41–53. https://doi.org/10.1002/humu.20401

Ip, J. Y., Schmidt, D., Pan, Q., Ramani, A. K., Fraser, A. G., Odom, D. T., & Blencowe, B. J. (2011). Global impact of RNA polymerase II elongation inhibition on alternative splicing regulation. *Genome Research*, *21*(3), 390–401. https://doi.org/10.1101/gr.111070.110

Jansen, A., & Verstrepen, K. J. (2011). Nucleosome positioning in Saccharomyces cerevisiae. *Microbiology and Molecular Biology Reviews: MMBR*, *75*(2), 301–320. https://doi.org/10.1128/MMBR.00046-10

Jeong, S. (2017). SR Proteins: Binders, Regulators, and Connectors of RNA. *Molecules and Cells*, *40*(1), 1–9. https://doi.org/10.14348/molcells.2017.2319

Jiao, X., Doamekpor, S. K., Bird, J. G., Nickels, B. E., Tong, L., Hart, R. P., & Kiledjian, M. (2017). 5' End Nicotinamide Adenine Dinucleotide Cap in Human Cells Promotes RNA Decay through DXO-Mediated deNADding. *Cell*, *168*(6), 1015-1027.e10. https://doi.org/10.1016/j.cell.2017.02.019

Jimeno-González, S., & Reyes, J. C. (2016). Chromatin structure and pre-mRNA processing work together. *Transcription*, *7*(3), 63–68. https://doi.org/10.1080/21541264.2016.1168507

Kadota, Y., Jam, F. A., Yukiue, H., Terakado, I., Morimune, T., Tano, A., Tanaka, Y., Akahane, S., Fukumura, M., Tooyama, I., & Mori, M. (2020). Srsf7 Establishes the Juvenile Transcriptome through Age-Dependent Alternative Splicing in Mice. *IScience*, *23*(3), 100929. https://doi.org/10.1016/j.isci.2020.100929

Kamma, H., Portman, D. S., & Dreyfuss, G. (1995). Cell type-specific expression of hnRNP proteins. *Experimental Cell Research*, *221*(1), 187–196. https://doi.org/10.1006/excr.1995.1366

Kashima, T., Rao, N., David, C. J., & Manley, J. L. (2007). HnRNP A1 functions with specificity in repression of SMN2 exon 7 splicing. *Human Molecular Genetics*, *16*(24), 3149–3159. https://doi.org/10.1093/hmg/ddm276

Kastner, B., Will, C. L., Stark, H., & Lührmann, R. (2019). Structural Insights into Nuclear pre-mRNA Splicing in Higher Eukaryotes. *Cold Spring Harbor Perspectives in Biology*, *11*(11), a032417. https://doi.org/10.1101/cshperspect.a032417

Kavalecz, N., Ág, N., Karaffa, L., Scazzocchio, C., Flipphi, M., & Fekete, E. (2019). A spliceosomal twin intron (stwintron) participates in both exon skipping and evolutionary exon loss. *Scientific Reports*, *9*(1), 9940. https://doi.org/10.1038/s41598-019-46435-x

Keren, H., Lev-Maor, G., & Ast, G. (2010b). Alternative splicing and evolution: Diversification, exon definition and function. *Nature Reviews. Genetics*, *11*(5), 345–355. https://doi.org/10.1038/nrg2776

Khatter, H., Vorländer, M. K., & Müller, C. W. (2017). RNA polymerase I and III: Similar yet unique. *Current Opinion in Structural Biology*, *47*, 88–94. https://doi.org/10.1016/j.sbi.2017.05.008

Kim, E., Goren, A., & Ast, G. (2008). Alternative splicing: Current perspectives. *BioEssays:*

News and Reviews in Molecular, Cellular and Developmental Biology, *30*(1), 38–47. https://doi.org/10.1002/bies.20692

Kim, K. K., Nam, J., Mukouyama, Y.-S., & Kawamoto, S. (2013). Rbfox3-regulated alternative splicing of Numb promotes neuronal differentiation during development. *The Journal of Cell Biology*, *200*(4), 443–458. https://doi.org/10.1083/jcb.201206146

Kobayashi, W., & Kurumizaka, H. (2019). Structural transition of the nucleosome during chromatin remodeling and transcription. *Current Opinion in Structural Biology*, *59*, 107–114. https://doi.org/10.1016/j.sbi.2019.07.011

Kolb, S. J., & Kissel, J. T. (2015). Spinal Muscular Atrophy. *Neurologic Clinics*, *33*(4), 831–846. https://doi.org/10.1016/j.ncl.2015.07.004

Kornblihtt, A. R. (2004). Multiple links between transcription and splicing. *RNA*, *10*(10), 1489–1498. https://doi.org/10.1261/rna.7100104

Kornblihtt, A. R., Schor, I. E., Alló, M., Dujardin, G., Petrillo, E., & Muñoz, M. J. (2013). Alternative splicing: A pivotal step between eukaryotic transcription and translation. *Nature Reviews Molecular Cell Biology*, *14*(3), 153–165. https://doi.org/10.1038/nrm3525

Kosti, A., de Araujo, P. R., Li, W.-Q., Guardia, G. D. A., Chiou, J., Yi, C., Ray, D., Meliso, F., Li, Y.-M., Delambre, T., Qiao, M., Burns, S. S., Lorbeer, F. K., Georgi, F., Flosbach, M., Klinnert, S., Jenseit, A., Lei, X., Sandoval, C. R., … Penalva, L. O. F. (2020). The RNA-binding protein SERBP1 functions as a novel oncogenic factor in glioblastoma by bridging cancer metabolism and epigenetic regulation. *Genome Biology*, *21*(1), 195. https://doi.org/10.1186/s13059-020-02115-y

Krecic, A. M., & Swanson, M. S. (1999). hnRNP complexes: Composition, structure, and function. *Current Opinion in Cell Biology*, *11*(3), 363–371. https://doi.org/10.1016/S0955-0674(99)80051-9

Lagha, M., Bothma, J. P., Esposito, E., Ng, S., Stefanik, L., Tsui, C., Johnston, J., Chen, K., Gilmour, D. S., Zeitlinger, J., & Levine, M. S. (2013). Paused Pol II coordinates tissue morphogenesis in the Drosophila embryo. *Cell*, *153*(5), 976–987. https://doi.org/10.1016/j.cell.2013.04.045

Lanfranco, M., Vassallo, N., & Cauchi, R. J. (2017). Spinal Muscular Atrophy: From Defective Chaperoning of snRNP Assembly to Neuromuscular Dysfunction. *Frontiers in Molecular Biosciences*, *4*, 41. https://doi.org/10.3389/fmolb.2017.00041

Langford, C. J., Klinz, F.-J., Donath, C., & Gallwitz, D. (1984). Point mutations identify the conserved, intron-contained TACTAAC box as an essential splicing signal sequence in yeast. *Cell*, *36*(3), 645–653. https://doi.org/10.1016/0092-8674(84)90344-1

Lavarone, E., Barbieri, C. M., & Pasini, D. (2019). Dissecting the role of H3K27 acetylation and methylation in PRC2 mediated control of cellular identity. *Nature Communications*, *10*(1), 1679. https://doi.org/10.1038/s41467-019-09624-w

Lee, Y., & Rio, D. C. (2015). Mechanisms and Regulation of Alternative Pre-mRNA Splicing. *Annual Review of Biochemistry*, *84*, 291–323. https://doi.org/10.1146/annurev-biochem-060614-034316

Lefcort, F., Mergy, M., Ohlen, S. B., Ueki, Y., & George, L. (2017). Animal and cellular models of familial dysautonomia. *Clinical Autonomic Research : Official Journal of the Clinical Autonomic Research Society*, *27*(4), 235–243. https://doi.org/10.1007/s10286-017-0438-2

Li, G., & Zhu, P. (2015). Structure and organization of chromatin fiber in the nucleus. *FEBS Letters*, *589*(20 Pt A), 2893–2904. https://doi.org/10.1016/j.febslet.2015.04.023

Li, S., Guo, W., Dewey, C. N., & Greaser, M. L. (2013). Rbm20 regulates titin alternative splicing as a splicing repressor. *Nucleic Acids Research*, *41*(4), 2659–2672. https://doi.org/10.1093/nar/gks1362

Linke, W. A., & Krüger, M. (2010). The giant protein titin as an integrator of myocyte signaling pathways. *Physiology (Bethesda, Md.)*, *25*(3), 186–198.

https://doi.org/10.1152/physiol.00005.2010
Liu, L., Cheung, T. H., Charville, G. W., Hurgo, B. M. C., Leavitt, T., Shih, J., Brunet, A., & Rando, T. A. (2013). Chromatin modifications as determinants of muscle stem cell quiescence and chronological aging. *Cell Reports*, *4*(1), 189–204. https://doi.org/10.1016/j.celrep.2013.05.043
Liu, N., Dai, Q., Zheng, G., He, C., Parisien, M., & Pan, T. (2015). N(6)-methyladenosine-dependent RNA structural switches regulate RNA-protein interactions. *Nature*, *518*(7540), 560–564. https://doi.org/10.1038/nature14234
Liu, X., Bushnell, D. A., & Kornberg, R. D. (2013). RNA polymerase II transcription: Structure and mechanism. *Biochimica et Biophysica Acta (BBA) - Gene Regulatory Mechanisms*, *1829*(1), 2–8. https://doi.org/10.1016/j.bbagrm.2012.09.003
López-Otín, C., Blasco, M. A., Partridge, L., Serrano, M., & Kroemer, G. (2013). The Hallmarks of Aging. *Cell*, *153*(6), 1194–1217. https://doi.org/10.1016/j.cell.2013.05.039
Luco, R. F., Allo, M., Schor, I. E., Kornblihtt, A. R., & Misteli, T. (2011). Epigenetics in Alternative Pre-mRNA Splicing. *Cell*, *144*(1), 16–26. https://doi.org/10.1016/j.cell.2010.11.056
Luco, R. F., Pan, Q., Tominaga, K., Blencowe, B. J., Pereira-Smith, O. M., & Misteli, T. (2010). Regulation of alternative splicing by histone modifications. *Science (New York, N.Y.)*, *327*(5968), 996–1000. https://doi.org/10.1126/science.1184208
M, B., P, H., S, D., C, H., & Wb, M. (2020). Alternative splicing in aging and longevity. *Human Genetics*, *139*(3). https://doi.org/10.1007/s00439-019-02094-6
Magaña-Acosta, M., & Valadez-Graham, V. (2020). Chromatin Remodelers in the 3D Nuclear Compartment. *Frontiers in Genetics*, *11*, 1344. https://doi.org/10.3389/fgene.2020.600615
Maniatis, T., & Reed, R. (2002). An extensive network of coupling among gene expression machines. *Nature*, *416*(6880), 499–506. https://doi.org/10.1038/416499a
Martinez-Contreras, R., Cloutier, P., Shkreta, L., Fisette, J.-F., Revil, T., & Chabot, B. (2007). HnRNP proteins and splicing control. *Advances in Experimental Medicine and Biology*, *623*, 123–147. https://doi.org/10.1007/978-0-387-77374-2_8
Maslon, M. M., Braunschweig, U., Aitken, S., Mann, A. R., Kilanowski, F., Hunter, C. J., Blencowe, B. J., Kornblihtt, A. R., Adams, I. R., & Cáceres, J. F. (2019). A slow transcription rate causes embryonic lethality and perturbs kinetic coupling of neuronal genes. *The EMBO Journal*, *38*(9), e101244. https://doi.org/10.15252/embj.2018101244
Matera, A. G., & Wang, Z. (2014b). A day in the life of the spliceosome. *Nature Reviews Molecular Cell Biology*, *15*(2), 108–121. https://doi.org/10.1038/nrm3742
Maures, T. J., Greer, E. L., Hauswirth, A. G., & Brunet, A. (2011). The H3K27 demethylase UTX-1 regulates C. elegans lifespan in a germline-independent, insulin-dependent manner. *Aging Cell*, *10*(6), 980–990. https://doi.org/10.1111/j.1474-9726.2011.00738.x
Mayer, O., Waldsich, C., Grossberger, R., & Schroeder, R. (2002). Folding of the td pre-RNA with the help of the RNA chaperone StpA. *Biochemical Society Transactions*. https://doi.org/10.1042/BST0301175
Mayerle, M., & Guthrie, C. (2017). Genetics and biochemistry remain essential in the structural era of the spliceosome. *Methods (San Diego, Calif.)*, *125*, 3–9. https://doi.org/10.1016/j.ymeth.2017.01.006
Mazin, P., Xiong, J., Liu, X., Yan, Z., Zhang, X., Li, M., He, L., Somel, M., Yuan, Y., Phoebe Chen, Y., Li, N., Hu, Y., Fu, N., Ning, Z., Zeng, R., Yang, H., Chen, W., Gelfand, M., & Khaitovich, P. (2013). Widespread splicing changes in human brain development and aging. *Molecular Systems Biology*, *9*(1), 633. https://doi.org/10.1038/msb.2012.67

Meijboom, K., Wood, M., & McClorey, G. (2017). Splice-Switching Therapy for Spinal Muscular Atrophy. *Genes*, *8*(6), 161. https://doi.org/10.3390/genes8060161

Min, I. M., Waterfall, J. J., Core, L. J., Munroe, R. J., Schimenti, J., & Lis, J. T. (2011). Regulating RNA polymerase pausing and transcription elongation in embryonic stem cells. *Genes & Development*, *25*(7), 742–754. https://doi.org/10.1101/gad.2005511

Miyamoto, S., Hidaka, K., Jin, D., & Morisaki, T. (2009). RNA-binding proteins Rbm38 and Rbm24 regulate myogenic differentiation via p21-dependent and -independent regulatory pathways. *Genes to Cells*, *14*(11), 1241–1252. https://doi.org/10.1111/j.1365-2443.2009.01347.x

Moore, L. D., Le, T., & Fan, G. (2013). DNA methylation and its basic function. *Neuropsychopharmacology: Official Publication of the American College of Neuropsychopharmacology*, *38*(1), 23–38. https://doi.org/10.1038/npp.2012.112

Morgan, M. A. J., & Shilatifard, A. (2020). Reevaluating the roles of histone-modifying enzymes and their associated chromatin modifications in transcriptional regulation. *Nature Genetics*, *52*(12), 1271–1281. https://doi.org/10.1038/s41588-020-00736-4

Morrison, O., & Thakur, J. (2021). Molecular Complexes at Euchromatin, Heterochromatin and Centromeric Chromatin. *International Journal of Molecular Sciences*, *22*(13), 6922. https://doi.org/10.3390/ijms22136922

Muñoz, M. J., Pérez Santangelo, M. S., Paronetto, M. P., de la Mata, M., Pelisch, F., Boireau, S., Glover-Cutter, K., Ben-Dov, C., Blaustein, M., Lozano, J. J., Bird, G., Bentley, D., Bertrand, E., & Kornblihtt, A. R. (2009). DNA damage regulates alternative splicing through inhibition of RNA polymerase II elongation. *Cell*, *137*(4), 708–720. https://doi.org/10.1016/j.cell.2009.03.010

Naftelberg, S., Schor, I. E., Ast, G., & Kornblihtt, A. R. (2015). Regulation of Alternative Splicing Through Coupling with Transcription and Chromatin Structure. *Annual Review of Biochemistry*, *84*(1), 165–198. https://doi.org/10.1146/annurev-biochem-060614-034242

Nakayama, K., & Kataoka, N. (2019). Regulation of Gene Expression under Hypoxic Conditions. *International Journal of Molecular Sciences*, *20*(13), E3278. https://doi.org/10.3390/ijms20133278

Noer, A., Lindeman, L. C., & Collas, P. (2009). Histone H3 modifications associated with differentiation and long-term culture of mesenchymal adipose stem cells. *Stem Cells and Development*, *18*(5), 725–736. https://doi.org/10.1089/scd.2008.0189

Norcliffe-Kaufmann, L., Axelrod, F. B., & Kaufmann, H. (2013). Developmental abnormalities, blood pressure variability and renal disease in Riley Day syndrome. *Journal of Human Hypertension*, *27*(1), 51–55. https://doi.org/10.1038/jhh.2011.107

Norcliffe-Kaufmann, L., Slaugenhaupt, S. A., & Kaufmann, H. (2017). Familial dysautonomia: History, genotype, phenotype and translational research. *Progress in Neurobiology*, *152*, 131–148. https://doi.org/10.1016/j.pneurobio.2016.06.003

Oesterreich, F. C., Bieberstein, N., & Neugebauer, K. M. (2011). Pause locally, splice globally. *Trends in Cell Biology*, *21*(6), 328–335. https://doi.org/10.1016/j.tcb.2011.03.002

Ohe, K., Yoshida, M., Nakano-Kobayashi, A., Hosokawa, M., Sako, Y., Sakuma, M., Okuno, Y., Usui, T., Ninomiya, K., Nojima, T., Kataoka, N., & Hagiwara, M. (2017). RBM24 promotes U1 snRNP recognition of the mutated 5′ splice site in the *IKBKAP* gene of familial dysautonomia. *RNA*, *23*(9), 1393–1403. https://doi.org/10.1261/rna.059428.116

Padgett, R. A. (2012). New connections between splicing and human disease. *Trends in Genetics: TIG*, *28*(4), 147–154. https://doi.org/10.1016/j.tig.2012.01.001 https://doi.org/10.1038/nrg1327

Pagani, F., & Baralle, F. E. (2004b). Genomic variants in exons and introns: Identifying the splicing spoilers. *Nature Reviews. Genetics*, *5*(5), 389–396.

https://doi.org/10.1038/nrg1327

Pagani, F., Stuani, C., Zuccato, E., Kornblihtt, A. R., & Baralle, F. E. (2003). Promoter architecture modulates CFTR exon 9 skipping. *The Journal of Biological Chemistry*, *278*(3), 1511–1517. https://doi.org/10.1074/jbc.M209676200

Perlman, R. L. (2016). Mouse models of human disease. *Evolution, Medicine, and Public Health*, *2016*(1), 170–176. https://doi.org/10.1093/emph/eow014

Pessa, H. K. J., Ruokolainen, A., & Frilander, M. J. (2006). The abundance of the spliceosomal snRNPs is not limiting the splicing of U12-type introns. *Rna*, *12*(10), 1883–1892. https://doi.org/10.1261/rna.213906

Piacentini, L., Fanti, L., Negri, R., Del Vescovo, V., Fatica, A., Altieri, F., & Pimpinelli, S. (2009). Heterochromatin protein 1 (HP1a) positively regulates euchromatic gene expression through RNA transcript association and interaction with hnRNPs in Drosophila. *PLoS Genetics*, *5*(10), e1000670. https://doi.org/10.1371/journal.pgen.1000670

Pope, S. D., & Medzhitov, R. (2018). Emerging Principles of Gene Expression Programs and Their Regulation. *Molecular Cell*, *71*(3), 389–397. https://doi.org/10.1016/j.molcel.2018.07.017

Proudfoot, N. J., Furger, A., & Dye, M. J. (2002). Integrating mRNA processing with transcription. *Cell*, *108*(4), 501–512. https://doi.org/10.1016/s0092-8674(02)00617-7

Qi, W., Zhao, K., Gu, J., Huang, Y., Wang, Y., Zhang, H., Zhang, M., Zhang, J., Yu, Z., Li, L., Teng, L., Chuai, S., Zhang, C., Zhao, M., Chan, H., Chen, Z., Fang, D., Fei, Q., Feng, L., … Li, E. (2017). An allosteric PRC2 inhibitor targeting the H3K27me3 binding pocket of EED. *Nature Chemical Biology*, *13*(4), 381–388. https://doi.org/10.1038/nchembio.2304

Ramanouskaya, T. V., & Grinev, V. V. (2017). The determinants of alternative RNA splicing in human cells. *Molecular Genetics and Genomics: MGG*, *292*(6), 1175–1195. https://doi.org/10.1007/s00438-017-1350-0

Ramsay, E. P., Abascal-Palacios, G., Daiß, J. L., King, H., Gouge, J., Pilsl, M., Beuron, F., Morris, E., Gunkel, P., Engel, C., & Vannini, A. (2020). Structure of human RNA polymerase III. *Nature Communications*, *11*(1), 6409. https://doi.org/10.1038/s41467-020-20262-5

Roscigno, R. F., Weiner, M., & Garcia-Blanco, M. A. (1993). A mutational analysis of the polypyrimidine tract of introns. Effects of sequence differences in pyrimidine tracts on splicing. *Journal of Biological Chemistry*, *268*(15), 11222–11229. https://doi.org/10.1016/S0021-9258(18)82114-7

Sahebi, M., Hanafi, M. M., van Wijnen, A. J., Azizi, P., Abiri, R., Ashkani, S., & Taheri, S. (2016). Towards understanding pre-mRNA splicing mechanisms and the role of SR proteins. *Gene*, *587*(2), 107–119. https://doi.org/10.1016/j.gene.2016.04.057

Sakharkar, M. K., Perumal, B. S., Sakharkar, K. R., & Kangueane, P. (2005). An analysis on gene architecture in human and mouse genomes. *In Silico Biology*, *5*(4), 347–365.

Sanford, J. R., Ellis, J., & Cáceres, J. F. (2005). Multiple roles of arginine/serine-rich splicing factors in RNA processing. *Biochemical Society Transactions*, *33*(Pt 3), 443–446. https://doi.org/10.1042/BST0330443

Schier, A. C., & Taatjes, D. J. (2020). Structure and mechanism of the RNA polymerase II transcription machinery. *Genes & Development*, *34*(7–8), 465–488. https://doi.org/10.1101/gad.335679.119

Schor, I. E., Fiszbein, A., Petrillo, E., & Kornblihtt, A. R. (2013). Intragenic epigenetic changes modulate NCAM alternative splicing in neuronal differentiation. *The EMBO Journal*, *32*(16), 2264–2274. https://doi.org/10.1038/emboj.2013.167

Schorling, D. C., Pechmann, A., & Kirschner, J. (2020). Advances in Treatment of Spinal Muscular Atrophy—New Phenotypes, New Challenges, New Implications for Care. *Journal of Neuromuscular Diseases*, *7*(1), 1–13. https://doi.org/10.3233/JND-190424

Schwartz, S., Meshorer, E., & Ast, G. (2009). Chromatin organization marks exon-intron structure. *Nature Structural & Molecular Biology*, *16*(9), 990–995. https://doi.org/10.1038/nsmb.1659

Schwörer, S., Becker, F., Feller, C., Baig, A. H., Köber, U., Henze, H., Kraus, J. M., Xin, B., Lechel, A., Lipka, D. B., Varghese, C. S., Schmidt, M., Rohs, R., Aebersold, R., Medina, K. L., Kestler, H. A., Neri, F., von Maltzahn, J., Tümpel, S., & Rudolph, K. L. (2016). Epigenetic stress responses induce muscle stem-cell ageing by Hoxa9 developmental signals. *Nature*, *540*(7633), 428–432. https://doi.org/10.1038/nature20603

Shukla, S., Kavak, E., Gregory, M., Imashimizu, M., Shutinoski, B., Kashlev, M., Oberdoerffer, P., Sandberg, R., & Oberdoerffer, S. (2011). CTCF-promoted RNA polymerase II pausing links DNA methylation to splicing. *Nature*, *479*(7371), 74–79. https://doi.org/10.1038/nature10442

Shukla, S., & Oberdoerffer, S. (2012). Co-transcriptional regulation of alternative pre-mRNA splicing. *Biochimica et Biophysica Acta (BBA) - Gene Regulatory Mechanisms*, *1819*(7), 673–683. https://doi.org/10.1016/j.bbagrm.2012.01.014

Shuman, S., & Schwer, B. (1995). RNA capping enzyme and DNA ligase: A superfamily of covalent nucleotidyl transferases. *Molecular Microbiology*, *17*(3), 405–410. https://doi.org/10.1111/j.1365-2958.1995.mmi_17030405.x

Siebold, A. P., Banerjee, R., Tie, F., Kiss, D. L., Moskowitz, J., & Harte, P. J. (2010). Polycomb Repressive Complex 2 and Trithorax modulate Drosophila longevity and stress resistance. *Proceedings of the National Academy of Sciences of the United States of America*, *107*(1), 169–174. https://doi.org/10.1073/pnas.0907739107

Sims, R. J., Millhouse, S., Chen, C.-F., Lewis, B. A., Erdjument-Bromage, H., Tempst, P., Manley, J. L., & Reinberg, D. (2007). Recognition of trimethylated histone H3 lysine 4 facilitates the recruitment of transcription postinitiation factors and pre-mRNA splicing. *Molecular Cell*, *28*(4), 665–676. https://doi.org/10.1016/j.molcel.2007.11.010

Singh, R. K., & Cooper, T. A. (2012). Pre-mRNA splicing in disease and therapeutics. *Trends in Molecular Medicine*, *18*(8), 472–482. https://doi.org/10.1016/j.molmed.2012.06.006

Slaugenhaupt, S. A., Blumenfeld, A., Gill, S. P., Leyne, M., Mull, J., Cuajungco, M. P., Liebert, C. B., Chadwick, B., Idelson, M., Reznik, L., Robbins, C. M., Makalowska, I., Brownstein, M. J., Krappmann, D., Scheidereit, C., Maayan, C., Axelrod, F. B., & Gusella, J. F. (2001). Tissue-Specific Expression of a Splicing Mutation in the IKBKAP Gene Causes Familial Dysautonomia. *Am. J. Hum. Genet.*, 8.

Slaugenhaupt, S. A., & Gusella, J. F. (2002). Familial dysautonomia. *Current Opinion in Genetics & Development*, *12*(3), 307–311. https://doi.org/10.1016/s0959-437x(02)00303-9

Staněk, D. (2017). Cajal bodies and snRNPs—Friends with benefits. *RNA Biology*, *14*(6), 671–679. https://doi.org/10.1080/15476286.2016.1231359

Stegeman, R., & Weake, V. M. (2017). Transcriptional Signatures of Aging. *Journal of Molecular Biology*, *429*(16), 2427–2437. https://doi.org/10.1016/j.jmb.2017.06.019

Sundaramoorthy, R., & Owen-Hughes, T. (2020). Chromatin remodelling comes into focus. *F1000Research*, *9*, F1000 Faculty Rev-1011. https://doi.org/10.12688/f1000research.21933.1

Swanson, M. S. (2015). Rectifying RNA splicing errors in hereditary neurodegenerative disease. *Proceedings of the National Academy of Sciences of the United States of America*, *112*(9), 2637–2638. https://doi.org/10.1073/pnas.1500976112

Tamaru, H. (2010). Confining euchromatin/heterochromatin territory: Jumonji crosses the line. *Genes & Development*, *24*(14), 1465–1478. https://doi.org/10.1101/gad.1941010

Tizzano, E. F., & Finkel, R. S. (2017). Spinal muscular atrophy: A changing phenotype

beyond the clinical trials. *Neuromuscular Disorders*, *27*(10), 883–889. https://doi.org/10.1016/j.nmd.2017.05.011

Tosolini, A. P., & Sleigh, J. N. (2017). Motor Neuron Gene Therapy: Lessons from Spinal Muscular Atrophy for Amyotrophic Lateral Sclerosis. *Frontiers in Molecular Neuroscience*, *10*, 405. https://doi.org/10.3389/fnmol.2017.00405

Ule, J., & Blencowe, B. J. (2019). Alternative Splicing Regulatory Networks: Functions, Mechanisms, and Evolution. *Molecular Cell*, *76*(2), 329–345. https://doi.org/10.1016/j.molcel.2019.09.017

Venkat Ramani, M. K., Yang, W., Irani, S., & Zhang, Y. (2021). Simplicity is the Ultimate Sophistication—Crosstalk of Post-translational Modifications on the RNA Polymerase II. *Journal of Molecular Biology*, *433*(14), 166912. https://doi.org/10.1016/j.jmb.2021.166912

Wang, C. M., Tsai, S. N., Yew, T. W., Kwan, Y. W., & Ngai, S. M. (2010). Identification of histone methylation multiplicities patterns in the brain of senescence-accelerated prone mouse 8. *Biogerontology*, *11*(1), 87–102. https://doi.org/10.1007/s10522-009-9231-5

Waszak, S. M., Robinson, G. W., Gudenas, B. L., Smith, K. S., Forget, A., Kojic, M., Garcia-Lopez, J., Hadley, J., Hamilton, K. V., Indersie, E., Buchhalter, I., Kerssemakers, J., Jäger, N., Sharma, T., Rausch, T., Kool, M., Sturm, D., Jones, D. T. W., Vasilyeva, A., … Pfister, S. M. (2020). Germline Elongator mutations in sonic hedgehog medulloblastoma. *Nature*, *580*(7803), 396–401. https://doi.org/10.1038/s41586-020-2164-5

Weaver, I. C. G., Korgan, A. C., Lee, K., Wheeler, R. V., Hundert, A. S., & Goguen, D. (2017). Stress and the Emerging Roles of Chromatin Remodeling in Signal Integration and Stable Transmission of Reversible Phenotypes. *Frontiers in Behavioral Neuroscience*, *11*. https://doi.org/10.3389/fnbeh.2017.00041

Wee, C. D., Havens, M. A., Jodelka, F. M., & Hastings, M. L. (2014). Targeting SR Proteins Improves SMN Expression in Spinal Muscular Atrophy Cells. *PLoS ONE*, *9*(12), e115205. https://doi.org/10.1371/journal.pone.0115205

Weyn-Vanhentenryck, S. M., Feng, H., Ustianenko, D., Duffié, R., Yan, Q., Jacko, M., Martinez, J. C., Goodwin, M., Zhang, X., Hengst, U., Lomvardas, S., Swanson, M. S., & Zhang, C. (2018). Precise temporal regulation of alternative splicing during neural development. *Nature Communications*, *9*(1), 2189. https://doi.org/10.1038/s41467-018-04559-0

Widen, S. G., Kedar, P., & Wilson, S. H. (1988). Human beta-polymerase gene. Structure of the 5'-flanking region and active promoter. *The Journal of Biological Chemistry*, *263*(32), 16992–16998.

Wilkinson, M. E., Charenton, C., & Nagai, K. (2020). RNA Splicing by the Spliceosome. *Annual Review of Biochemistry*, *89*, 359–388. https://doi.org/10.1146/annurev-biochem-091719-064225

Will, C. L., & Luhrmann, R. (2011). Spliceosome Structure and Function. *Cold Spring Harbor Perspectives in Biology*, *3*(7), a003707–a003707. https://doi.org/10.1101/cshperspect.a003707

Williams, L. H., Fromm, G., Gokey, N. G., Henriques, T., Muse, G. W., Burkholder, A., Fargo, D. C., Hu, G., & Adelman, K. (2015). Pausing of RNA polymerase II regulates mammalian developmental potential through control of signaling networks. *Molecular Cell*, *58*(2), 311–322. https://doi.org/10.1016/j.molcel.2015.02.003

Yang, J., Hung, L.-H., Licht, T., Kostin, S., Looso, M., Khrameeva, E., Bindereif, A., Schneider, A., & Braun, T. (2014). RBM24 Is a Major Regulator of Muscle-Specific Alternative Splicing. *Developmental Cell*, *31*(1), 87–99. https://doi.org/10.1016/j.devcel.2014.08.025

Yano, M., Hayakawa-Yano, Y., Mele, A., & Darnell, R. B. (2010). Nova2 regulates neuronal

migration through an RNA switch in disabled-1 signaling. *Neuron*, *66*(6), 848–858. https://doi.org/10.1016/j.neuron.2010.05.007

Yokoyama, A. (2019). RNA Polymerase II-Dependent Transcription Initiated by Selectivity Factor 1: A Central Mechanism Used by MLL Fusion Proteins in Leukemic Transformation. *Frontiers in Genetics*, *9*, 722. https://doi.org/10.3389/fgene.2018.00722

Zhang, Y., Sun, Z., Jia, J., Du, T., Zhang, N., Tang, Y., Fang, Y., & Fang, D. (2021). Overview of Histone Modification. In D. Fang & J. Han (Eds.), *Histone Mutations and Cancer* (pp. 1–16). Springer. https://doi.org/10.1007/978-981-15-8104-5_1

Zhu, J., Li, L., Tong, J., Hui, C., Wong, C. H., Lo, K. W., Chan, R., Ai, Q. Y., Hui, E. P., Chan, A. T., To, K. F., Tao, Q., & Ma, B. B. (2020). Targeting the polycomb repressive complex-2 related proteins with novel combinational strategies for nasopharyngeal carcinoma. *American Journal of Cancer Research*, *10*(10), 3267–3284.

Chapter 7 – Acknowledgements

Innanzitutto, ringrazio il mio tutore, Prof. Paolo Pinton ed il mio co-tutore, Prof. Franco Pagani, per avermi supportato durante questo percorso. Un ringraziamento (e merito) ulteriore va a Franco per la fiducia, l'aiuto e la pazienza dimostrati in questi anni.

Ringrazio gli attuali membri del laboratorio, Giulia ed Erica, e quelli che ormai sono migrati altrove per i suggerimenti, i consigli e i bei momenti trascorsi insieme.

Un grazie di cuore va a Martina, sempre presente.

Ringrazio inoltre tutti i miei amici, sia della vecchia che della nuova guardia, che hanno condiviso con me un sacco di lagne e di noie ma anche di risate, di cene e di bevute nel corso degli anni. Una particolare menzione tra i diversi luoghi cittadini va a "Robi Scussa", luogo di ritrovo chi ci accoglie in qualsiasi stagione e che ci ha alleviato la sete tante volte ma mai troppe.

Ringrazio genitori, nonni, zii, cugini e quella cicciona della Chicca per il supporto in questi anni.

Un sentito ringraziamento va al Prof. David Bentley della University of Colorado School of Medicine che ci ha gentilmente inviato i costrutti cinetici della Polimerasi II permettendoci di aprire un intero capitolo di questo progetto.

...THE END?